Demetalation of Copper Undecaarylcorroles: Molecular Structures of a Free-Base Undecaarylisocorrole and a Gold Undecaarylcorrole

Jan Capar,[a] Job Zonneveld,[a] Steffen Berg,[a] Johan Isaksson,[a] Kevin J. Gagnon,[b] Kolle E. Thomas,*[,a] and Abhik Ghosh*[,a]

[a] Department of Chemistry and Center for Theoretical and Computational Chemistry, University of Tromsø, N-9037 Tromsø, Norway; Email: thomas.kolle@uit.no; abhik.ghosh@uit.no; [b] Advanced Light Source, Lawrence Berkeley National Laboratory, Berkeley, CA 94720-8229

Abstract. Copper undecaarylcorroles were found to undergo acid-induced demetalation with unusual ease under both reductive and nonreductive conditions. The resulting free-base undecaarylcorroles were found to be rather reactive, readily photooxygenating to yield 5/10-hydroxyisocorroles and biliverdines. The use of nonreductive conditions led to fairly good yields of undecaarylisocorroles, a new class of sterically hindered ligands, of which one proved amenable to single-crystal X-ray structural analysis. In one case, interaction of an undecaarylisocorrole with gold(III) acetate resulted in aromatization of the macrocycle and a gold undecaarylcorrole. The Au complex exhibited Au-N distances of 1.941(3)-1.965(3) Å, and no significant nonbonded interactions involving the gold. The significant solubility of this complex in organic solvents, compared with the relative insolubility of gold *β*-octabromo-*meso*-triarylcorroles, appears to be related to the lack of aurophilic and metallophilic interactions.

Introduction. Metallocorroles,[1,2] particularly copper corroles, are typically much more readily functionalized and elaborated in a controlled manner than free-base corroles. Subsequent demetalation then has the potential to yield novel, substituted free-base corrole ligands. Unfortunately, the demetalation of metallocorroles is generally more difficult than that of common metalloporphyrins, requiring both strong acid and an excess of a reductant such as a Fe(II) or Sn(II) salt.[3,4,5,6,7] A notable success of this 'reductive demetalation' approach has been the synthesis of free-base *β*-octabromocorroles[5,4,7,8] and their subsequent use as ligands.[9,10] Here we report that copper undecaarylcorroles[11,12,13] demetalate with unusual ease, in a matter of minutes, on exposure to acid, under both reductive and nonreductive conditions.

In what initially appeared to be a setback, free-base undecaarylcorroles were found to be rather reactive, readily reacting with ambient oxygen to generate 5-hydroxy- and 10-hydroxy-undecaarylisocorroles as well as open-chain dioxo compounds. As shown in Figure 1, isocorroles are fascinating ligands in their own right: they are porphyrin-like by virtue of their diprotic or dianionic character and corrole-like in affording a spatially constricted cavity for metal coordination.[14,15,16,17,18] They are thus promising platforms for unusual transition metal spin states. In a pertinent study, Bröring and coworkers have reported that thiacorroles, which are structurally similar to isocorroles, give rise to intermediate-spin iron(III) complexes.[19] A second remarkable feature of isocorroles is their strong absorption in the near-infrared,[17] which is of great relevance to photodynamic therapy.[20] Reported herein are optimized syntheses for a family of sterically hindered undecaarylisocorrole ligands, including the first, single-crystal X-ray structure of a free-base undecaarylisocorrole.

Furthermore, we have attempted to determine whether undecaarylisocorrole ligands can be rearomatized on metal complexation, yielding novel undecaarylcorrole complexes. This is an important question because, as of today, only copper and cobalt undecaarylcorroles have been reported.[11-13] New metalloundecaarylcorroles are of considerable interest as shape-selective catalysts and other functional materials. As shown in Figure 2, we found that at least one free-base undecaarylisocorrole could be smoothly converted to the corresponding gold undecaarylcorrole. The same gold complex could also be obtained from a gold *β*-octabromo-*meso*-triarylcorrole via a tedious, week-long Suzuki coupling procedure. Remetalation and aromatization of isocorroles to corroles, when feasible, thus promises to be a useful transformation.

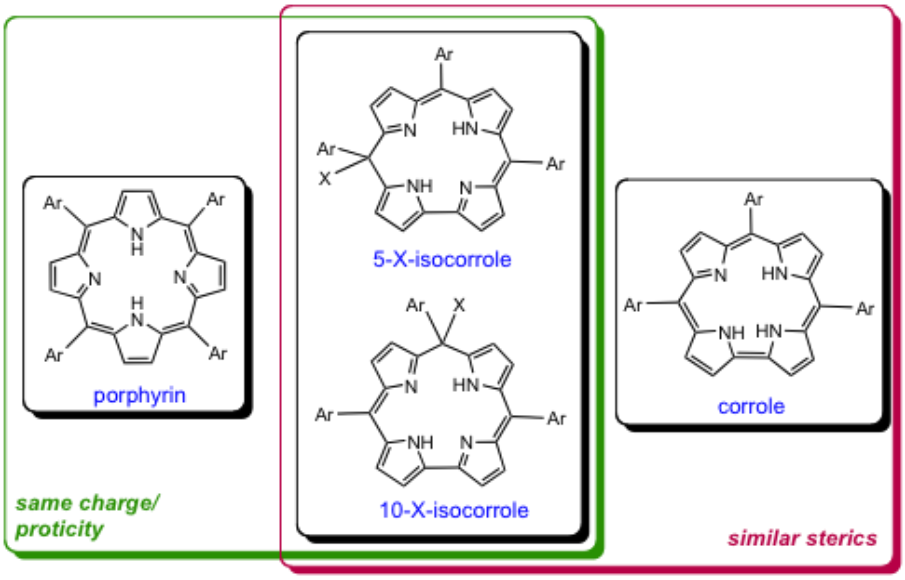

Figure 1. Steric and electronic relationships between porphyrin, corrole, and isocorrole ligands. Whereas porphyrin and isocorroles share the same proticity (both coordinate as dianionic ligands), isocorroles and corroles share similar, constricted coordination cavities.

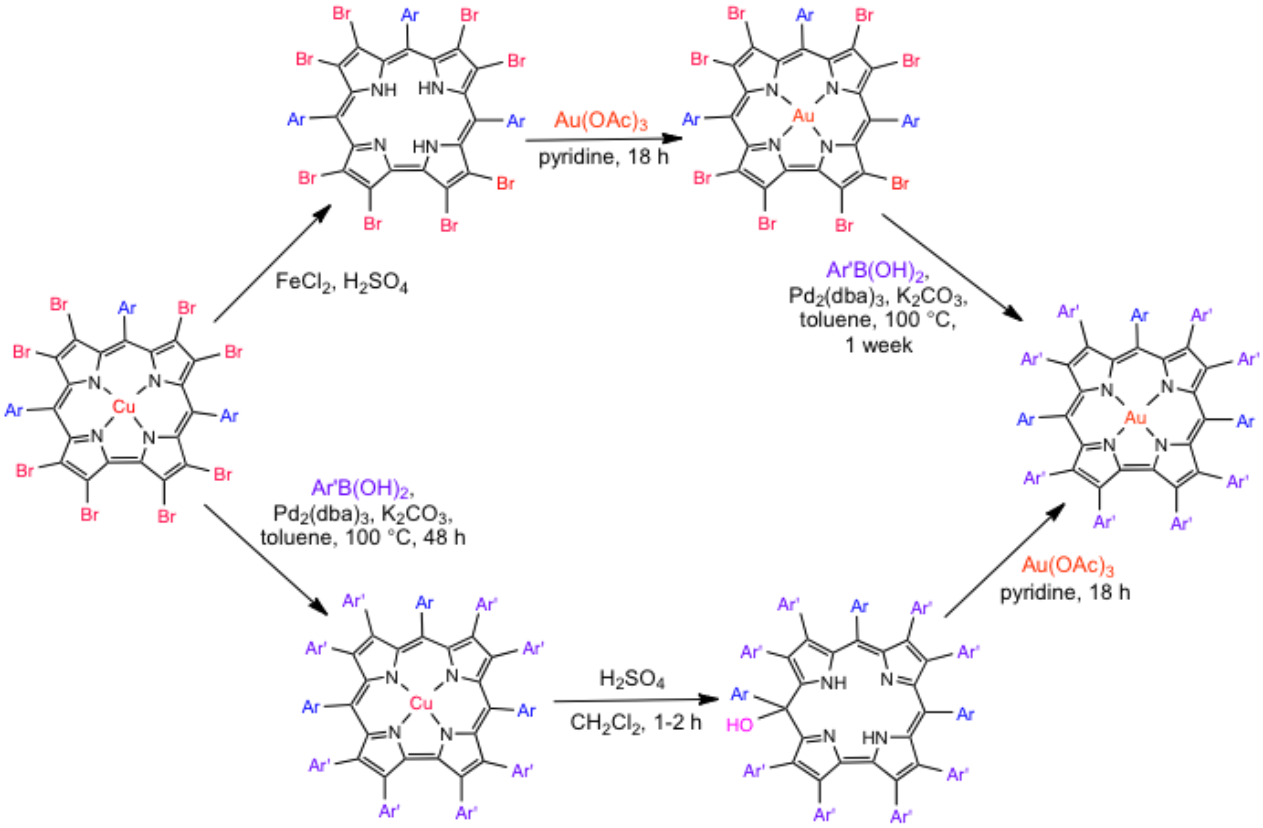

Figure 2. Two alternative synthetic routes to a gold undecaarylcorrole.

Results and Discussion

(a) Demetallation of copper undecaarylcorroles and isocorrole formation. Four different copper undecaarylcorroles were demetallated in this study, copper *β*-octakis(*p*-X-phenyl)-*meso*-tris(*p*-methylphenyl)corrole, where X = H, F, and CF_3, and copper *β*-octakis(*p*-trifluoromethylphenyl)-*meso*-triphenylcorrole (Figure 3). For brevity, we will refer to these complexes as $Cu[X_8Me_3]$. We will also refer to the corresponding free-base corroles as $H_3[X_8Me_3]$ and the isocorroles as $H_2[X_8Me_3(5\text{-}OH)]$. Reductive demetallation of $Cu[X_8Me_3]$ with concentrated sulfuric acid and ~10 equiv of anhydrous $FeCl_2$ led to ~70% yields of the free-base corroles, $H_3[X_8Me_3]$, in a matter of minutes, but in the presence of air and light, free-base undecaarylcorroles quickly decomposed to open-chain dioxotetrapyrroles such as biliverdines and small quantitites of the isocorroles, $H_2[X_8Me_3(5/10\text{-}OH)]$. Eliminating reductive conditions (i.e., $FeCl_2$) proved to be an effective way of improving the yield of isocorroles, the key targets of this study, as did the presence of an organic solvent such as dichloromethane. The final optimized conditions, involving demetallation in dichloromethane and concentrated sulfuric acid, led to 50-65% yields of highly stable, free-base isocorroles, with negligible quantities of corroles.

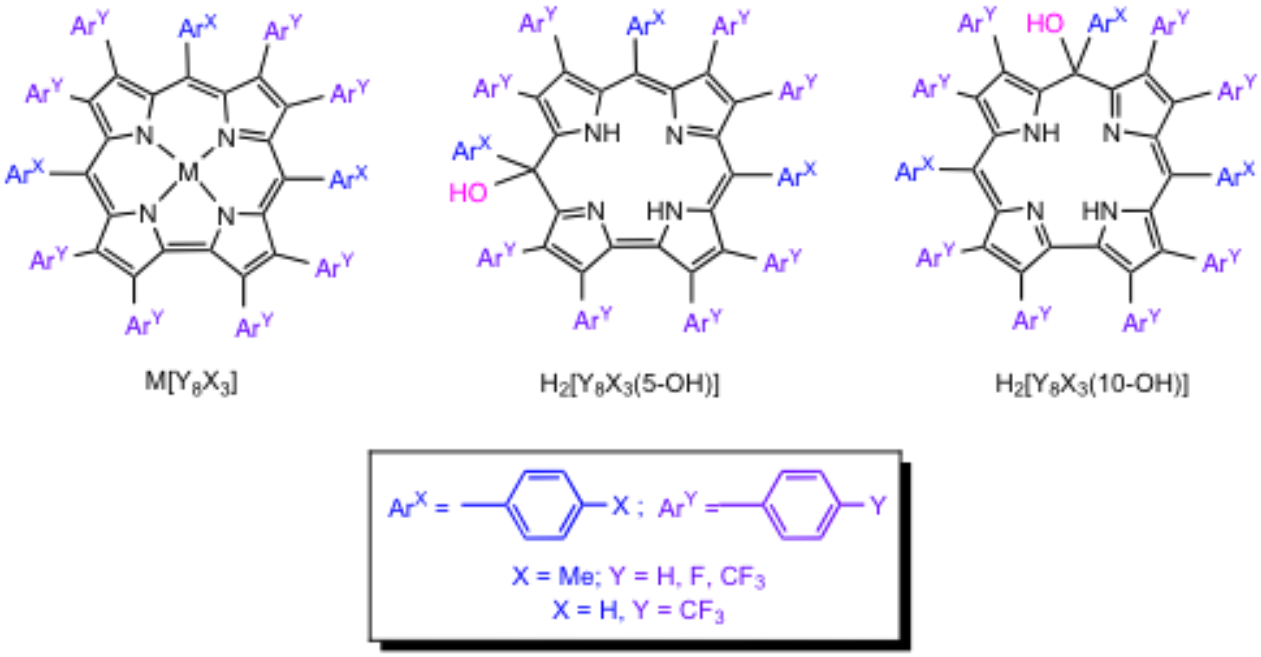

Figure 3. Corrole and Isocorrole derivatives investigated in this study.

Each demetallation led to both 5- and 10-OH isocorroles, with the former dominating. Although not separable by column chromatography, the two regioisomers could be separated by preparative thin-layer chromatography. Except for one case, $H_2[(CF_3)_8Me_3(10\text{-}OH)]$, however, the pure 10-regioisomer was not obtained in large enough quantities for full characterization. Examples of preferential formation of one or the other regioisomer occur in the literature.[21,22,23] Thus, a convenient isocorrole synthesis, involving DDQ oxidation of *meso*-triarylcorroles in methanol, was found to lead preferentially to 5-OMe isocorroles.[18] On the other hand, nonreductive demetallation of $Cu[Br_8H_3]$ (i.e., copper *β*-octabromo-*meso*-triphenylcorrole) with $H_2SO_4/CHCl_3$ led to preferential formation of the 10-OH isocorrole, $H_2[Br_8H_3(10\text{-}OH)]$.[3] A combination of electronic and steric factors is presumably responsible for the preponderance of one isomer over the other.

Literature reports suggest that the oxygen in 5/10-OH isocorroles arises from O_2 rather than water, although the latter has not been strictly ruled out.[22,23] To determine the source of oxygen in the isocorroles obtained in this study, we carried out isotope labeling experiments with $H_2{}^{18}O$ and $^{18}O_2$. The freshly purified, vacuum-dried corrole $H_3[(CF_3)_8Me_3]$, upon stirring in anhydrous dichloromethane and $H_2{}^{18}O$ under argon, showed no evidence of ^{18}O incorporation with electrospray ionization (ESI) mass spectrometry (MS). In contrast, bubbling $^{16}O_2$ into a solution of pure $H_3[(CF_3)_8Me_3]$ in anhydrous dichloromethane revealed the incorporation of both one and two oxygen atoms via ESI-MS. Flushing the ESI mass spectrometer with $^{18}O_2$ also resulted in the incorporation of both one and two ^{18}O atoms into $H_3[(CF_3)_8Me_3]$, confirming the strong affinity of free-base undecaarylcorroles for dioxygen. A plausible pathway for the oxidative decomposition of free-base corroles, based on both literature precedence[22,23,24,25] and our own experiments, is depicted in Figure 4.

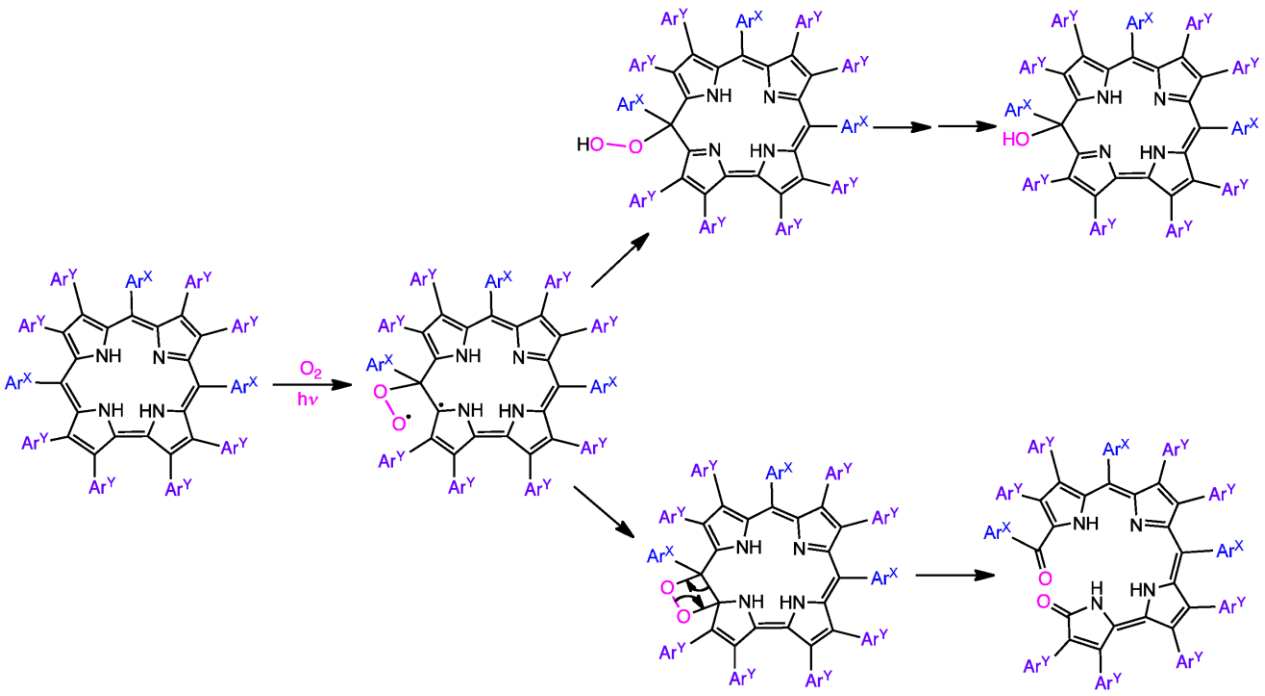

Figure 4. Proposed pathway for photooxygenation of a free-base undecaarylcorrole.

A single-crystal X-ray structure could be obtained for the free-base undecaarylisocorrole $H_2[(CF_3)_8Me_3(5\text{-}OH)]$ (Figure 5, Table 1). Despite the considerable steric crowding, the macrocyclic skeleton of $H_2[(CF_3)_8Me_3(5\text{-}OH)]$ was found to be essentially planar, as for other free-base isocorroles, but in sharp contrast to free-base corroles, which are generally strongly buckled as a result of steric repulsion among the three inner hydrogens.[26] The two central hydrogens could be unambiguously located for $H_2[(CF_3)_8Me_3(5\text{-}OH)]$.

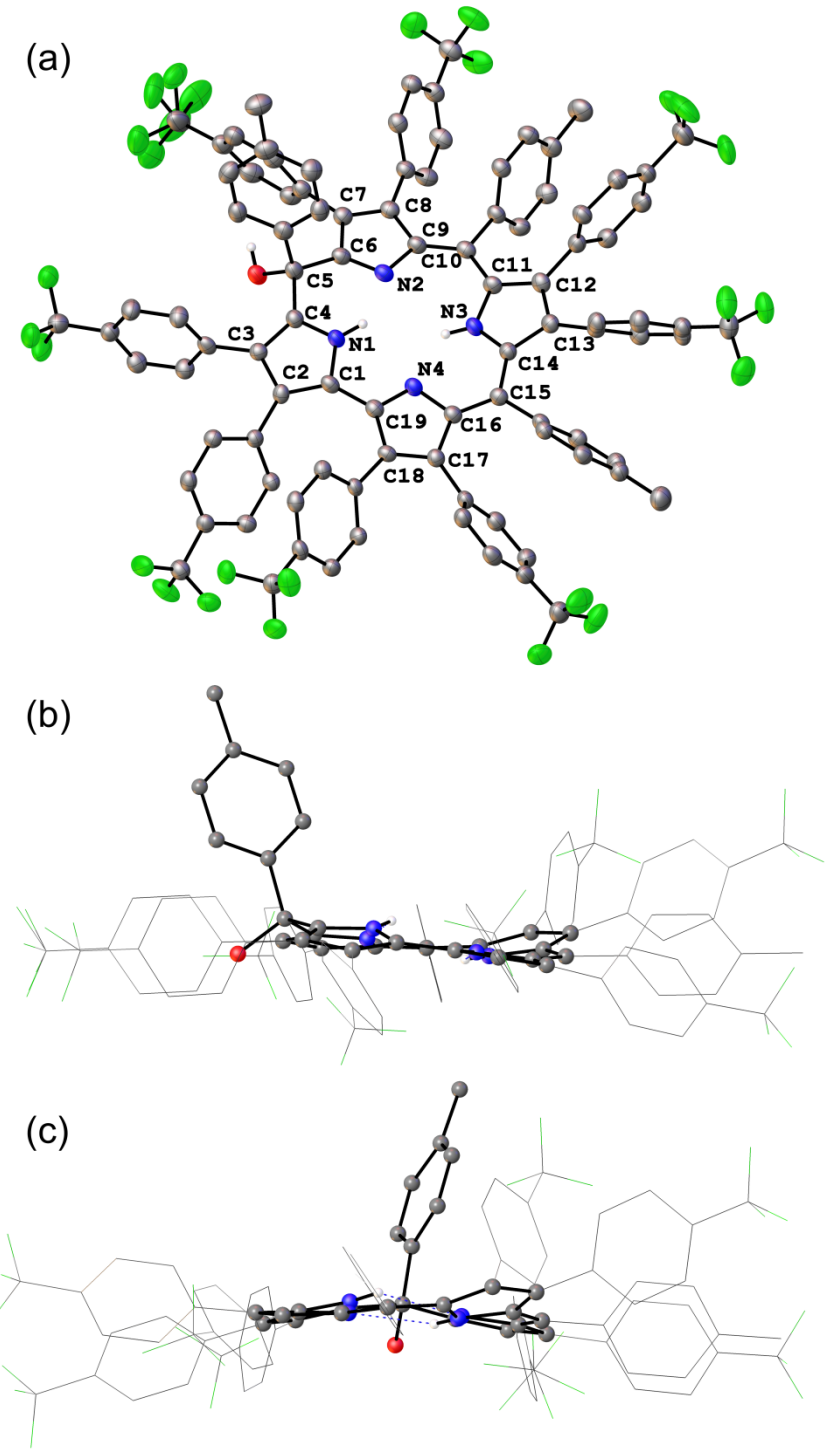

Figure 5. X-ray structure of free-base undecaarylisocorrole $H_2[(CF_3)_8Me_3(5\text{-}OH)]$: (a) top view and (b, c) side views.

Table 1. Crystallographic data for $H_2[(CF_3)_8Me_3(5\text{-}OH)]$.

Sample	$H_2[(CF_3)_8Me_3(5\text{-}OH)]$	$Au[(CF_3)_8H_3]$
Chemical formula	$C_{96}H_{56}F_{24}N_4$	$C_{95}H_{51}F_{24}N_4Cl_4Au$
Formula mass	1737.44	2043.16
Crystal system	Triclinic	Triclinic
Space group	*P* 1	*P* -1
λ (Å)	0.7749	0.7749
a (Å)	12.783(3)	15.4998(6)
b (Å)	18.085(4)	16.8410(6)
c (Å)	18.600(4)	16.9639(6)
α (deg.)	102.363(3)	106.229(2)
β (deg.)	108.203(3)	91.961(2)
γ (deg.)	96.468(3)	106.901(2)
Z	2	2
V ($Å^3$)	3914.7(15)	4035.8(3)
Temperature (K)	100(2)	100(2)
Density (g/cm^3)	1.474	1.681
Measured reflections	40303	78866
Unique reflections	15237	29236
Parameters	1169	1256
Restraints	66	646
R_{int}	0.0670	0.0524
θ range (deg.)	2.587 – 28.553	2.165 – 36.007
R_1, wR_2 all data	0.0683, 0.2226	0.0459, 0.1140
S (GooF) all data	1.024	1.030
Max/min res. Dens. ($e/Å^3$)	0.410/-0.349	2.151/-1.956

(b) Synthesis and molecular structure of a gold undecaarylcorrole. Given the oxidative instability of free-base undecaarylcorroles, we were intrigued by the question whether metal insertion into a free-base undecaarylisocorrole might proceed with concomitant aromatization, thereby providing a pathway to novel metalloundecaarylcorroles. Although a full exploration of this question, involving different isocorroles and metal ions, has not yet been carried out, we were gratified to discover that interaction of free-base $H_3[(CF_3)_8H_3(5\text{-}OH)]$ and gold(III) acetate in pyridine leads to the fully aromatized undecaarylcorrole complex $Au[(CF_3)_8H_3]$ in yields of ~40%.[27,28] We are currently examining the generality of this process and will report on our findings in due course.

Unlike many gold β-octabromocorrole complexes, which tend to be quite insoluble, presumably because of intermolecular metallophilic Au…Br interactions,[27] $Au[(CF_3)_8H_3]$ was

found to be moderately soluble. X-ray quality crystals were obtained and single-crystal structure determination revealed a planar Au-corrole, Au-N distances of 1.941(3)-1.965(3) Å, and no significant nonbonded interactions involving the gold (Figure 6).[29] The planarity of the gold corrole may be contrasted with the strong nonplanarity of copper corroles, which is believed to be due to ligand noninnocence. Silver corroles exhibit more variable behavior in this regard. Thus, whereas simple silver *meso*-triarylcorroles are only slightly saddled, a recent X-ray structure has provided an example of a strongly saddled silver *β*-octabromocorrole.[30] The substantial variations in corrole geometry in the silver case has been attributed to variations in noninnocent character among the different ligands. By contrast, corrole ligands in gold corroles are thought to be innocent.

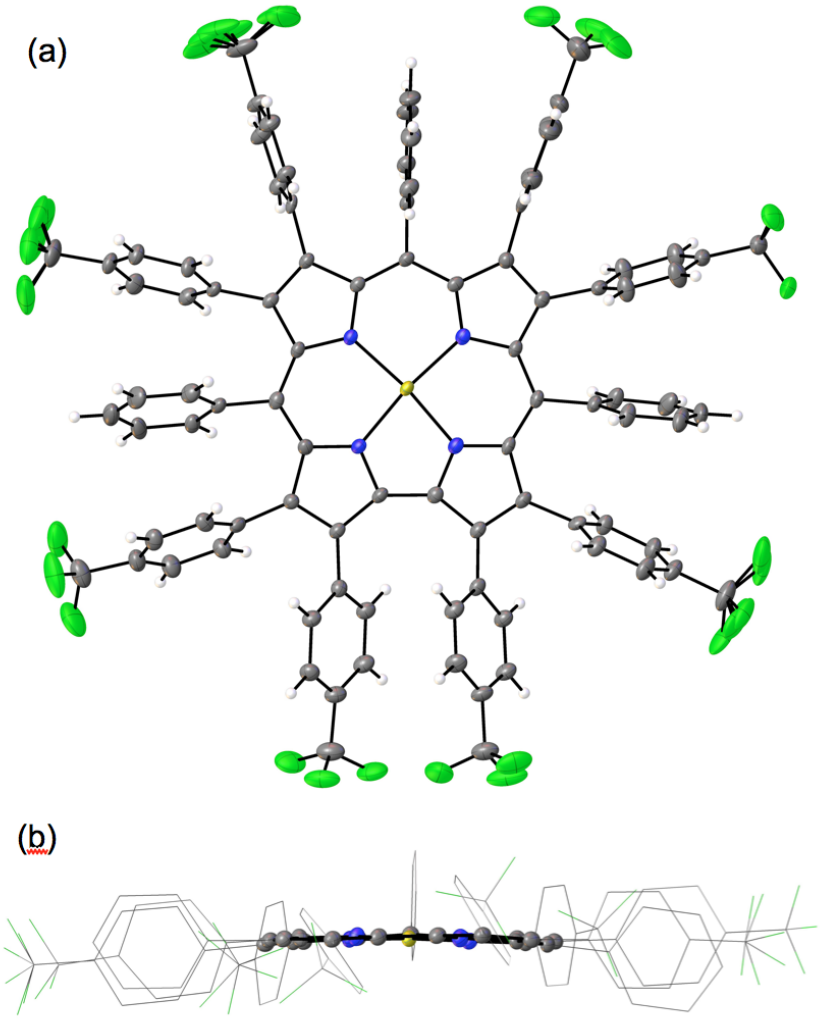

Figure 6. X-ray structure of the gold undecaarylcorrole Au[$(CF_3)_8H_3$]: (a) top view and (b) side view.

Conclusion

In summary, copper undecaarylcorroles were found to demetallate with unusual ease under standard reductive demetallation conditions. The free-base undecaarylcorroles, however, proved to be light- and oxygen-sensitive, readily oxidizing to biliverdines and 5/10-OH isocorroles. Nonreductive conditions could be devised that led to good yields 65-80% of 5/10-OH undecaarylisocorroles, a new class of sterically hindered and relatively stable macrocyclic ligands. Interaction of one such ligand with gold(III) acetate resulted in rearomatization of the macrocycle and a gold undecaarylcorrole, which proved amenable to single-crystal X-ray diffraction analysis. Unlike the rather insoluble gold *β*-octabromo-*meso*-triarylcorroles, the gold undecaarylcorrole was found to be moderately soluble in organic solvents. The relatively high solubility appears to be related to the lack of intermolecular aurophilic and metallophilic interactions involving the gold atom.

Experimental section

Materials. All reagents and solvents were used as purchased unless stated otherwise. Anhydrous toluene (Sigma-aldrich) was stored over pre-activated 3 Å molecular sieves. Silica gel 150 (35-70 μm particle size, Davisil) was used for flash chromatography and silica gel 60 plates (20 × 20 cm; 0.5 mm thick, Merck) were used for preparative thin-layer chromatography (PLC). Copper *β*-octabromo-*meso*-tris(4-methylphenyl)corrole, Cu[Br_8Me_3] and copper *β*-octabromo-*meso*-triphenylcorrole, Cu[Br_8H_3], served as the starting materials for copper undecaarylcorroles and were synthesized as previously described.[31] Copper *β*-octakis(*p*-trifluoromethylphenyl)-*meso*-triphenylcorrole], Cu[$(CF_3)_8H_3$], was also synthesized according to a literature method.[11]

Instrumentation. Ultraviolet-visible (UV-vis) spectra were recorded with CH_2Cl_2 as solvent on an HP 8453 spectrophotometer. ^{1}H NMR spectra were obtained at 298 K on either a Mercury Plus Varian spectrometer (400 MHz) in $CDCl_3$ (referenced to 7.26 ppm), in CD_2Cl_2 (referenced to 5.30 ppm), and in C_6D_6 (referenced to 7.20 ppm) or a Varian Inova spectrometer (600MHz) equipped with a cryogenically cooled inverse triple-resonance probe in 1,1,2,2-tetrachloroethane-*d*$_2$ ($CDCl_2$-$CDCl_2$, referenced to 5.91ppm). ^{19}F NMR spectra (376 MHz) were recorded at 298-333K on a Mercury Plus Varian spectrometer and referenced to 2,2,2-trifluoroethanol-*d*$_3$ (δ= -77.8 ppm). Electrospray ionization mass spectra were recorded on an LTQ Orbitrap XL spectrometer.

General Procedure for the Synthesis of Copper Undecaarylcorroles. The syntheses were carried essentially according to the procedure reported by Ghosh and coworkers. Into a 50-mL three-necked round-bottomed flask equipped with a magnetic stirring bar and a reflux condenser were introduced Cu[Br_8Me_3], the arylboronic acid of choice (40 equiv), potassium carbonate (40 equiv), and $Pd_2(dba)_3{\cdot}CHCl_3$ (0.1 equiv). After degassing with argon, dry toluene (10 mL) was added. After purging with argon for 10 min, the suspension was stirred at 100−105 °C under argon for 1−2 days. Progress of the reaction was monitored by mass spectrometry. When product formation appeared to have stabilized, the reaction mixture was cooled to room temperature, diluted with 10 mL of CH_2Cl_2, and washed with saturated aqueous $NaHCO_3$ and then with distilled water. The CH_2Cl_2 phase was dried with anhydrous Na_2SO_4, filtered, and evaporated. The brown residue obtained was chromatographed on a silica gel column with hexane/CH_2Cl_2 as eluent. The product eluted as a dark brown band, which was collected and evaporated to dryness. The residue was purified by preparative thin-layer chromatography (PLC), as detailed below for each corrole.

Synthesis of Copper 2,3,7,8,12,13,17,18-octakis(4-fluorophenyl)-*meso*-tris(*p*-methylphenyl)corrole, Cu[F_8Me_3]. The reaction employed 0.025 mol (32 mg) of Cu[Br_8TMePC] and was complete after ~2 days (45 h). Both the column chromatography and subsequent PLC were carried out with 3:1 hexane/CH_2Cl_2 as eluent. The pure product Cu[F_8Me_3] (26.6 mg, 76%) eluted as the most intense brown band. UV-vis (CH_2Cl_2): λ_{max}, nm (ε x 10^{-4}, M^{-1} cm^{-1}): 448 (3.56), 644 (0.32). ^{1}H NMR ($CDCl_3$, 400 MHz, δ in ppm): δ 6.87 (d, *J*=8.0 Hz, 2H, 10-*o*, 4-CH_3Ph), 6.80-6.74 (m, 4H, 2,18-*o*, 4-FPh; 4H, 5,15-*o*, 4-CH_3Ph), 6.57-6.51 (m, 4H, 3,17-*o*, 4-FPh; 4H, 2,18-*m*, 4-FPh), 6.47-6.26 (m, 4H, 8,12-*o*, 4-FPh; 4H, 7,13-*o*, 4-FPh; 4H, 3,17-*m*, 4-FPh; 4H, 5,15-*m*, 4-CH_3Ph; 4H, 7,13-*m*, 4-FPh; 4H, 8,12-*m*, 4-FPh; 2H, 10-*m*, 4-CH_3Ph), 2.02 (s, 6H, 5,15-*p*, 4-CH_3Ph), 1.91 (s, 3H, 10-*p*, 4- CH_3Ph). ^{19}F NMR ($CDCl_3$): δ -116.31 to -116.39 (m, 2F), -118.08 to -118.21 (m, 4F), -118.62 to -118.70 (m, 2F). MS (HR-ESI major isotopomer): M^+ = 1380.34 (expt), 1380.34 (calcd).

Synthesis of Copper 2,3,7,8,12,13,17,18-Octakis(4-trifluoromethylphenyl)-5,10,15-tris(4-methylphenyl)corrole, Cu[$(CF_3)_8Me_3$]. The reaction employed 0.020 mol (25 mg) of Cu[Br_8TMePC] and was complete after 24 h. Both the column chromatography and subsequent PLC were carried out with 3:1 hexane/CH_2Cl_2 as eluent. The pure product Cu[$(CF_3)_8Me_3$] (18.4 mg, 52%) eluted as the most intense brown band. UV-vis (CH_2Cl_2): λ_{max}, nm (ε x 10^{-4}, M^{-1} cm^{-1}): 454 (4.34), 642 (0.44), 841 (0.59). ^{1}H NMR ($CDCl_3$, 600 MHz, δ in ppm): δ 7.09 (d, *J*=4.0 Hz,

4H, 2,18-*o*, 4-CF_3Ph), 6.97 (d, *J*=4.0 Hz, 4H, 2,18-*m*, 4-CF_3Ph), 6.94 (d, *J*=4.0 Hz, 4H, 3,17-*o*, 4-CF_3Ph), 6.89 (d, *J*=4.0 Hz, 4H, 7,13-*o*, 4-CF_3Ph), 6.85 (d, *J*=4.0 Hz, 4H, 8,12-*o*, 4-CF_3Ph), 6.81 (d, *J*=8.0 Hz, 2H, 10-*o*, 4-CH_3Ph), 6.75 (d, *J*=4.0 Hz, 4H, 3,17-*m*, 4-CF_3Ph), 6.69 (d, *J*=8.0 Hz, 4H, 5,15-*o*, 4-CH_3Ph), 6.62 (d, *J*=8.0 Hz, 8H, 7,8,12,13-*m*, 4-CF_3Ph), 6.25 (d, *J*=4.0 Hz, 4H, 5,15-*m*, 4-CH_3Ph), 6.19 (d, *J*=8.0 Hz, 2H, 10-*m*, 4-CH_3Ph), 1.93 (s, 6H, 5,15-*p*, 4-CH_3Ph), 1.82 (s, 3H, 10-*p*, 4-CH_3Ph). ^{19}F NMR ($CDCl_3$): δ -63.07 (s, 6F), -63.17 (s, 6F), -63.29 (s, 6F), -63.46 (s, 6F). MS (HR-ESI major isotopomer): M^+= 1780.31 (expt), 1780.32 (calcd).

Synthesis of Copper 2,3,7,8,12,13,17,18-octaphenyl-5,10,15-tris(4-methylphenyl)corrole, Cu[H_8Me_3]. The reaction employed 0.021 mol (27 mg) of Cu[Br_8TMePC] and was complete after 48 h. Column chromatography was carried out with hexane/CH_2Cl_2 as eluent, while 3:1 *n*-hexane/CH_2Cl_2 was used for the PLC. The pure product Cu[H_8Me_3] (12.1 mg, 46%) eluted as the most intense brown band. UV-vis (CH_2Cl_2): λ_{max}, nm (ε x 10^{-4}, M^{-1} cm^{-1}): 448 (6.17), 544 (0.77), 645 (0.49). ^{1}H NMR (CD_2Cl_2, 600 MHz, δ in ppm): δ 6.86 (d, *J*=8.4 Hz, 2H, 10-*o*, 4-CH_3Ph), 6.85-6.82 (m, 4H, 2,18-*o*, Ph; 2H, 2,18-*p*, Ph), 6.80-6.76 (m, 4H, 2,18-*m*, Ph), 6.74 (d, *J*=7.8 Hz, 4H, 5,15-*o*, 4-CH_3Ph), 6.72-6.68 (m, 2H, 3,17-*p*, Ph), 6.65-6.63 (m, 4H, 3,17-*o*, Ph; 4H, 3,17-*m*, Ph), 6.62-6.58 (m, 2H, 7,13-*p*, Ph; 4H, 7,13-*m*, Ph), 6.58-6.57 (m, 2H, 8,12-*p*, Ph), 6.57-6.54 (m, 4H, 8,12-*m*, Ph; 4H, 8,12-*o*, Ph), 6.54-6.52 (m, 4H, 7,13-*o*, Ph), 6.19 (d, *J*=7.2 Hz, 4H, 5,15-*m*, 4-CH_3Ph), 6.16 (d, *J*=7.8 Hz, 2H, 10-*m*, 4-CH_3Ph), 1.90 (s, 6H, 5,15-*p*, 4-CH_3Ph), 1.80 (s, 3H, 10-*p*, 4- CH_3Ph). MS (HR-ESI major isotopomer): M^+= 1237.42 (expt), 1237.42 (calcd).

Undecaarylisocorrole H_2[F_8Me_3(5-OH)]. Into a 50 mL round-bottomed flask was placed 25 mg (0.018 mmol) of Cu[F_8Me_3] and dissolved in 3 mL of CH_2Cl_2. Subsequently, 3 mL of concentrated H_2SO_4 (95-97%, Merck) was added. The mixture was then stirred and sonicated at room temperature. Progress of the reaction was monitored by ESI mass spectrometry. After 2 h, the reaction mixture was carefully poured into 300 mL of distilled H_2O and then extracted with $CHCl_3$. The organic phase was washed once with distilled water and twice with saturated aqueous $NaHCO_3$. Upon washing with $NaHCO_3$, the color of the organic phase changed from brown to green. The organic phase was then dried with anhydrous Na_2SO_4, filtered, and the filtrate rotary-evaporated to dryness. The residue obtained was chromatographed on a silica gel column with CH_2Cl_2/1%-MeOH. The product was further purified by PLC with 2:3 *n*-hexane/CH_2Cl_2; upon completion of the PLC, the pure product H_2[F_8Me_3(5-OH)] (14.4 mg, 60%) was obtained as the most intense green band in the middle of the plate. UV-vis (CH_2Cl_2): λ_{max}, nm (ε x 10^{-4}, M^{-1} cm^{-}

^{1}): 433 (3.37), 683 (0.69). ^{1}H NMR (C_6D_6, 600 MHz, δ in ppm): δ 8.05 (d, *J* = 8.1 Hz, 2H, 5-*o*, 4-CH_3Ph), 7.01 (d, *J* = 8.3 Hz, 2H, 5-*m*, 4-FPh), 6.81 (d, *J* = 8.1 Hz, 1H, 10-*o*, 4-CH_3Ph), 6.80 (d, *J* = 8.6 Hz, 2H, 3-*o*, 4-FPh), 6.70 (d, *J* = 8.0 Hz, 1H, 7-*o*, 4-FPh), 6.69 (t, *J* = 7.6 Hz, 1H, 7-*m*, 4-FPh), 6,60 (d, *J* = 8.6 Hz, 2H, 2-*o*, 4-FPh), 6.55 (t, *J* = 8.5 Hz, 2H, 3-*m*, 4-FPh), 6.44 (overlapping, 1H, 7-*o*, 4-FPh), 6.42 (o, 12-*o*, 4-FPh), 6.36 (o, 1H, 7-*m*, 4-FPh), 6.33 (o, 1H, 10-*m*, 4-CH_3Ph), 6.29 (o, 1H, 8-*m*, 4-FPh), 6.25 (t, *J* = 8.8 Hz, 2H, 2-*m*, 4-FPh), 6.20 (o, 1H, 8-*o*, 4-FPh), 6.11 (o, 1H, 8-*m*, 4-FPh), 6.07 (d, *J* = 8.4 Hz, 1H, 10-*o*, 4-CH_3Ph), 6.02 (t, *J* = 8.5 Hz, 0.5H, 12-*m*, 4-FPh), 5.65 (d, *J* = 7.8 Hz, 1H, 10-*m*, 4-CH_3Ph), 2.29 (s, 1H, -OH), 2.05 (s, 3H, 5-*p*, 4-CH_3Ph), 1.86 (s, 3H, 15-*p*, 4-CH_3Ph), 1.72 (s, 3H, 10-*p*, 4-CH_3Ph). ^{19}F NMR ($CDCl_3$): δ -115.96 to -116.08 (m, 1F), -116.25 to -116.36 (m, 1F), -116.45 to -116.59 (m, 1F), -117.38 to -117.49 (m, 1F), -117.79 to -117.88 (m, 1F), -117.95 to -118.09 (m, 2F), -118.25 to -118.35 (m, 1F). MS (HR-ESI major isotopomer): M^+ = 1337.44 (expt), 1337.44 (calcd).

Undecaarylisocorroles H_2[$(CF_3)_8Me_3$(5-OH)] and H_2[$(CF_3)_8Me_3$(10-OH)]. Into a 50 mL round-bottomed flask, 20 mg (0.0112 mmol) of Cu[$(CF_3)_8Me_3$] was added and dissolved in 4 mL of CH_2Cl_2. Subsequently, 2 mL of concentrated H_2SO_4 (95-97%, Merck) was added. The mixture was stirred and sonicated at room temperature. The progress of the reaction was monitored by ESI mass spectrometry. After 4 hours the reaction was quenched by pouring the mixture into 300 mL distilled H_2O and then extracted with $CHCl_3$. The brown organic phase was washed once with distilled water and once with saturated aqueous $NaHCO_3$. Upon washing with $NaHCO_3$ the color of organic phase changed from brown to green. The organic phase was dried with anhydrous Na_2SO_4, filtered and evaporated under vacuum. The residue obtained was chromatographed on a silica gel column with 2:1 *n*-hexane/CH_2Cl_2. The product was further purified by PLC with 2:1 *n*-hexane/CH_2Cl_2. The most intense green band in the middle of the plate was pure H_2[$(CF_3)_8Me_3$ (5-OH)] (11 mg, 57%) and the most intense light-green band below that was H_2[$(CF_3)_8Me_3$(10-OH)] (3.7 mg, 19%). X-ray quality crystals of H_2[$(CF_3)_8Me_3$(5-OH)] were grown by slow diffusion of *n*-heptane into the benzene solution. Analytical data for the two isomers are as follows.

Undecaarylisocorrole H_2[$(CF_3)_8Me_3$(5-OH)]. UV-vis (CH_2Cl_2): λ_{max}, nm (ε x 10^{-4}, M^{-1} cm^{-1}): 435 (4.19), 683 (0.92). ^{1}H NMR (C_6D_6, 600 MHz, δ in ppm): δ 7.95 (d, *J* = 8.0 Hz, 2H, 5-*o*, 4-CH_3Ph), 7.22 (d, *J* = 8.0 Hz, 1H, 7-*m*, 4-CF_3Ph), 7.05 (d, *J* = 8.0 Hz, 2H, 3-*m*, 4-CF_3Ph), 7.03 (d, *J* = 8.1 Hz, 2H, 5-*m*, 4-CH_3Ph), 6.87 (d, *J* = 7.9 Hz, 2H, 3-*o*, 4-CF_3Ph), 6.75 (d, *J* = 8.4 Hz, 1H, 7-*m*, 4-CF_3Ph), 6.72 (d, *J* = 8.0 Hz, 1H, 7-*o*, 4-CF_3Ph), 6.68 (o, 1H, 10-*o*, 4-CH_3Ph), 6.61 (d,

J = 8.6 Hz, 1H, 8-*m*, 4-CF_3Ph), 6.61 (o, 2H, 12-*m*, 4-CF_3Ph), 6.61 (o, 1H, 15-*m*, 4-CH_3Ph), 6.6 (o, 2H, 2-*m*, 4-CF_3Ph), 6.6 (o, 2H, 2-*o*, 4-CF_3Ph), 6.57 (o, 1H, 15-*m*, 4-CH_3Ph), 6.53 (d, *J* = 8.2 Hz, 1H, 8-*m*, 4-CF_3Ph), 6.44 (d, *J* = 8.4 Hz, 1H, 7-*o*, 4-CF_3Ph), 6.37 (broad, 1H, 15-*o*, 4-CH_3Ph), 6.35 (d, *J* = 8.6 Hz, 1H, 8-*o*, 4-CF_3Ph), 6.26 (b, 1H, 15-*o*, 4-CH_3Ph), 6.17 (d, *J* = 7.9 Hz, 1H, 10-*m*, 4-CH_3Ph), 6.13 (d, *J* = 8.2 Hz, 1H, 8-*o*, 4-CF_3Ph), 5.93 (d, *J* = 7.8 Hz, 1H, 10-*o*, 4-CH_3Ph), 5.48 (d, *J* = 7.8 Hz, 1H, 10-*m*, 4-CH_3Ph), 2.07 (s, 3H, 5-*p*, 4-CH_3Ph), 1.97 (s, 1H, -OH), 1.86 (s, 3H, 15-*p*, 4-CH_3Ph), 1.68 (s, 3H, 10-*p*, 4-CH_3Ph). ^{19}F NMR (C_6D_6, 60°C): δ -62.58 (s, 3F), -62.72 (s, 9F), -62.88 (s, 3F), -62.95 (s, 3F), -63.06 (s, 3F), -63.32 (s, 3F). MS (HR-ESI major isotopomer): M^+ = 1738.42 (expt), 1738.42 (calcd).

Undecaarylisocorrole H_2[$(CF_3)_8Me_3$(10-OH)]. UV-vis (CH_2Cl_2): λ_{max}, nm (ε x 10^{-4}, M^{-1} cm^{-1}): 458 (1.86), 658 (0.26). ^{1}H NMR (C_6D_6, 600 MHz, δ in ppm): δ 7.46 (d, *J* = 8.3 Hz, 2H, 10-*o*, 4-CH_3Ph), 6.95 (d, *J* = 8.1 Hz, 4H, 12-*m*, 4-CF_3Ph), 6.80 (d, *J* = 8.2 Hz, 4H, 18-*m*, 4-CF_3Ph), 6.77 (d, *J* = 8.1 Hz, 2H, 10-*m*, 4-CH_3Ph), 6.72 (d, *J* = 8.3 Hz, 4H, 18-*o*, 4-CF_3Ph), 6.68 (d, *J* = 8.0 Hz, 4H, 17-*m*, 4-CF_3Ph), 6.68 (b, 12-*o*, 4-CF_3Ph), 6.62 (d, *J* = 8.0 Hz, 4H, 13-*m*, 4-CF_3Ph), 6.40 (d, *J* = 7.9 Hz, 4H, 17-*o*, 4-CF_3Ph), 6.30 (d, *J* = 8.0 Hz, 4H, 13-*o*, 4-CF_3Ph), 6.28 (d, *J* = 7.9 Hz, 4H, 15-*o*, 4-CH_3Ph), 5.86 (d, *J* = 7.8 Hz, 4H, 15-*m*, 4-CH_3Ph), 2.39 (s, 1H, -OH), 1.98 (s, 3H, 10-*p*, 4-CH_3Ph), 1.80 (s, 6H, 5,15-*p*, 4-CH_3Ph). ^{19}F NMR ($CDCl_3$): δ -63.06 (s, 6F), -63.15 (s, 6F), -63.19 (s, 6F), -63.54 (s, 6F). MS (HR-ESI major isotopomer): M^+= 1738.42 (expt), 1738.42 (calcd).

Single-crystal X-ray diffraction analysis of Undecaarylisocorrole H_2[$(CF_3)_8Me_3$(5-OH)]. X-ray data for H_2[$(CF_3)_8Me_3$(5-OH)] were collected on beamline 11.3.1 at the Advanced Light Source, Lawrence Berkeley National Laboratory. Samples were mounted on MiTeGen® kapton loops and placed in a 100(2) K nitrogen cold stream provided by an Oxford Cryostream 700 Plus low temperature apparatus on the goniometer head of a Bruker D8 diffractometer equipped with a APEX-II CCD detector. Diffraction data were collected with synchrotron radiation monochromated using silicon(111) to a wavelength of 0.7749(1)Å. An approximate full-sphere of data was collected using a ω scans with scan rates of 3 seconds per 0.5 degree with 2θ = -36°. The structures were solved by intrinsic phasing (SHELXT) and refined by full-matrix least squares on F^2 (SHELXL-2014). All non-hydrogen atoms were refined anisotropically. Hydrogen atoms were geometrically calculated and refined as riding atoms. The hydrogen atoms on the nitrogen and oxygen atoms were found in the Fourier difference map and allowed to ride on their respective N or O atoms. Additional crystallographic information has been summarized in Table

1 and full details can be found in the crystallographic information file provided in the Supplementary Information.

Undecaarylisocorrole $H_2[H_8Me_3(5\text{-}OH)]$. Into a 50 mL round-bottomed flask, 12 mg (0.0097 mmol) of $Cu[H_8Me_3]$ was added and dissolved in 2 mL of CH_2Cl_2. Subsequently, 2 mL of concentrated H_2SO_4 (95-97%, Merck) was added. The mixture was stirred and sonicated at room temperature. The progress of the reaction was monitored by ESI mass spectrometry. After 2 hours the reaction was quenched by pouring the mixture into 300 mL distilled H_2O and then extracted with $CHCl_3$. The brown organic phase was washed once with distilled water and once with saturated aqueous $NaHCO_3$. Upon washing with $NaHCO_3$ the color of organic phase changed from brown to green. The organic phase was dried with anhydrous Na_2SO_4, filtered and evaporated under vacuum. The residue obtained was chromatographed on a silica gel column with CH_2Cl_2/5%-MeOH. The product was further purified by PLC with 1:2 *n*-hexane/CH_2Cl_2. The olive-green band at the bottom of the plate was pure $H_2[H_8Me_3(5\text{-}OH)]$. Yield: 5.6 mg, 48%. UV-vis (CH_2Cl_2): λ_{max}, nm (ε x 10^{-4}, M^{-1} cm^{-1}): 439 (0.69), 689 (0.15). ^1H NMR (C_6D_6, 600 MHz, δ in ppm): δ 8.22 (d, *J* = 7.8 Hz, 2H, 5-*o*, 4-CH_3Ph), 7.07 (d, *J* = 7.2 Hz, 2H, 3-*o*, Ph), 7.04 (d, *J* = 8.1 Hz, 2H, 5-*m*, 4-CH_3Ph), 7.03 (o, 7-*o*, Ph), 7.0 (b, 1H, 10-*o*, 4-CH_3Ph), 6.94 (d, *J* = 7.2 Hz, 2H, 2-*o*, Ph), 6.94 (o, 7-*p*, Ph), 6.86 (t, *J* = 7.5 Hz, 2H, 3-*m*, Ph), 6.81 (d, *J* = 7.2 Hz, 1H, 3-*p*, Ph), 6.77 (o, 7-*m*, Ph), 6.73 (o, 7-*m*, Ph), 6.66 (o, 7-*o*, Ph), 6.56 (t, *J* = 6.8 Hz, 2H, 2-*m*, Ph), 6.56 (o, 15-*o*, 4-CH_3Ph), 6.55 (o, 8-*m*, Ph), 6.51 (12-*m*, Ph), 6.48 (o, 15-*m*, 4-CH_3Ph), 6.43 (o, 8-*m*, Ph), 6.37 (b, 1H, 10-*m*, 4-CH_3Ph), 6.23 (b, 1H, 10-*o*, 4-CH_3Ph), 5.56 (b, 1H, 10-*m*, 4-CH_3Ph), 2.52 (s, 1H, -OH), 2.08 (s, 3H, 5-*p*, 4-CH_3Ph), 1.82 (s, 3H, 15-*p*, 4-CH_3Ph), 1.68 (s, 3H, 10-*p*, 4-CH_3Ph). MS (HR-ESI major isotopomer): M^+= 1193.52 (expt), 1193.52 (calcd).

Undecaarylisocorrole $H_2[(CF_3)_8H_3(5\text{-}OH)]$. To a solution of $Cu[(CF_3)_8H_3]$ (25 mg, 0.014 mmol) in CH_2Cl_2 (7.0 mL) was added dropwise 1 mL H_2SO_4 (95-97%) and the resulting suspension was stirred for 30 min. The mixture was poured into cold, distilled water and extracted with CH_2Cl_2. The green organic phase was washed once with distilled H_2O and once with saturated aqueous $NaHCO_3$, dried with anhydrous Na_2SO_4, and filtered. After concentration to a minimum volume, the organic phase was chromatographed on a silica gel column with 1:1 hexane/CH_2Cl_2, whereupon the isocorrole isomers eluted as a green band. PLC with 3:2 hexane/CH_2Cl_2 yielded the 5-OH-isocorrole (17mg, 0.01, 71.6%) as the first intense green band. Free base $H_3[(CF_3)_8H_3]$ (1.8 mg, 7%) followed as a second, thinner green band, closely followed by a third, bright green band containing the 10-OH-isocorrole (2.5 mg, 11%). The latter two

products were not fully characterized because of the small quantities obtained so analytical data are only reported for the 5-OH isomer. UV-Vis (CH_2Cl_2): λ_{max}, nm (ε x 10^{-4}, $M^{-1}cm^{-1}$): 433 (4.30), 681 (0.98). ^{1}H NMR (C_6D_6): δ 8.0 (d, 2H, 5-*o*, Ph), 7.20 (m, 1H, 7-*m*, 4-CF_3Ph), 7.15 (t, 2H, 5-*m*, Ph); 7.05 - 7.0 (m , 3H, *5-p*, Ph and 3-*m*, 4-CF_3Ph), 6.82 (d, 2H, 3-*o*, 4-CF_3Ph), 6.75 (d, 1H, 10-*o*, Ph), 6.75- 6.56 {m, 7-*m* (1H, 4-CF_3Ph), 2-*o*, *m* (4H, 4-CF_3Ph), 8-*m* (1H, 4-CF_3Ph), 7-*o* (1H, 4-CF_3Ph), 15-*m* (2H, Ph)}, 6.54 (d, 1H, 8-*m*, 4-CF_3Ph), 6.42 (d, 1H, 7-*o*, 4-CF_3Ph), 6.40 – 6.25 {m, 15-*p* (1H, Ph), 10-*m* (1H, Ph), 8-*o* (2H, 4-CF_3Ph), 15-*o* (2H, Ph)}, 6.20 (t, 1H, 10-*p*, Ph), 6.10 (d, 1H, 8-*o*, 4-CF_3Ph), 6.0 (d, 1H, 10-*o*, Ph), 5.65 (t, 1H, 10-*m*, Ph). ^{19}F NMR $(C_6D_6)_2$: δ -62.88 (s, 3F), -63.02 (s, 3F), -63.41 to -63.46 (m, 3F), -63.48 (s, 6F), -63.53 (s, 3F), -63.61 (s, 3F), -63.71 to -63.76 (m, 3F). HRMS (ESI^+, major isotopomer): $[M + H]^+$ = 1696.3692 (expt), 1696.3708 (calcd). Elemental analysis. Found (calcd) : C, 65.86 (65.88); H, 3.20 (2.97), N, 3.27 (3.30).

Synthesis of gold *β*-octakis(*p*-trifluoromethylphenyl)-*meso*-triphenylcorrole, $Au[(CF_3)_8H_3]$. Gold(III) acetate (11 mg, 5 equiv) was added to a green solution of a mixture of the isomeric isocorroles $H_2[(CF_3)_8H_3$(5/10-OH)] (15 mg, 0.009mmol) pyridine (5.0 mL). After overnight stirring, the resulting reddish-brown suspension was evaporated and the residue eluted through silica gel with 7:3 hexane/CH_2Cl_2, yielding the gold undecaarylcorrole as the first red band (7 mg, 41.5%). Vapour diffusion of hexane into a CH_2Cl_2 solution yielded tiny rectangular needles of x-ray quality in approximately a month. UV-Vis (CH_2Cl_2): λ_{max}, nm (ε x 10^{-4}, $M^{-1}cm^{-1}$): 434 (6.08), 544 (0.58). 580 (2.0). ^{1}H NMR (600 MHz, $(CDCl_2)_2$): δ 7.29 (d, *J* = 8.2 Hz, 4H, 2,18-*o*,4-CF_3Ph), 7.15 (d, 4H, 5, 15-*o*, Ph), 7.09 (d, 2H, 10-*o*, Ph), 7.05 (d, *J* = 8.1 Hz, 4H, 3,17-*o*, 4-CF_3Ph), 7.02 (d, *J* = 8.1 Hz, 4H, 2,18-*m*,4-CF_3Ph), 6.96 (d, *J* = 7.9 Hz, 4H, 3,17-*m*, 4-CF_3Ph), 6.93 – 6.89 (m, 8H, 7, 8, 12,13-*m*, 4-CF_3Ph), 6.87 (d, *J* = 8.0 Hz, 4H, 7,13-*o*, 4-CF_3Ph), 6.82 (d, *J* = 7.9 Hz, 4H, 8,12-*o*, 4-CF_3Ph), 6.74 (t, *J* = 7.7 Hz, 2H, 5,15-*p*, Ph), 6.65 (t, *J* = 7.6 Hz, 1H, 10-*p*, Ph), 6.49 (t, *J* = 7.7 Hz, 4H, 5,15-*m*, Ph), 6.41 (t, *J* = 7.7 Hz, 2H, 10-*m*, Ph). ^{19}F NMR ($CDCl_3$): δ -63.31 (s, 12F); -63.42 (s, 6F); -63.49 (s, 6F). HRMS (ESI^+, major isotopomer): $[M]^+$ = 1873.3112 (expt), 1873.3110 (calcd). Elemental analysis. Found (calcd) : C, 59.90 (59.63); H, 2.77 (2.53), N, 3.11 (2.99).

Single-crystal X-ray diffraction analysis of the gold undecaarylcorrole $Au[(CF_3)_8H_3]$. X-ray data for $Au[(CF_3)_8H_3]$ were collected on beamline 11.3.1 at the Advanced Light Source, Lawrence Berkeley National Laboratory. A red tablet with dimensions 50 x 40 x 15 μm^3 was mounted on a MiTeGen® kapton loop and placed in a 100(2) K nitrogen cold stream provided by an Oxford Cryostream 700 Plus low temperature apparatus on the goniometer head of a Bruker

D8 diffractometer equipped with a PHOTON100 CMOS detector operating in shutterless mode. Diffraction data were collected with synchrotron radiation monochromated using silicon(111) to a wavelength of 0.7749(1) Å. An approximate full-sphere of data was collected using a combination of ϕ and ω scans with scan speeds of 1 second per degree for the ϕ scans, and 1 and 3 seconds per degree for the ω scans at 2θ = 0 and -45°, respectively. The structures were solved by intrinsic phasing (SHELXT) and refined by full-matrix least squares on F^2 (SHELXL-2014). All non-hydrogen atoms were refined anisotropically. Hydrogen atoms were geometrically calculated and refined as riding atoms. Additional crystallographic information has been summarized in Table 1 and full details can be found in the crystallographic information file provided in the Supporting Information.

Supporting information. UV-vis, ^{1}H NMR, and high-resolution mass spectra (42 pages); crystallographic information files for $H_2[(CF_3)_8Me_3(5\text{-}OH)]$ and $Au[(CF_3)_8H_3]$.

Acknowledgement. This work was supported by the of the Research Council of Norway (FRINATEK project 231086, AG) and the Advanced Light Source, Berkeley, California (CMB, KJG). The Advanced Light Source is supported by the Director, Office of Science, Office of Basic Energy Sciences, of the U.S. Department of Energy under Contract No. DE-AC02-05CH11231.

References

[1] For a review on applications of corroles, see: I. Aviv-Harel, Z. Gross, Chem. Eur. J. 15 (2009) 8382–8394.

[2] For more specialized reviews on metallocorroles, see:

(a) K. E. Thomas, A. B. Alemayehu, J. Conradie, C. M. Beavers, A. Ghosh, Acc. Chem. Res. 45 (2012) 1203–1214.

(b) J. H. Palmer, Struct. Bond. 142 (2012) 49–89.

(c) H. L. Buckley, J. Arnold, Dalton Trans. 44 (2015) 30–36.

[3] C. Capar, K. E. Thomas, A. Ghosh, J. Por. Phthalocya. 12 (2008) 964–967.

[4] F. Mandoj, S. Nardis, G. Pomarico, R. Paolesse, J. Por. Phthalocya. 12 (2008) 19–26.

[5] H. Y. Liu, L. Chen, F. Yam, H. Y. Zhan, X. Ying, X. L. Wang, H. F. Jiang, C. K. Chang, Chin. Chem. Lett. 19 (2008) 1000–1003.

[6] T. H. Ngo, W.Van Rossom, W. Dehaen, W. Maes, Org. Biomol. Chem. 7 (2009) 439–443.

[7] (a) C. Capar, L.-K. Hansen, J. Conradie, A. Ghosh, J. Por. Phthalocya. 14 (2010) 509–512.
(b) J. Capar, J. Conradie, C. M. Beavers, A. Ghosh, J. Phys. Chem. A 119 (2015) 3452–3457.
[8] J. Capar, S. Berg, K. E. Thomas, C. M. Beavers, K. J. Gagnon, A. Ghosh, J. Inorg. Biochem. 153 (2015) 162–166.
[9] Synthesis of gold octabromocorroles:
(a) A. Alemayehu, A. Ghosh, J. Por. Phthalocya. 15 (2011) 106–110.
(b) E. Rabinovitch, I. Goldberg, Z. Gross, Chem. Eur. J. 17 (2011) 12294–12301.
[10] Synthesis of diboron octabromocorroles: A. M. Albrett, K. E. Thomas, S. Maslek, A. Młodzianowska, J. Conradie, C. M. Beavers, A. Ghosh, P. J. Brothers, Inorg. Chem. 53 (2014) 5486–5493.
[11] S. Berg, K. E. Thomas, C. M. Beavers, A. Ghosh, Inorg. Chem. 51, (2012) 9911–9916.
[12] D. Gao, G. Canard, M. Giorgi, T. S. Balaban, Eur. J. Inorg. Chem. (2012) 5915–5920.
[13] D. Gao, G. Canard, M. Giorgi, P. Vanloot, T. S. Balaban, Eur. J. Inorg. Chem. (2013) 279–287.
[14] J. I. Setsune, A. Tsukajima, J. Watanabe, Tetrahedron Lett. 47 (2006) 1817–1820.
[15] G. Pomarico, X. Xiao, S. Nardis, R. Paolesse, F. R. Fronczek, K. M. Smith, Y. Fang, Z. Ou, K. M. Kadish, Inorg. Chem. 49 (2010) 5766–5774.
[16] D. L. Flint, R. L. Fowler, T. D. LeSaulnier, A. C. Long, A. Y. O'Brien, G. R. Geier, J. Org. Chem. 75 (2010) 553–563.
[17] R. Costa, G. R. Geier, C. J. Ziegler, Dalton Trans. 40 (2011) 4384–4386.
[18] S. Nardis, G. Pomarico, F. R. Fronczek, M. G. H. Vicente, R. Paolesse, Tetrahedron Lett. 48 (2007) 8643–8646.
[19] D. Sakow, D. Baabe, B. Böker, O. Burghaus, M. Funk, C. Kleeberg, D. Menzel, C. Pietzonka, M. Bröring, Chem. Eur. J. 20 (2014) 2913–2924.
[20] M. Ethirajan, Y. Chen, P. Joshi, R. K. Pandey, Chem. Soc. Rev. 40 (2011) 340–362.
[21] M. Stefanelli, J. Shen, W. Zhu, M. Mastroianni, F. Mandoj, S. Nardis, Z. Ou, K. M. Kadish, F. R. Fronczek, K. M. Smith, R. Paolesse, Inorg. Chem. 48 (2009) 6879–6887.
[22] P. Świder, A. Nowak-Król, R. Voloshchuk, J. P. Lewtak, D. T. Gryko, W. Danikiewicz, J. Mass Spectrom. 45 (2010) 1443–1451.
[23] J. Wojaczyński, M. Duszak, L. Latos-Grazyński, Tetrahedron 69 (2013) 10445–10449.
[24] C. Tardieux, C. P. Gros, R. Guilard, J. Heterocycl. Chem. 35 (1998) 965–970.

[25] G. R. Geier, J. F. B. Chick, J. B. Callinan, C. G. Reid, W. P. Auguscinski, J. Org. Chem. 69 (2004) 4159–4169.

[26] For an extensive study of free-base corrole conformation, see: J. Capar, J. Conradie, C. M. Beavers, A. Ghosh, J. Phys. Chem. A. 119 (2015) 3452–3457.

[27] Syntheses of gold corroles:

(a) K. E. Thomas, A. B. Alemayehu, J. Conradie, C. M. Beavers, A. Ghosh, Inorg. Chem. 50 (2011) 12844–12851.

(b) K. E. Thomas, C. M. Beavers, A. Ghosh, Mol. Phys. 110 (2012) 2439–2444.

[28] Gold corroles have found applications as organic solar cells and as reagents for photo-dynamic therapy of cancer:

(a) S.-L. Lai, L. Wang, C. Yang, M.-Y. Chan, X. Guan, C.-C. Kwok, C.-M. Che, Adv. Func. Mat. 24 (2014) 4655–4665.

(b) R. D. Teo, H. B. Gray, P. Lim, J. Termini, E. Domeshek, Z. Gross, Chem. Comm. 50 (2014) 13789–13792.

[29] Aurophilic interactions of approximately 4.93-4.35 Å have been observed in a crystal structure of a gold triarylcorrole.**Feil! Bokmerke er ikke definert.**[a]

[30] For X-ray structures of Cu and Ag octabromocorroles, see:

(a) A. B. Alemayehu, L.-K. Hansen, A. Ghosh, Inorg. Chem. 49 (2010) 7608–7610.

(b) K. E. Thomas, H. Vazquez-Lima, Y. Fang, Y. Song, K. J. Gagnon, C. M. Beavers, K. M. Kadish, A. Ghosh, Chem. Eur. J. 21 (2015) 16839–16847.

[31] I. H. Wasbotten, T. Wondimagegn, A. Ghosh, J. Am. Chem. Soc. 124 (2002) 8104–8116.

Supporting Information

Demetalation of Copper Undecaarylcorroles: Molecular Structures of a Free-Base Undecaarylisocorrole and a Gold Undecaarylcorrole

Jan Capar,[a] Job Zonneveld,[a] Steffen Berg,[a] Johan Isaksson,[a] Kevin J. Gagnon,[b] Kolle E. Thomas,*[,a] and Abhik Ghosh*[,a]

[a] Department of Chemistry and Center for Theoretical and Computational Chemistry, University of Tromsø, N-9037 Tromsø, Norway; Email: thomas.kolle@uit.no; abhik.ghosh@uit.no; [b] Advanced Light Source, Lawrence Berkeley National Laboratory, Berkeley, CA 94720-8229

Table of Contents

A. Copper undecaarylcorroles

(a) UV-vis spectra of copper undecaarylcorroles

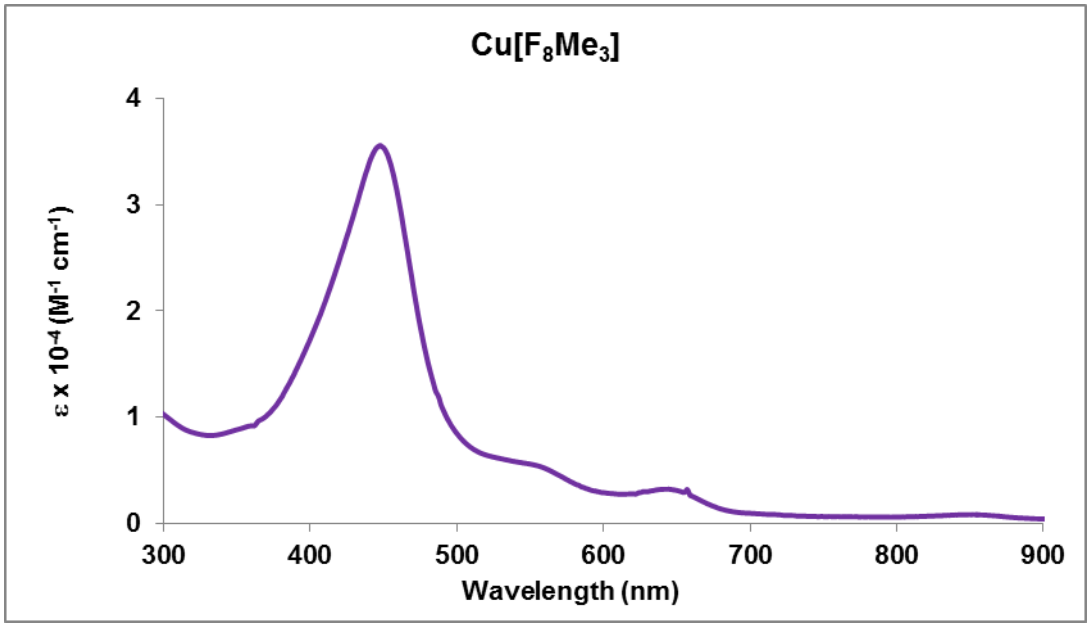

Figure S1. UV-vis spectrum of Cu[F_8Me_3].

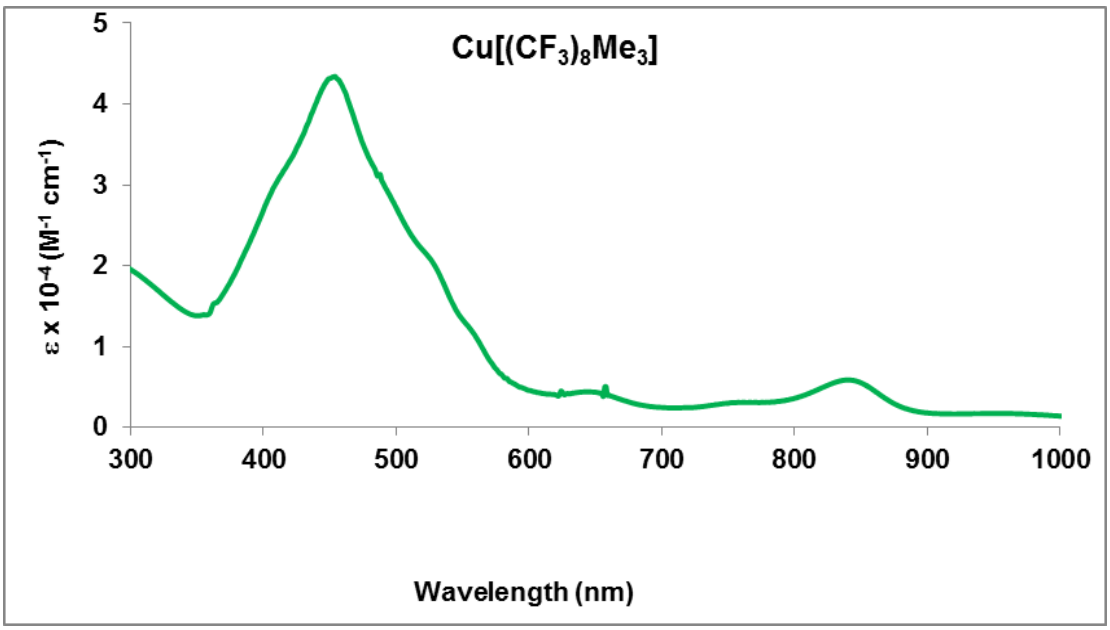

Figure S2. UV-vis spectrum of Cu[$(CF_3)_8Me_3$].

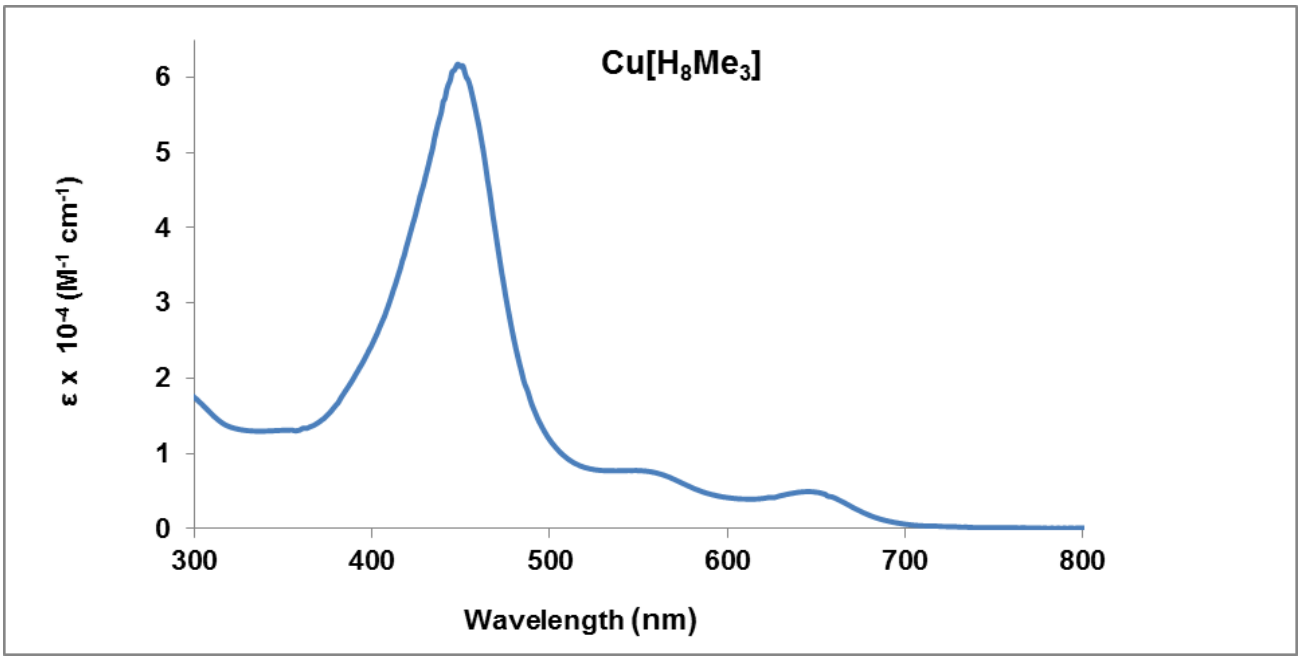

Figure S3. UV-vis spectrum of Cu[H_8Me_3].

(b) NMR spectra of copper undecaarylcorroles

NMR spectra of Cu[F_8Me_3]

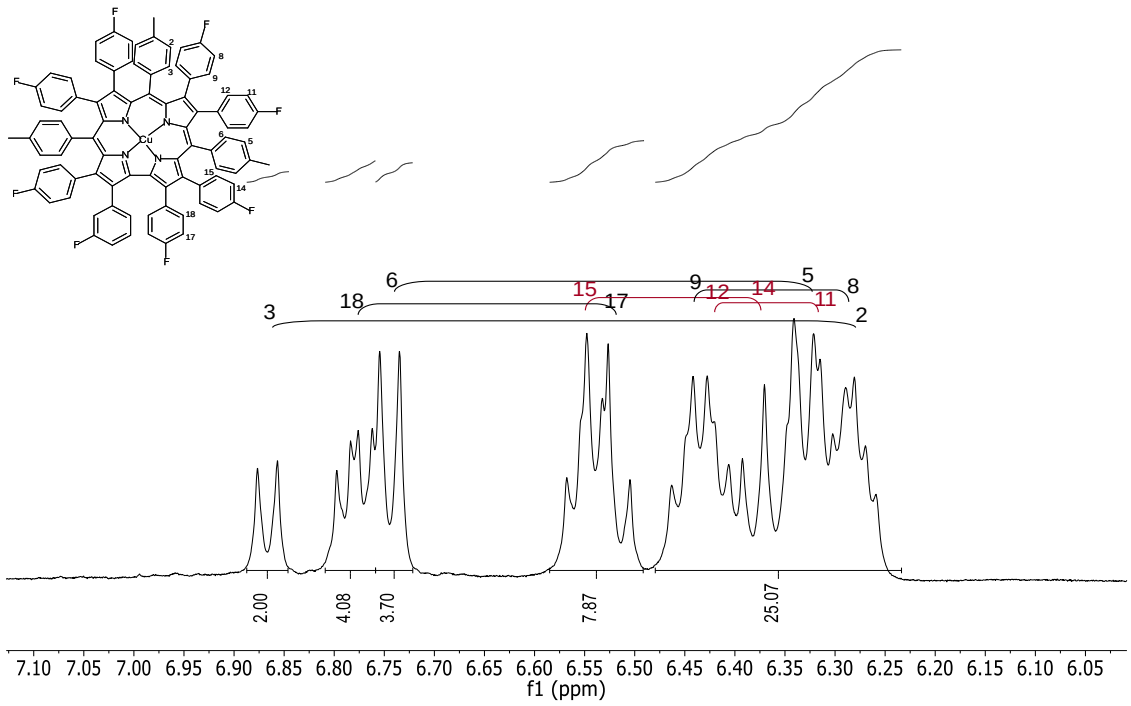

Figure S4. Aromatic region in the ^1H NMR spectrum of Cu[F_8Me_3] in $CDCl_3$.

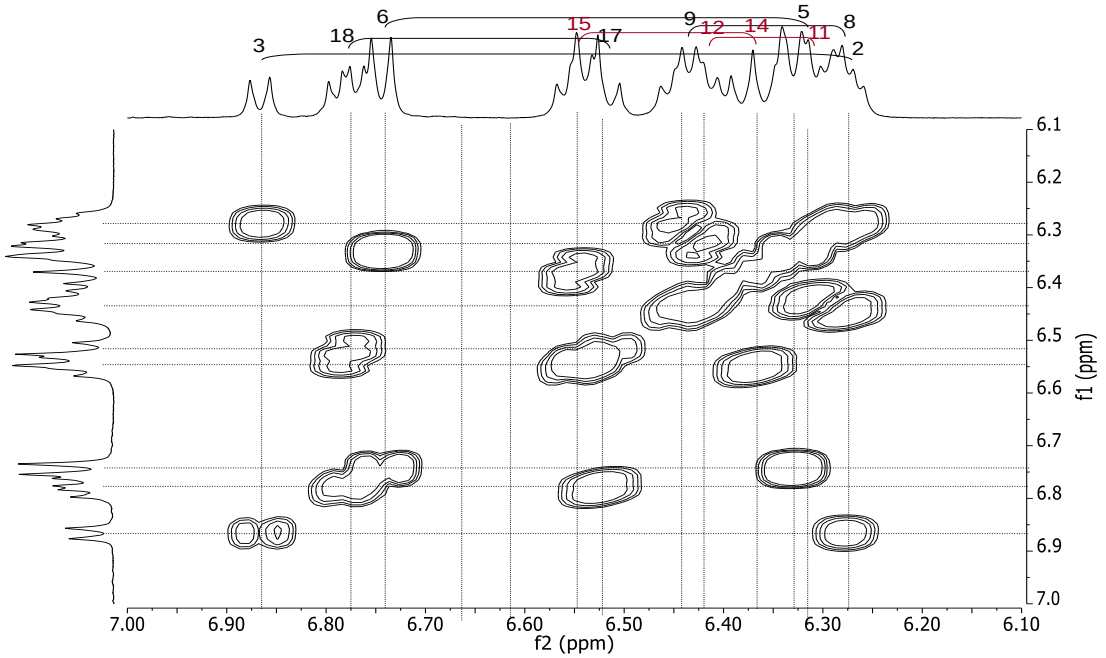

Figure S5. $^1H,^1H$ COSY of Cu[F_8Me_3] in $CDCl_3$ for the aromatic region.

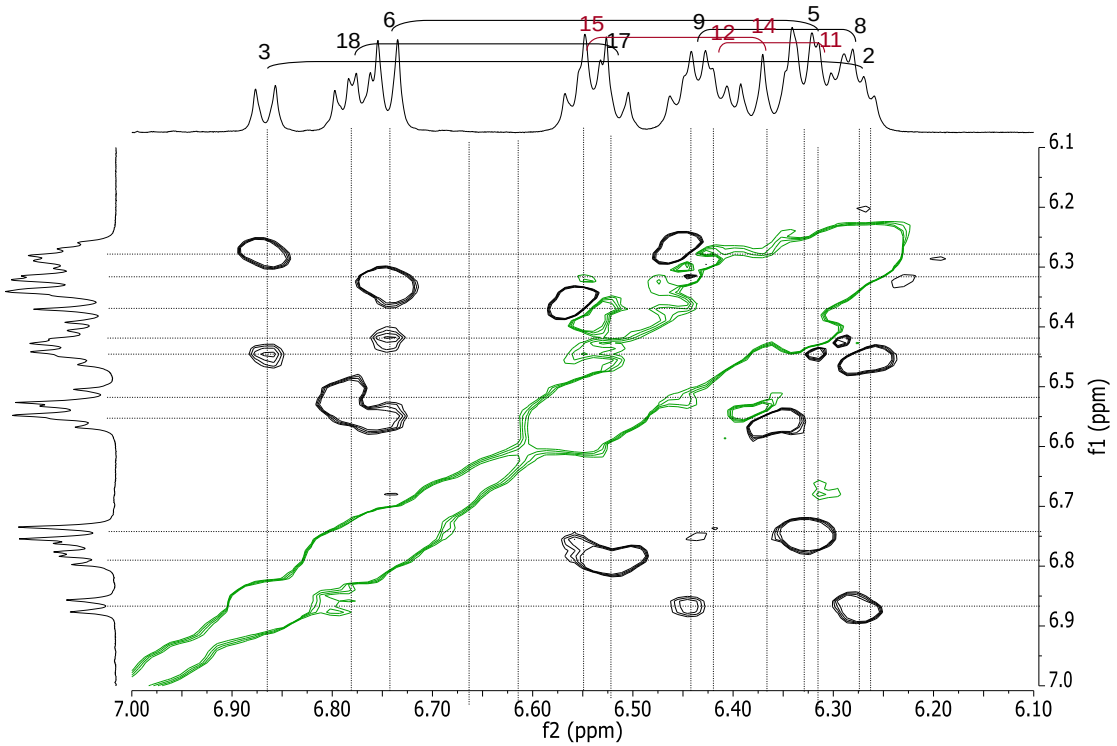

Figure S6. $^{1}H,^{1}H$ ROESY (300ms, $CDCl_3$) of $Cu[F_8Me_3]$ for the aromatic region.

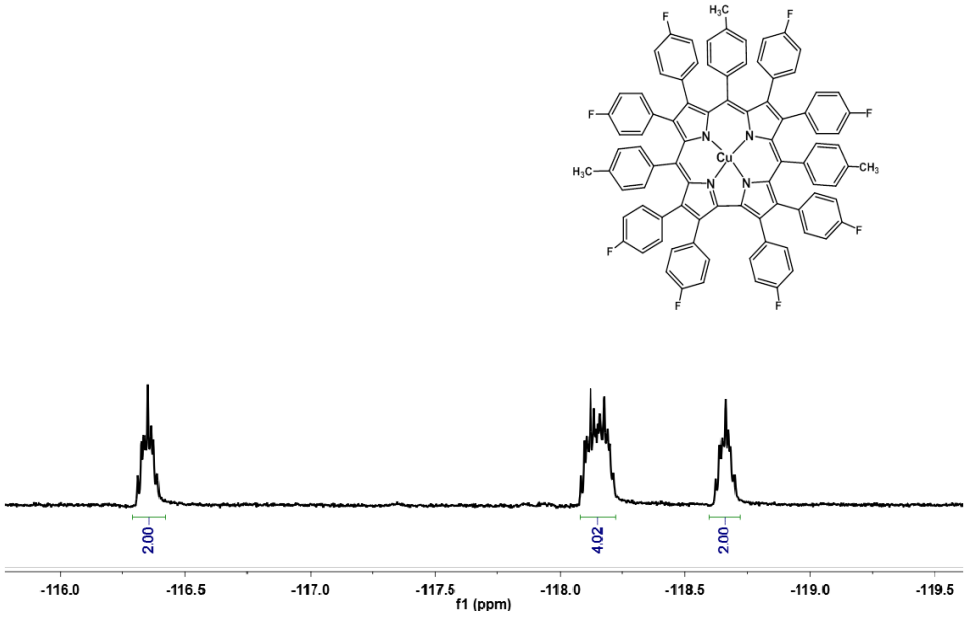

Figure S7. ^{19}F NMR spectrum of $Cu[F_8Me_3]$ in $CDCl_3$.

NMR spectra of Cu[$(CF_3)_8Me_3$]

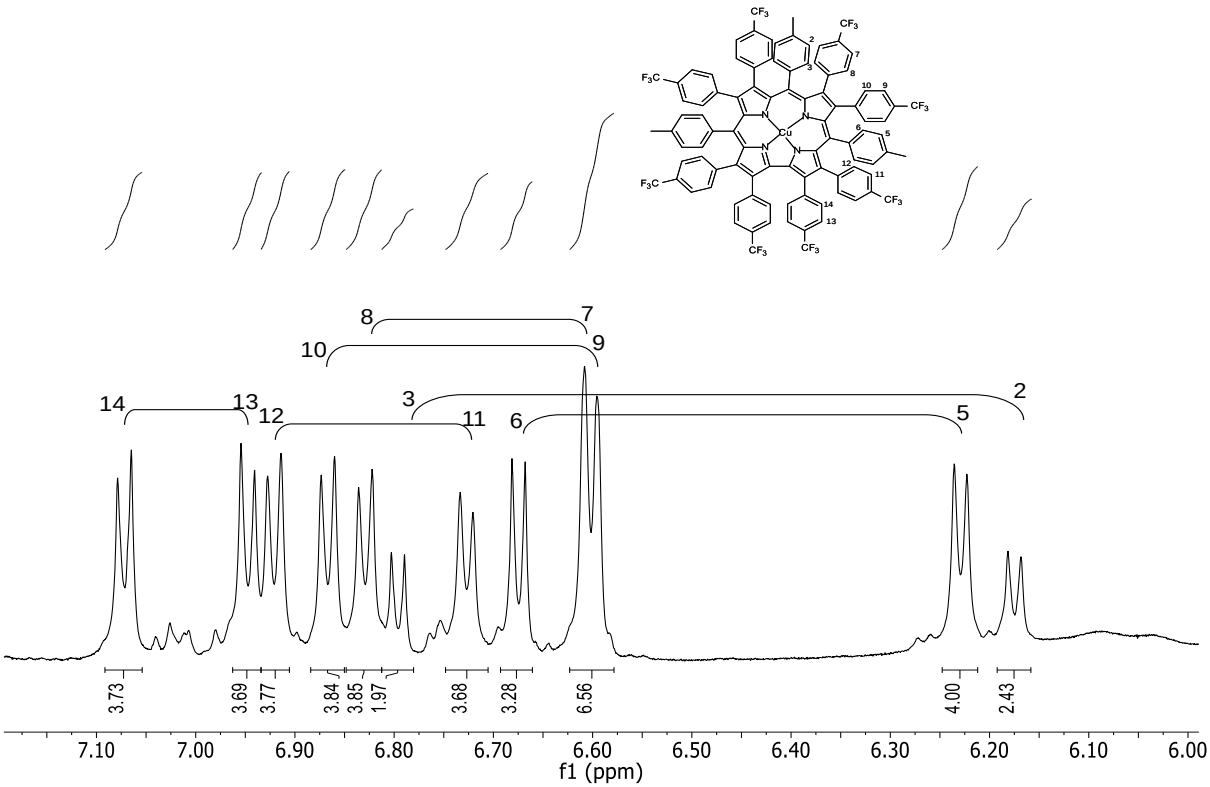

Figure S8. Aromatic region in the ^{1}H NMR spectrum of Cu[$(CF_3)_8Me_3$] in $CDCl_3$.

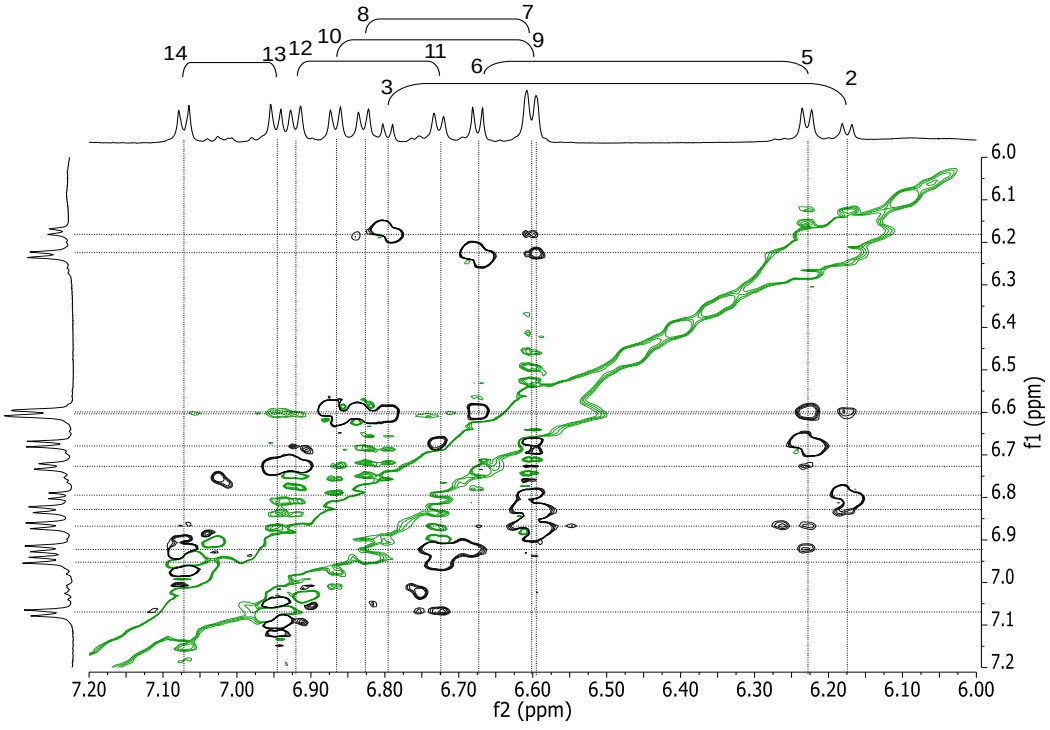

Figure S9. ^{1}H,^{1}H ROESY (300ms, $CDCl_3$) of Cu[$(CF_3)_8Me_3$] for the aromatic region.

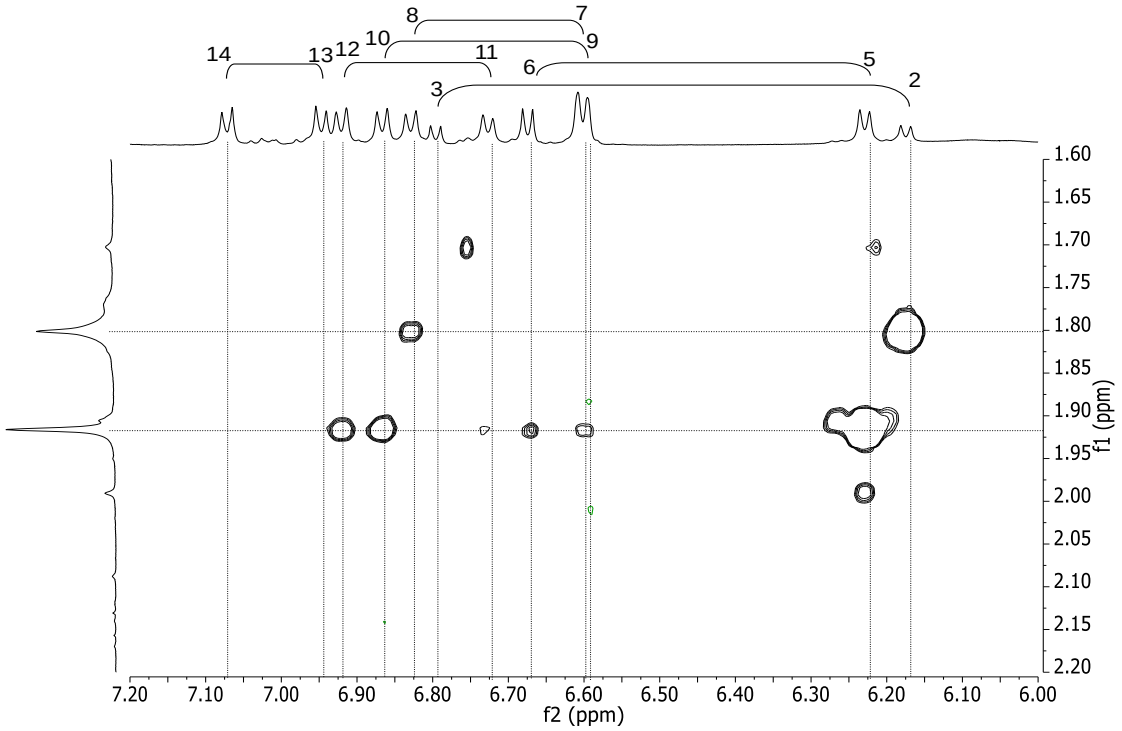

Figure S10. $^{1}H,^{1}H$ ROESY (300ms, $CDCl_3$) of $Cu[(CF_3)_8Me_3]$ for the aromatic/methyl region.

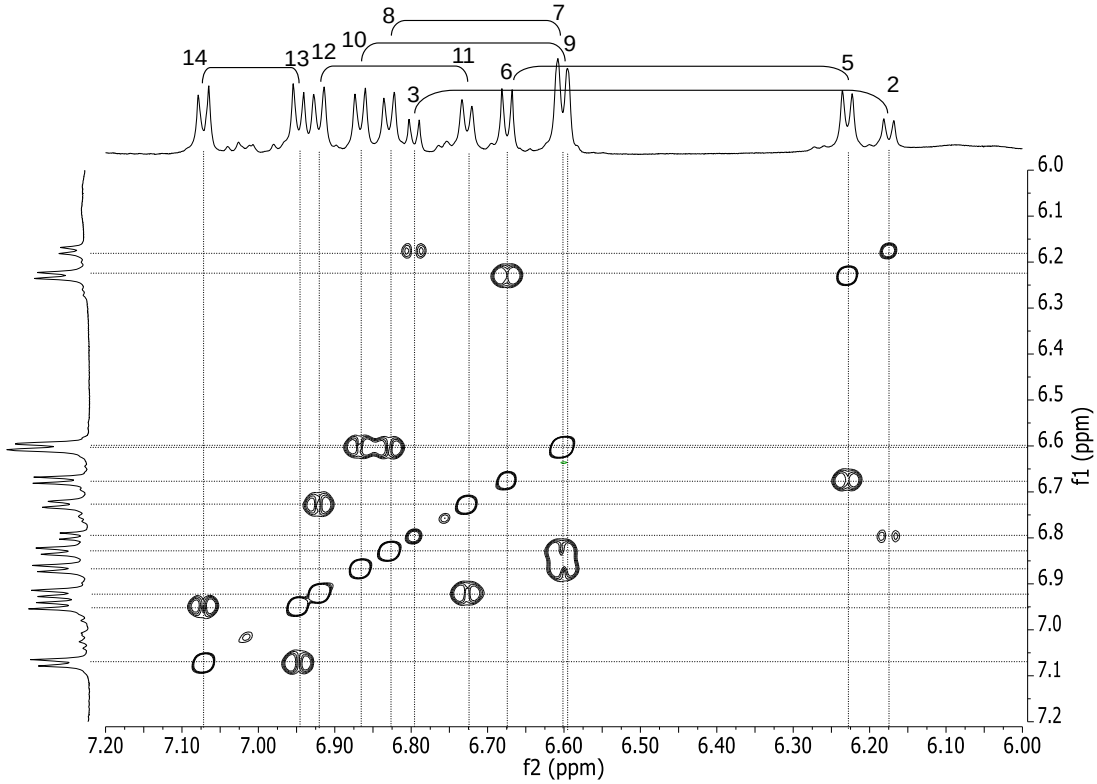

Figure S11. $^{1}H,^{1}H$ TOCSY (80ms, $CDCl_3$) of $Cu[(CF_3)_8Me_3]$ for the aromatic region.

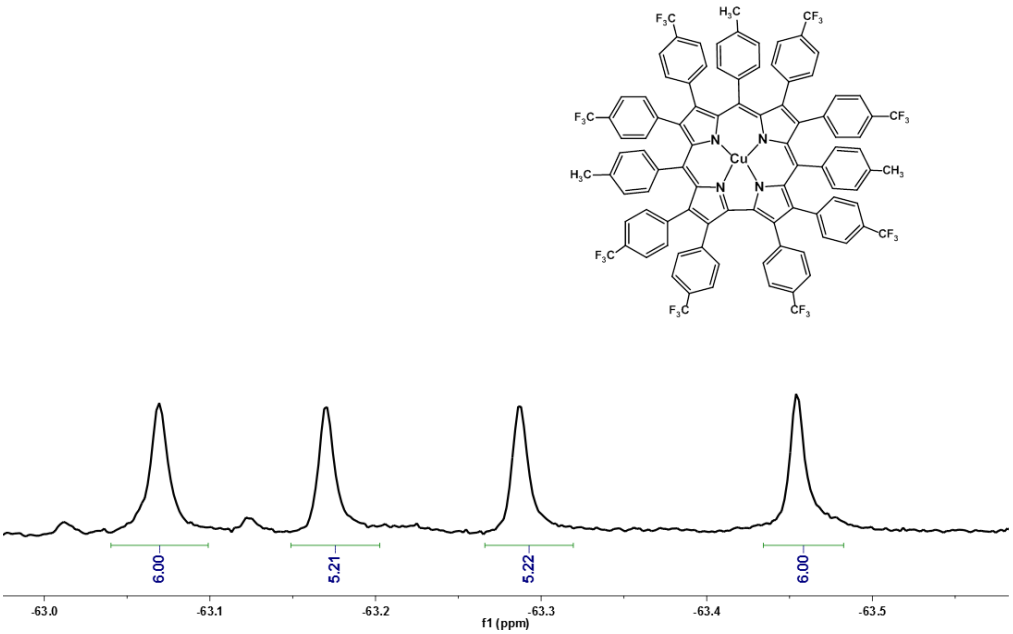

Figure S12. ^{19}F NMR spectrum of $Cu[(CF_3)_8Me_3]$ in $CDCl_3$.

NMR spectra of $Cu[(Ph)_8Me_3]$

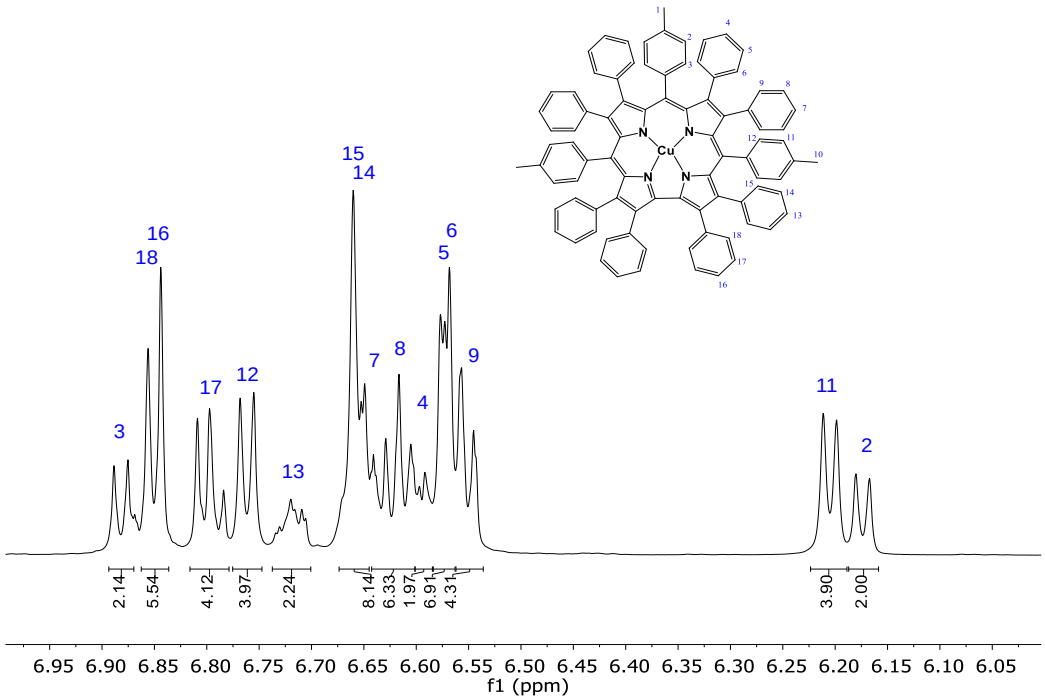

Figure S13. Aromatic region in the ^1H NMR spectrum of $Cu[H_8Me_3]$ in CD_2Cl_2.

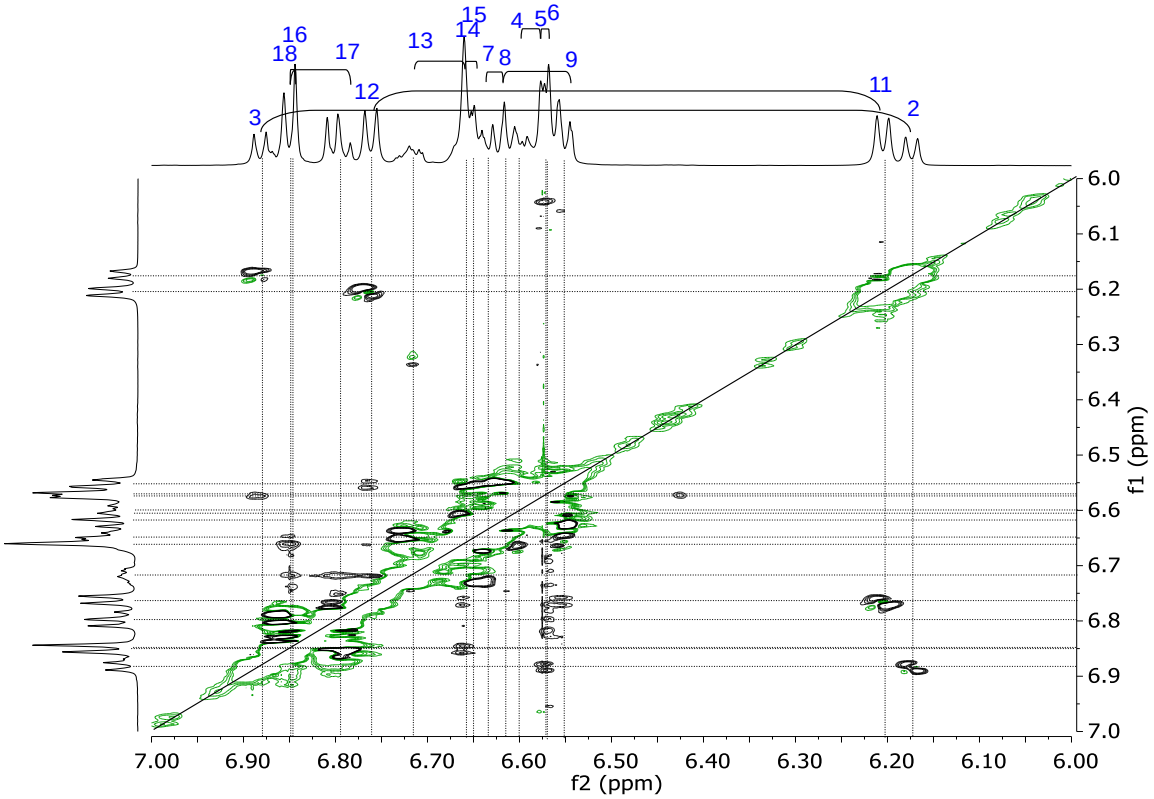

Figure S14. ^{1}H,^{1}H ROESY (300ms, CD_2Cl_2) of Cu[H_8Me_3] for the aromatic region.

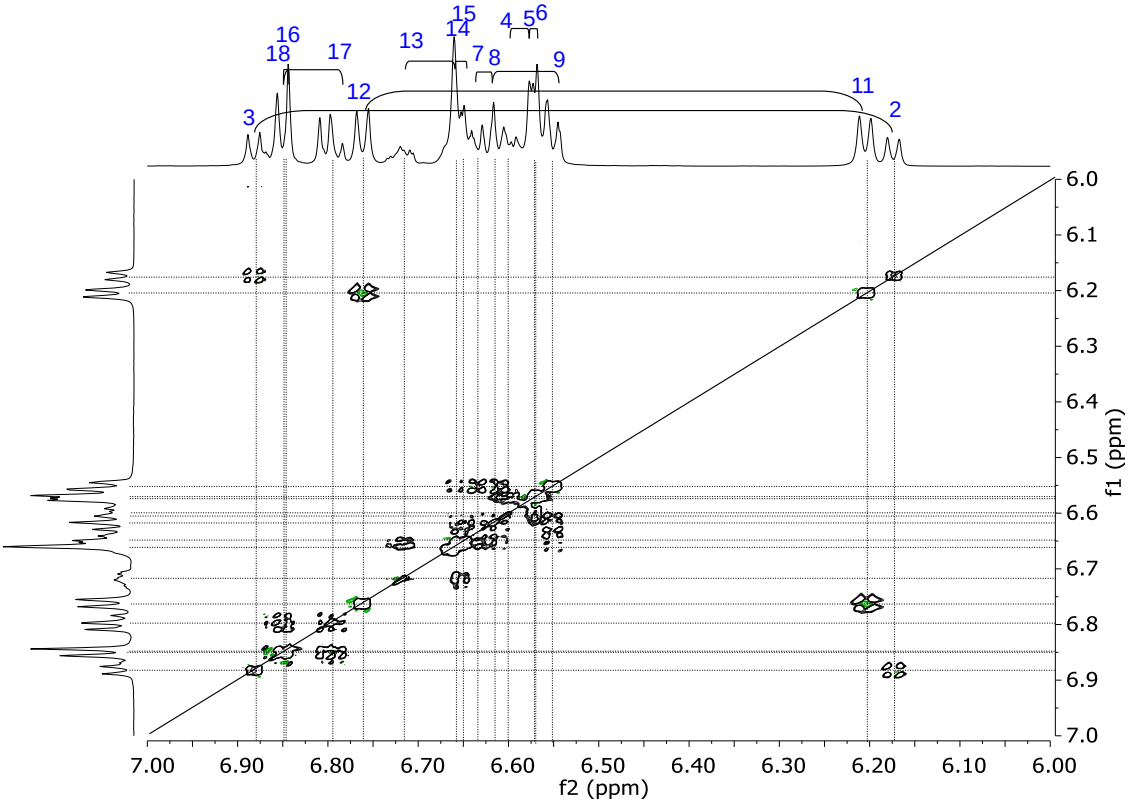

Figure S15. ^{1}H,^{1}H TOCSY (80ms, CD_2Cl_2) of Cu[H_8Me_3] for the aromatic region.

(c) HR-MS of copper undecaarylcorroles

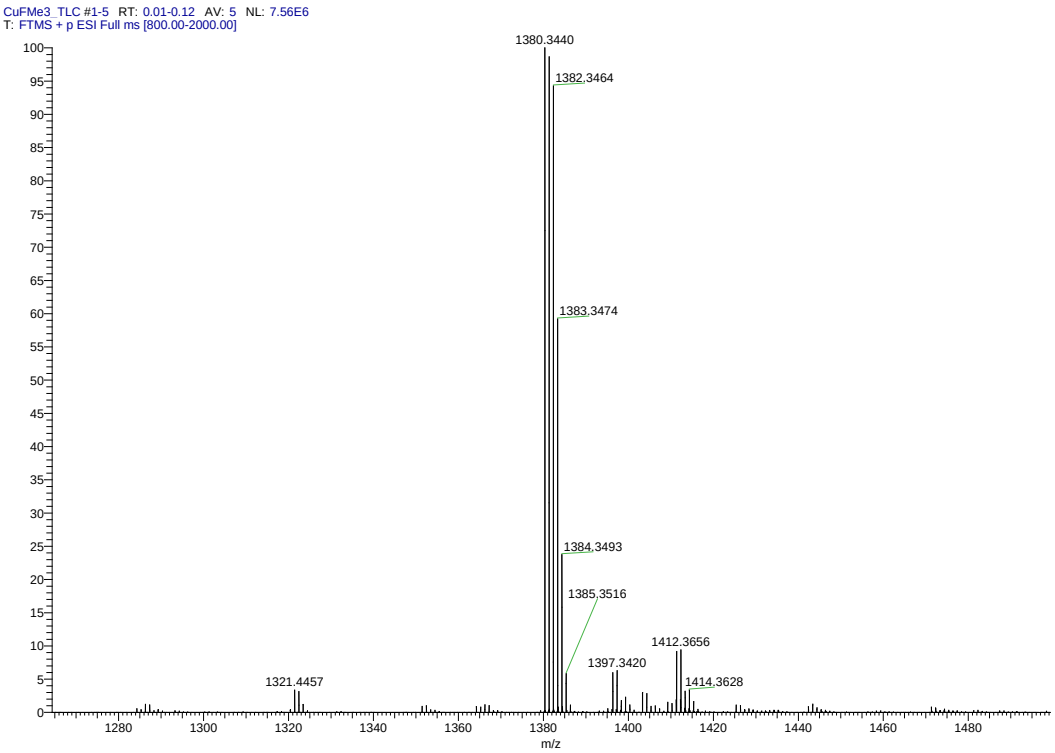

Figure S16. HR-ESI mass spectrum of Cu[F_8Me_3].

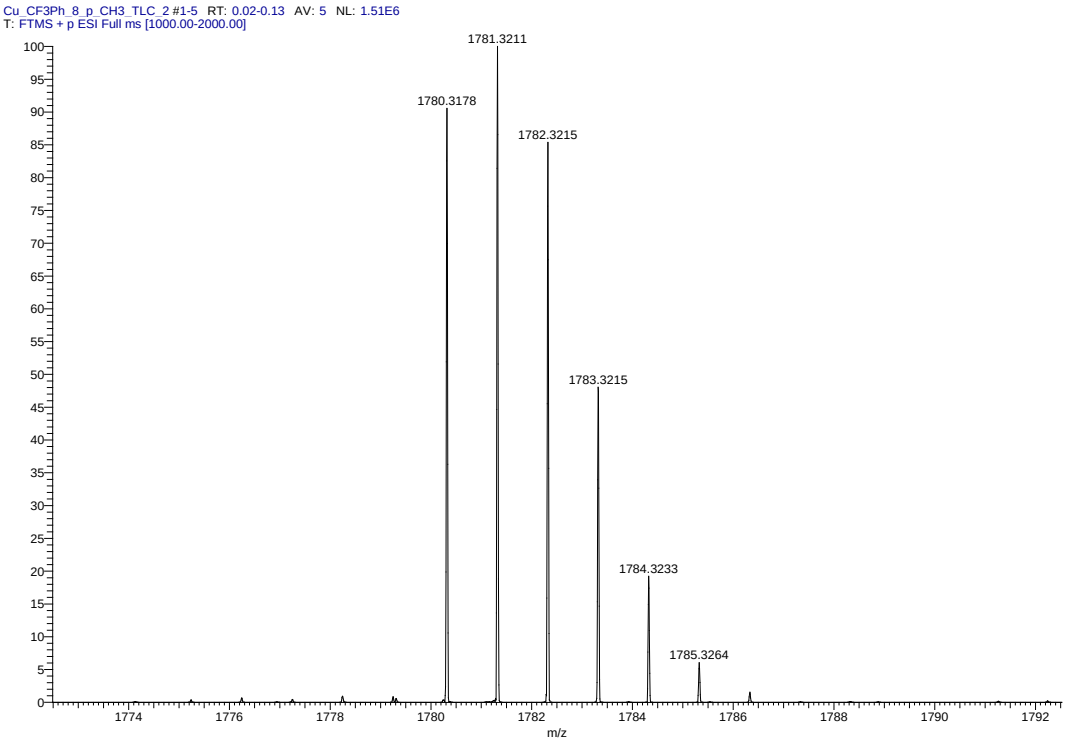

Figure S17. HR-ESI mass spectrum of Cu[$(CF_3)_8Me_3$].

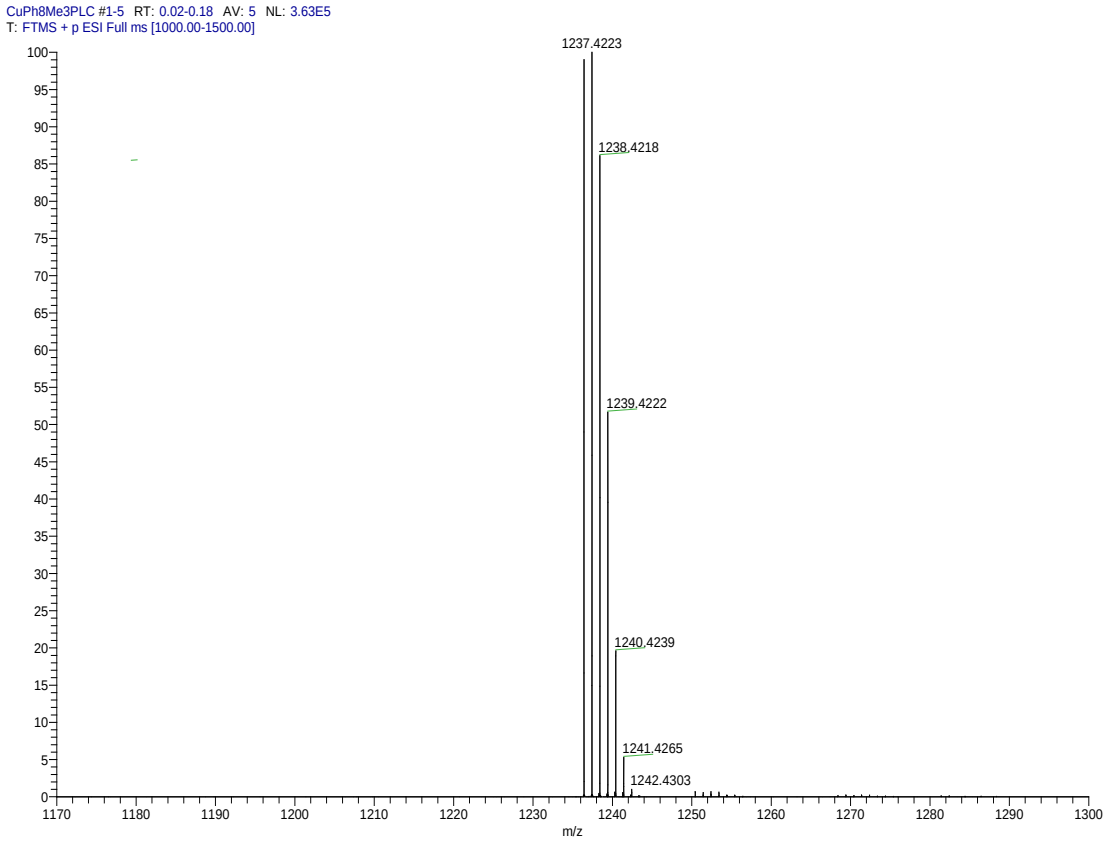

Figure S18. HR-ESI mass spectrum of Cu[H_8Me_3].

B. Free base undecaarylisocorroles

(a) UV-vis spectra of free base undecaarylisocorroles

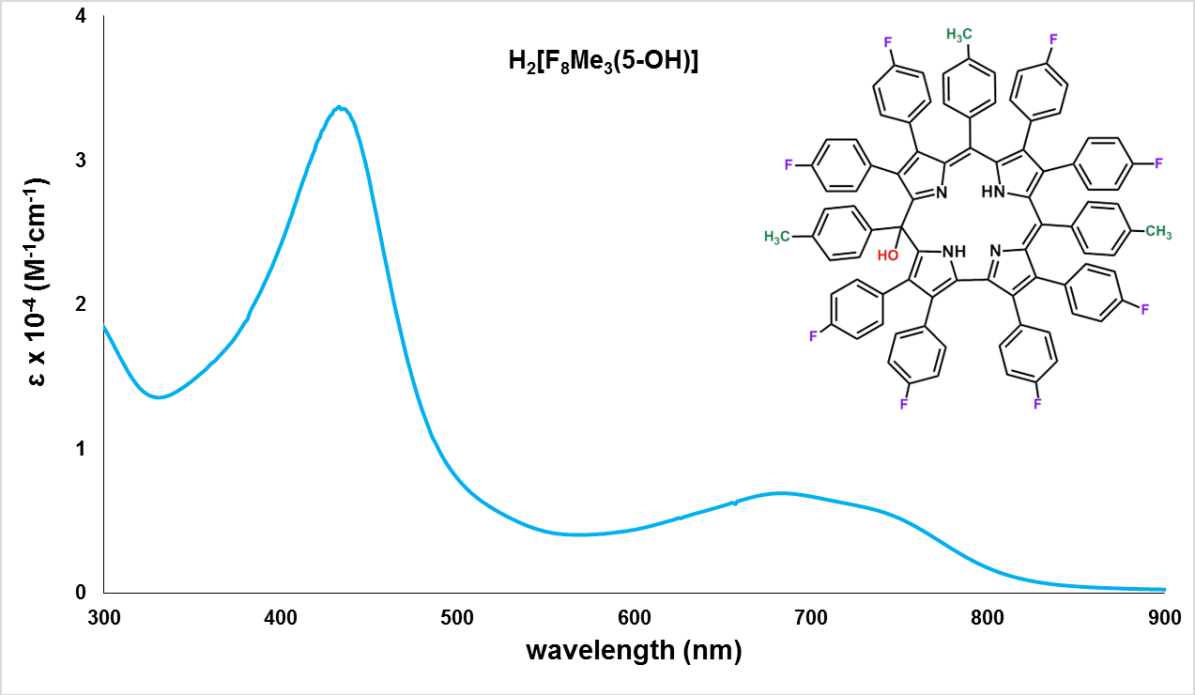

Figure S19. UV-vis spectrum of $H_2[F_8Me_3(5\text{-}OH)]$.

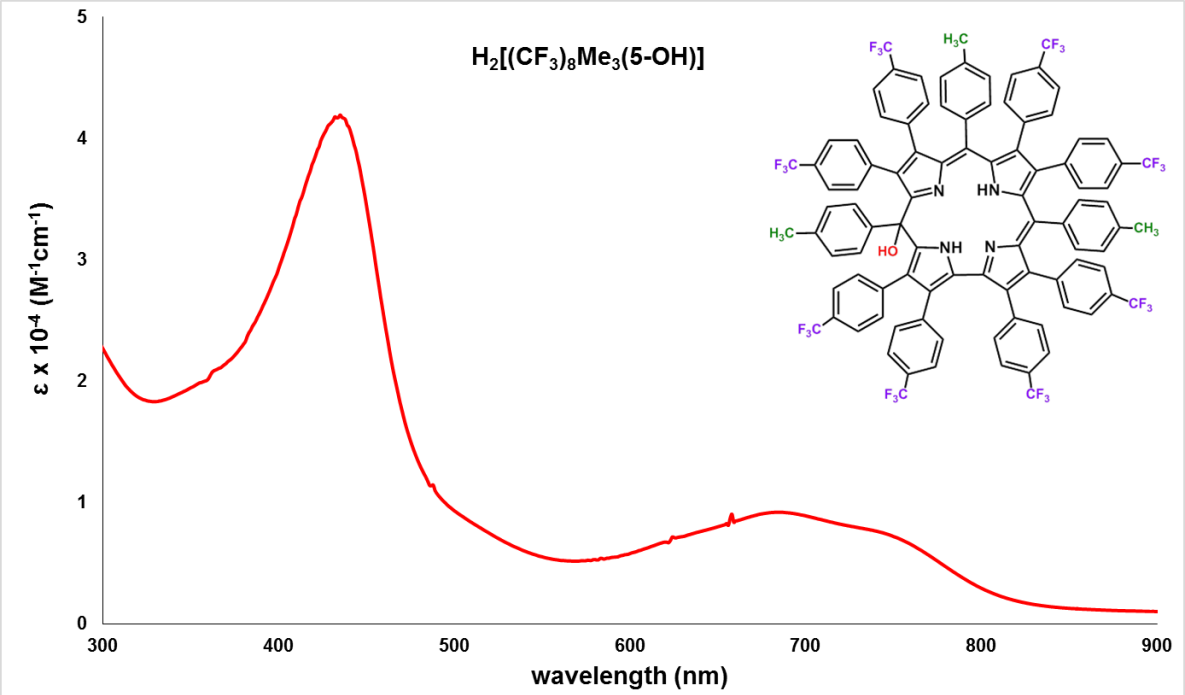

Figure S20. UV-vis spectrum of $H_2[(CF_3)_8Me_3(5\text{-}OH)]$.

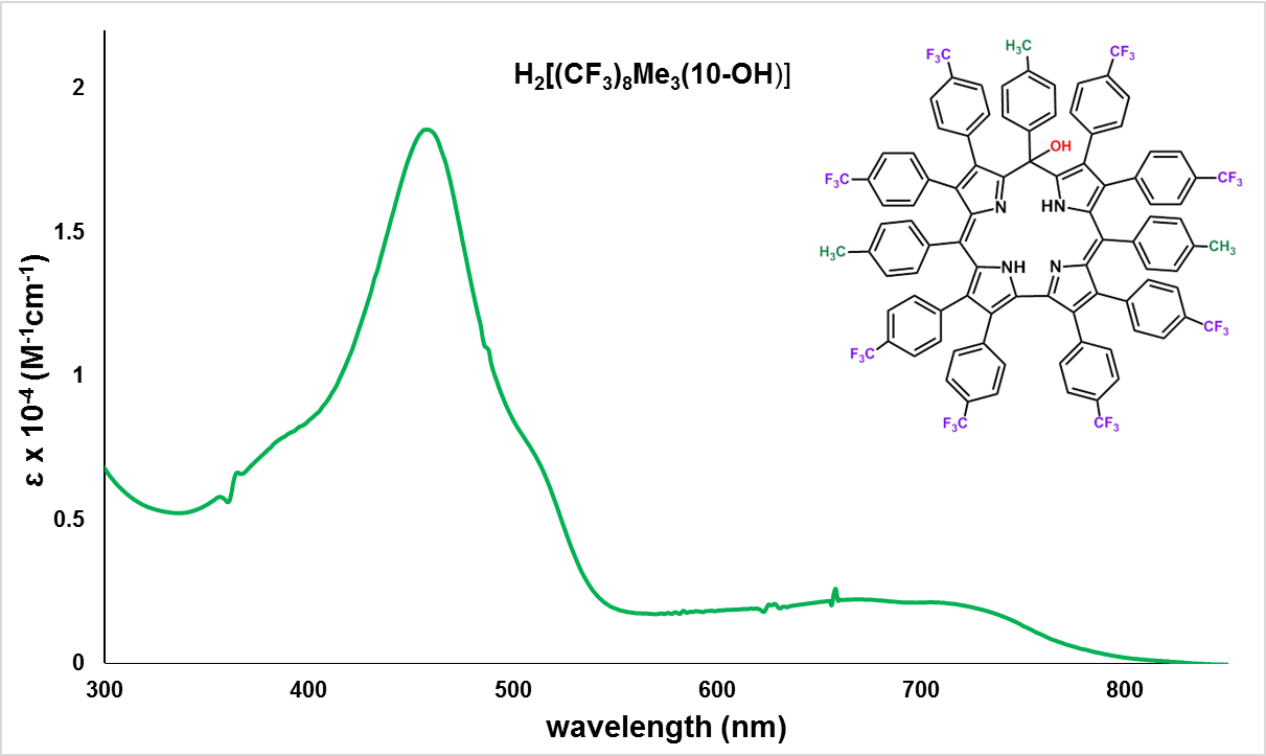

Figure S21. UV-vis spectrum of $H_2[(CF_3)_8Me_3(10\text{-}OH)]$.

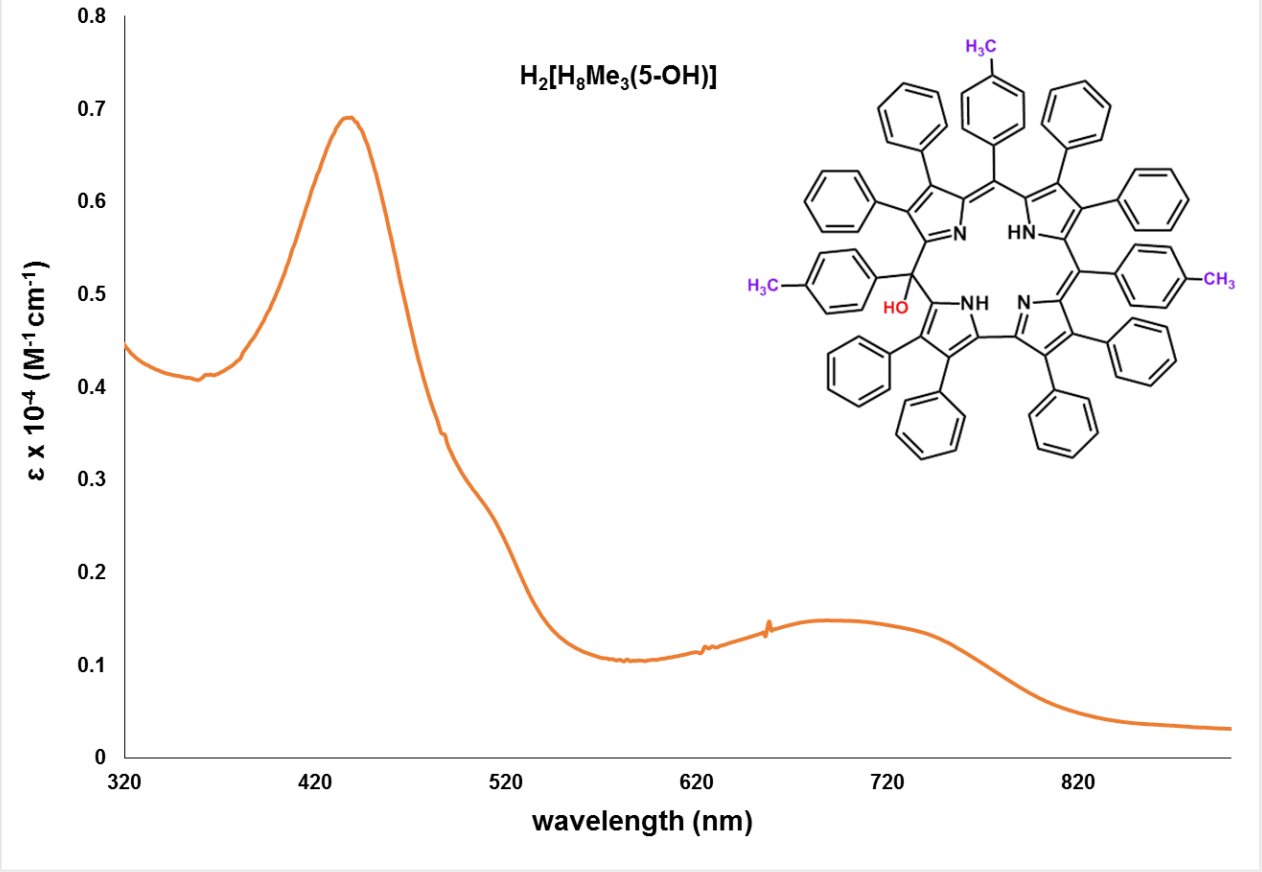

Figure S22. UV-vis spectrum of $H_2[H_8Me_3(5\text{-}OH)]$.

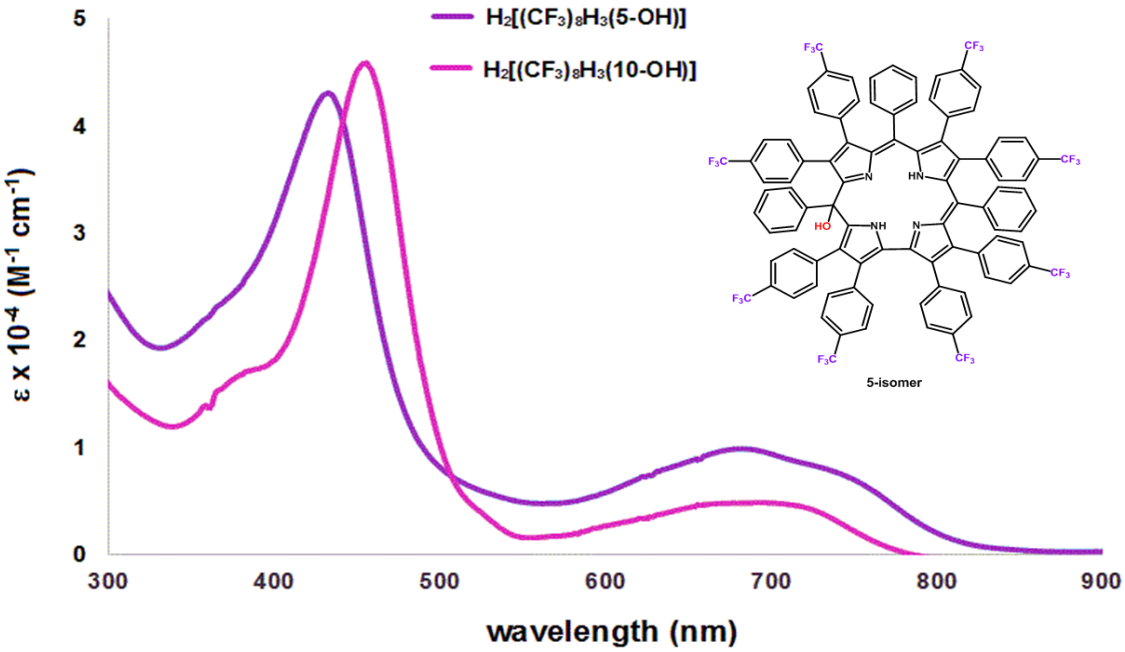

Figure S23. UV-vis spectra of $H_2[(CF_3)_8H_3(5\text{-}OH)]$ and $H_2[(CF_3)_8H_3(10\text{-}OH)]$.

(b) NMR spectra of free base undecaarylisocorroles

NMR spectra of $H_2[F_8Me_3(5\text{-}OH)]$

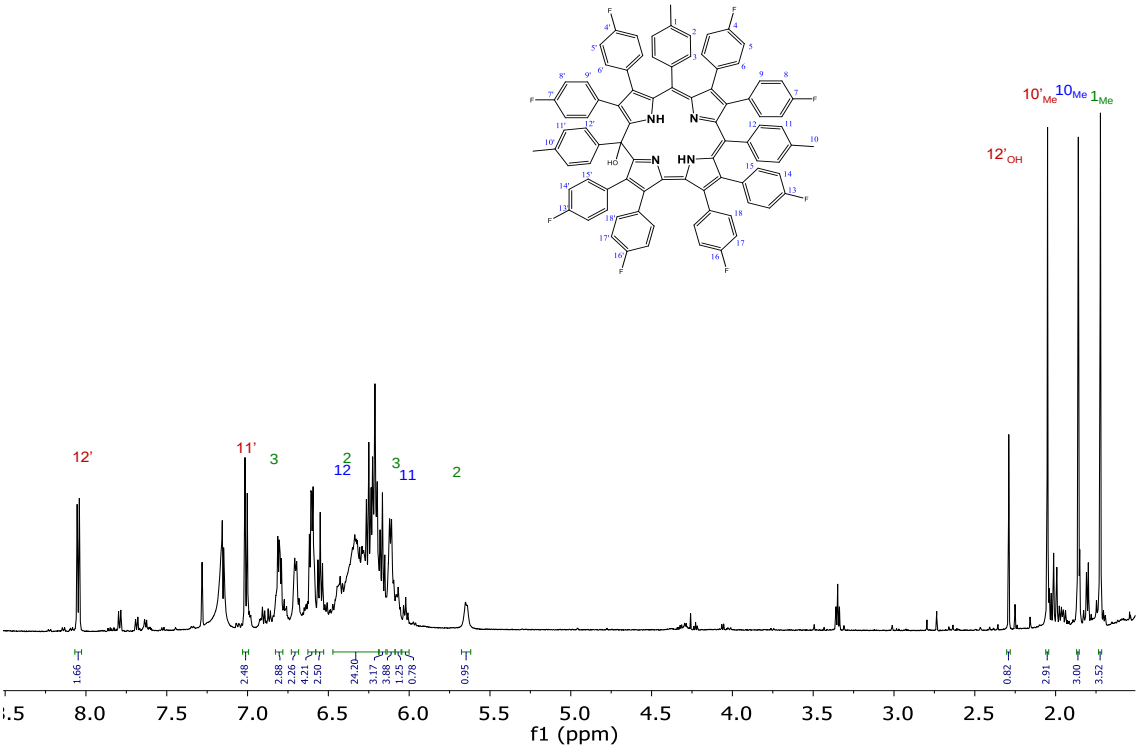

Figure S24. ^{1}H NMR spectrum of $H_2[F_8Me_3(5\text{-}OH)]$ in benzene-d_6.

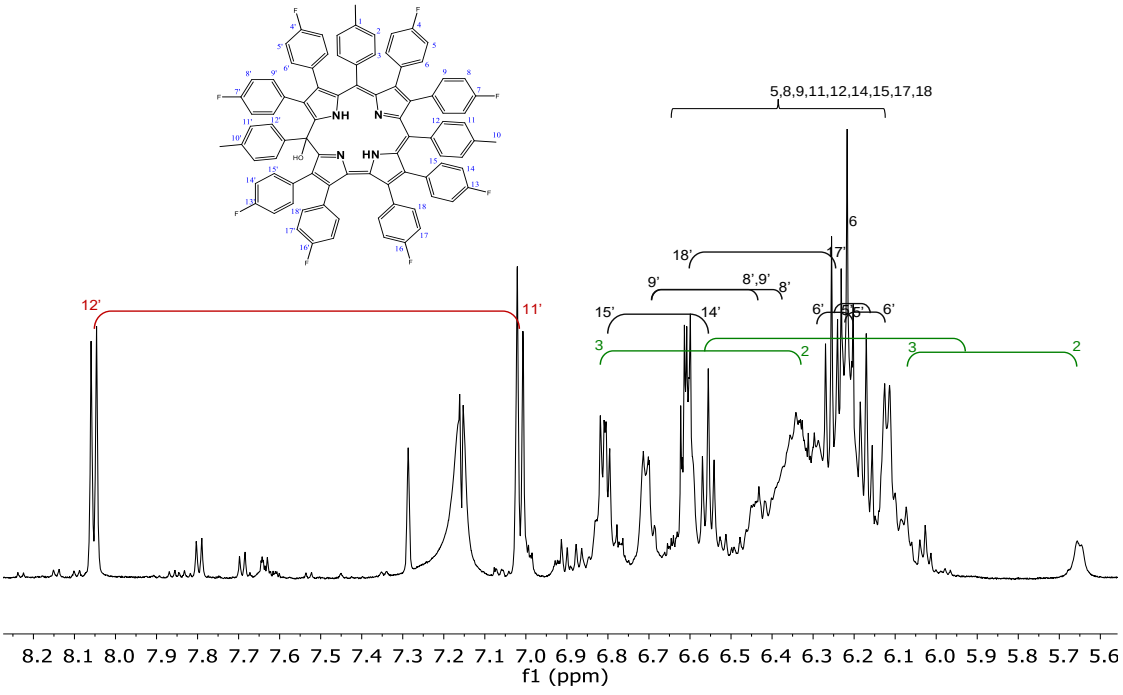

Figure S25. Aromatic region of the ^{1}H NMR spectrum of $H_2[F_8Me_3(5\text{-}OH)]$ in benzene-d_6.

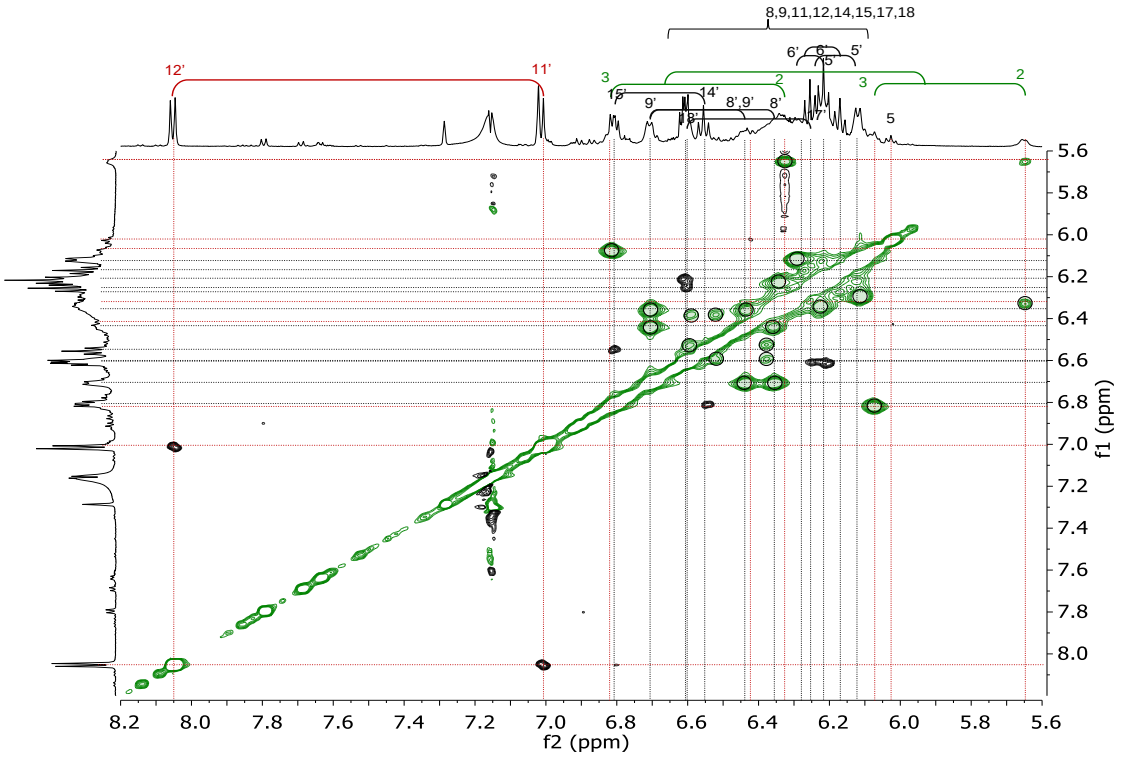

Figure S26. ^{1}H,^{1}H ROESY (300ms, benzene-d_6) of H_2[F_8Me_3(5-OH)] for the aromatic region. Conformational exchange peaks (same sign as diagonal) are shown as circles.

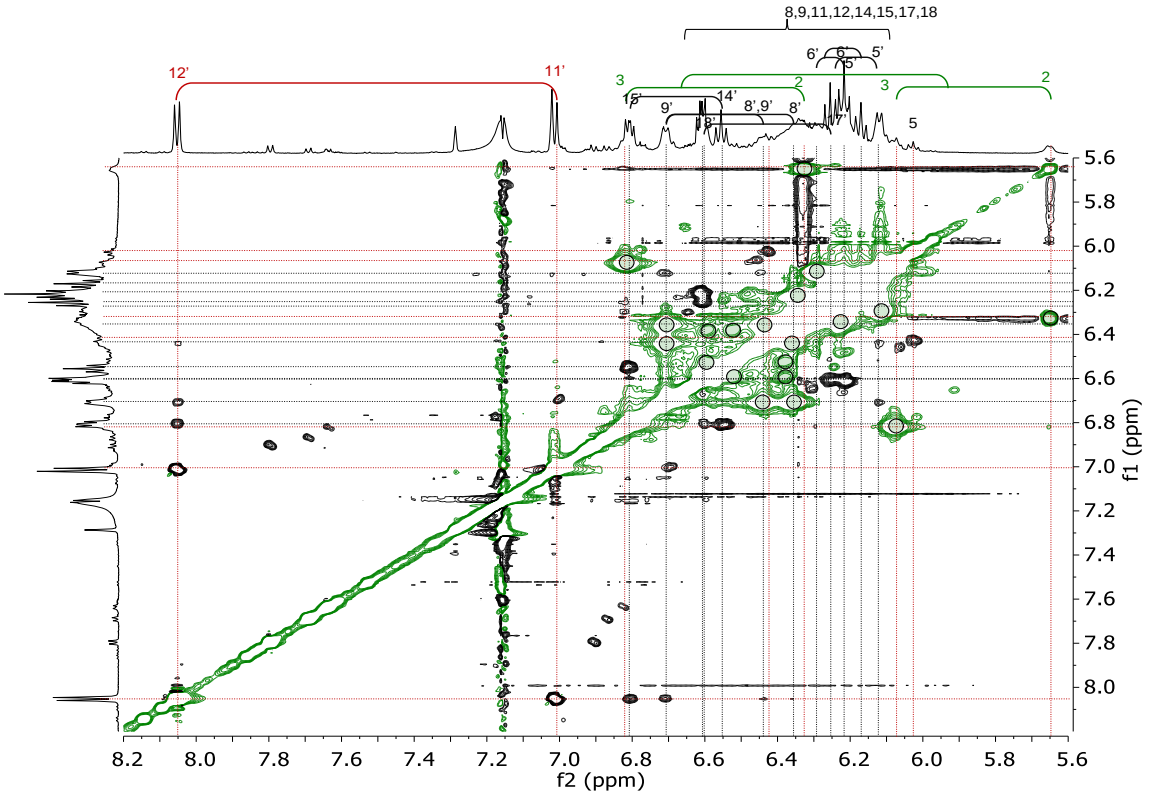

Figure S27. ^{1}H,^{1}H ROESY (300ms, benzene-d_6) of H_2[F_8Me_3(5-OH)] in the aromatic region. Conformational exchange peaks from ROESY are shown as circles.

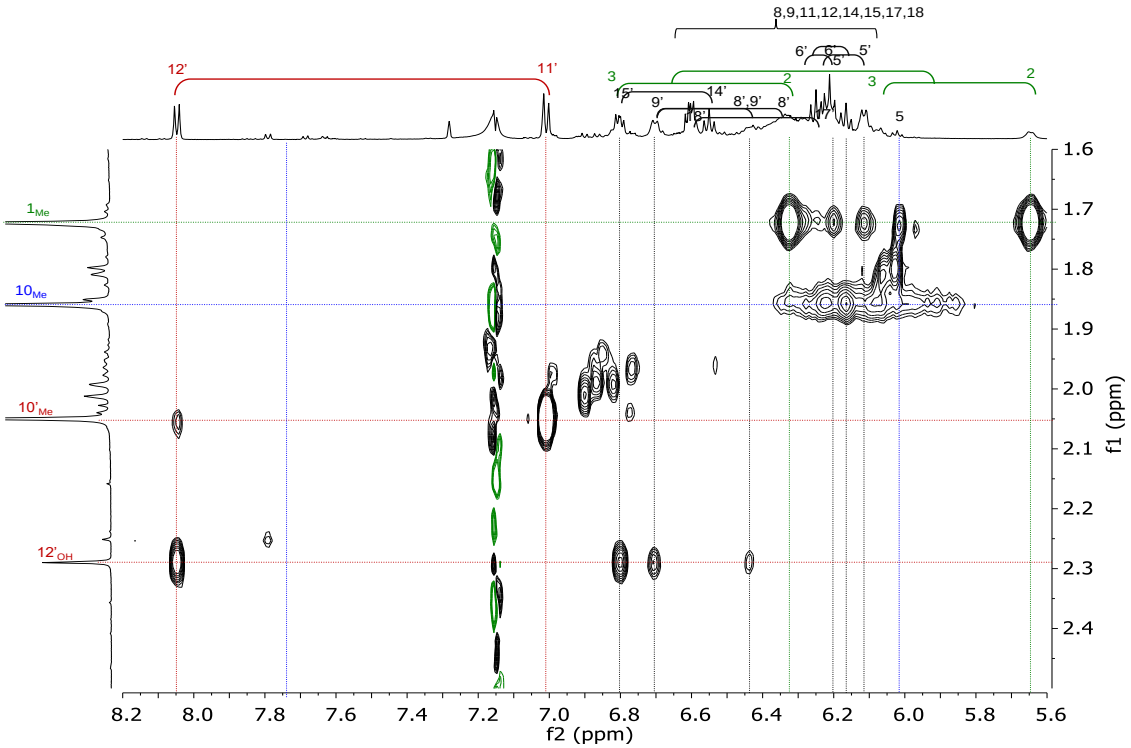

Figure S28. ^{1}H,^{1}H ROESY (300ms, benzene-d_6) spectrum of $H_2[F_8Me_3(5\text{-}OH)]$ for the aromatic/methyl region.

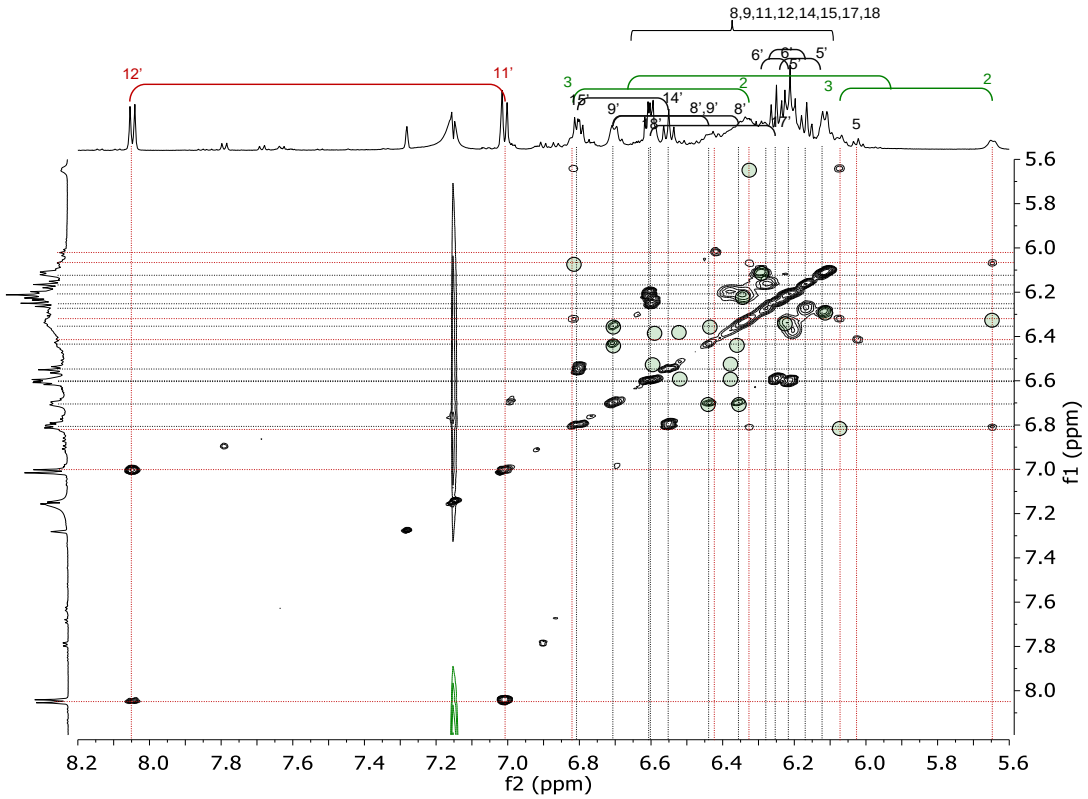

Figure S29. ^{1}H,^{1}H TOCSY (80ms, benzene-d_6) of $H_2[F_8Me_3(5\text{-}OH)]$ for the aromatic region. Conformational exchange peaks from ROESY are shown in circles.

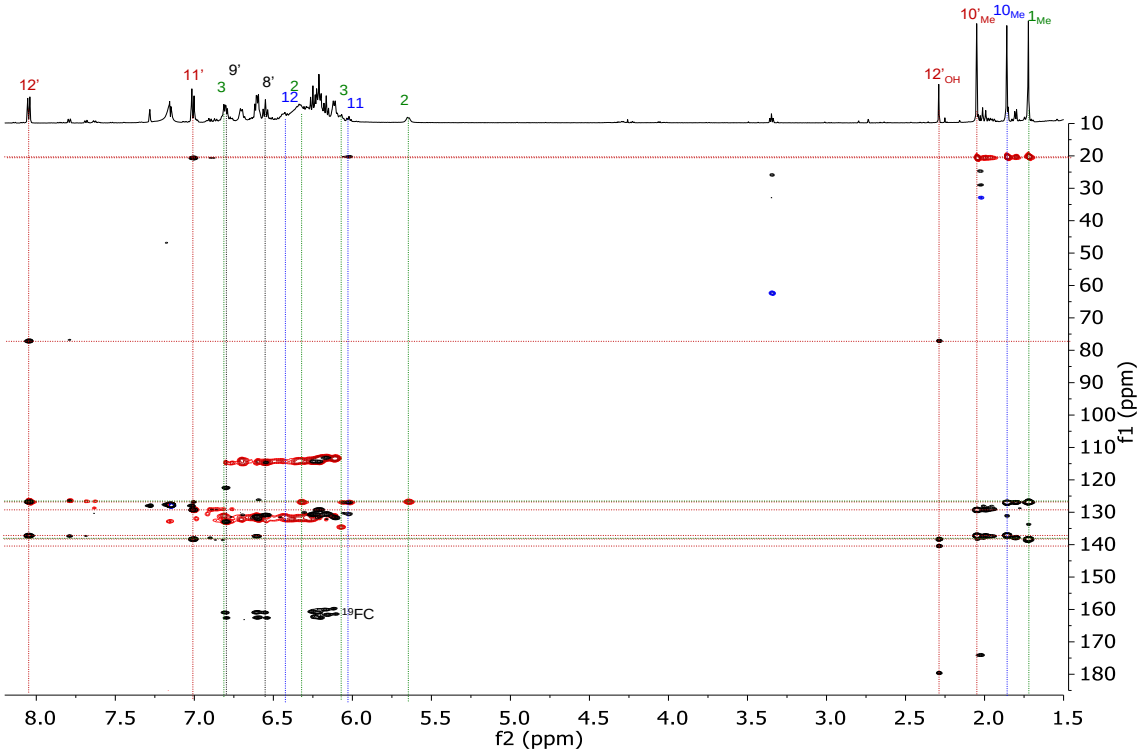

Figure S30. $^{1}H,^{13}C$ HSQC and HMBC spectra (in benzene-d_6) of $H_2[F_8Me_3(5\text{-}OH)]$ superimposed.

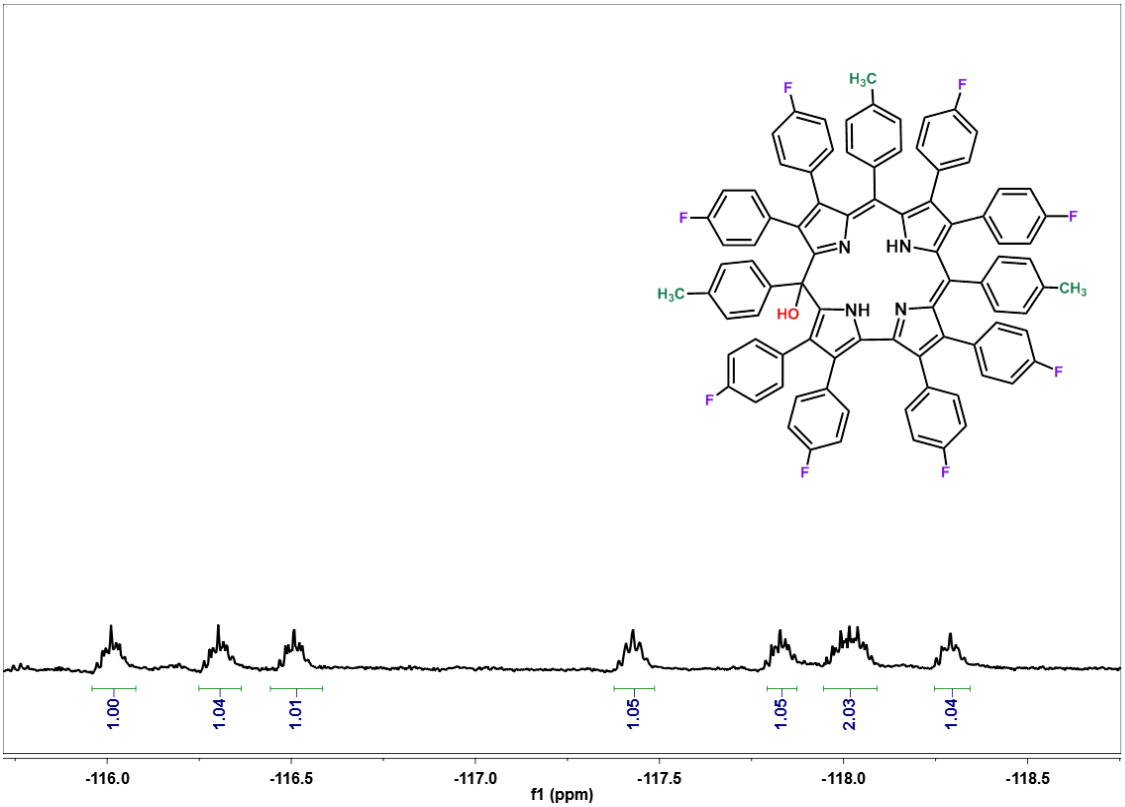

Figure S31. ^{19}F NMR spectrum of $H_2[F_8Me_3(5\text{-}OH)]$ in $CDCl_3$ at 298K.

NMR spectra of $H_2[(CF_3)_8Me_3(5\text{-}OH)]$

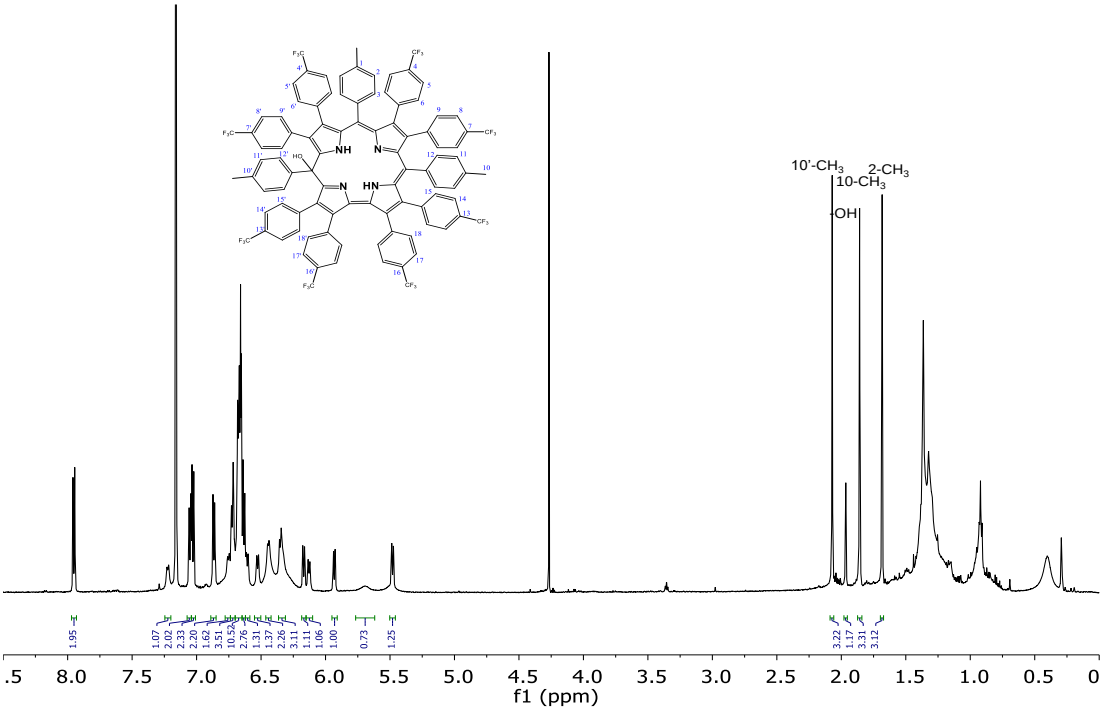

Figure S32. ^{1}H NMR spectrum of $H_2[(CF_3)_8Me_3(5\text{-}OH)]$ in benzene-d_6.

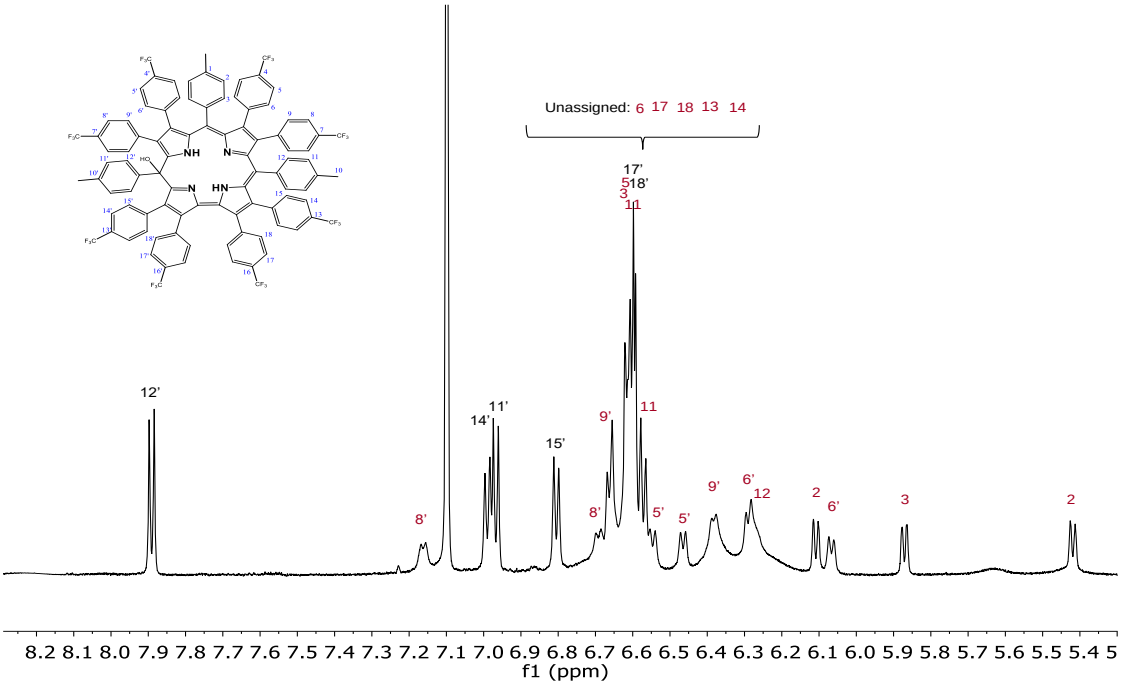

Figure S33. Aromatic region of the ^{1}H NMR spectrum of $H_2[(CF_3)_8Me_3(5\text{-}OH)]$ in benzene-d_6.

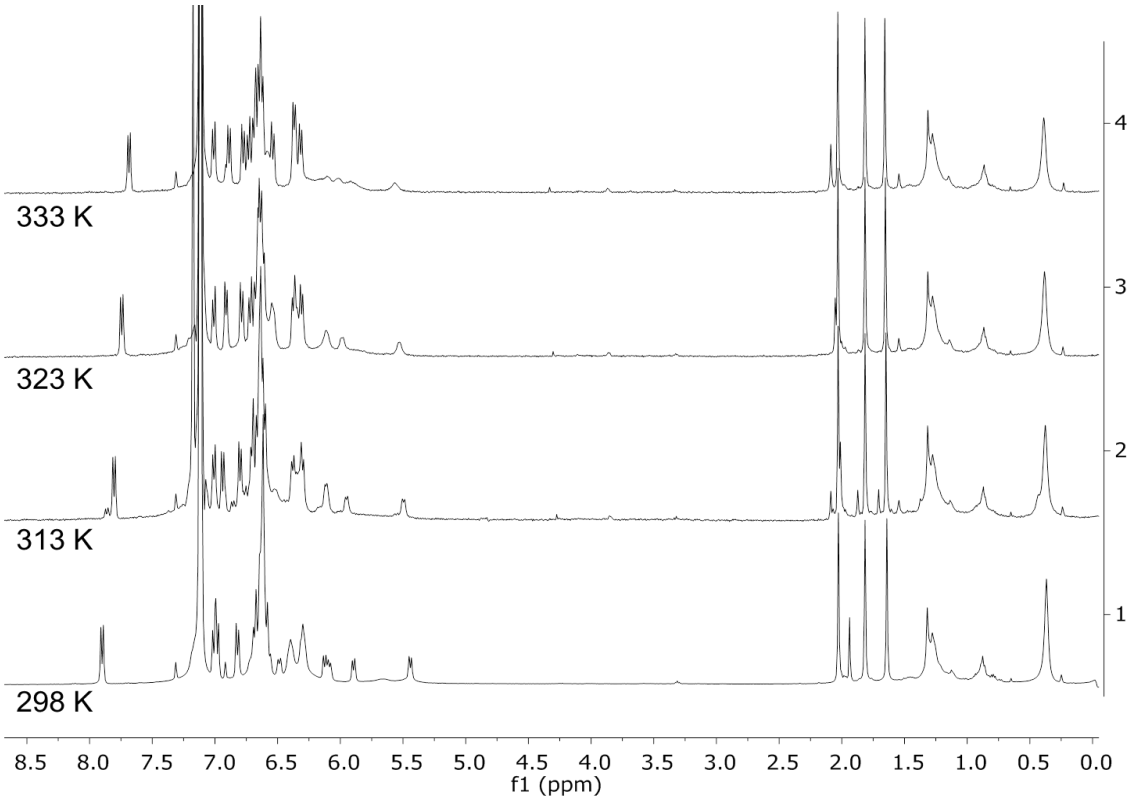

Figure S34. Variable temperature ^{1}H NMR spectra of $H_2[(CF_3)_8Me_3(5\text{-}OH)]$ in benzene-d_6.

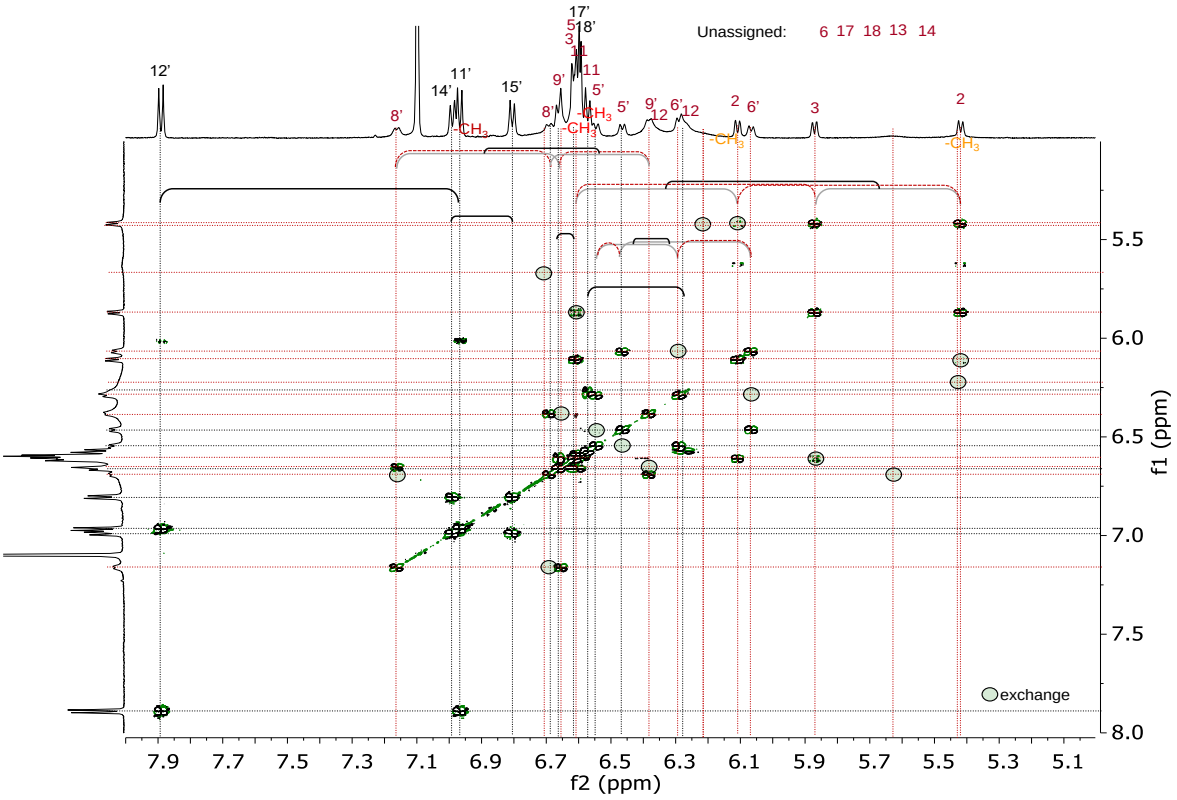

Figure S35. ^{1}H,^{1}H DQFCOSY (benzene-d_6) of $H_2[(CF_3)_8Me_3(5\text{-}OH)]$ for the aromatic region. Exchange peaks from ROESY are shown as circles.

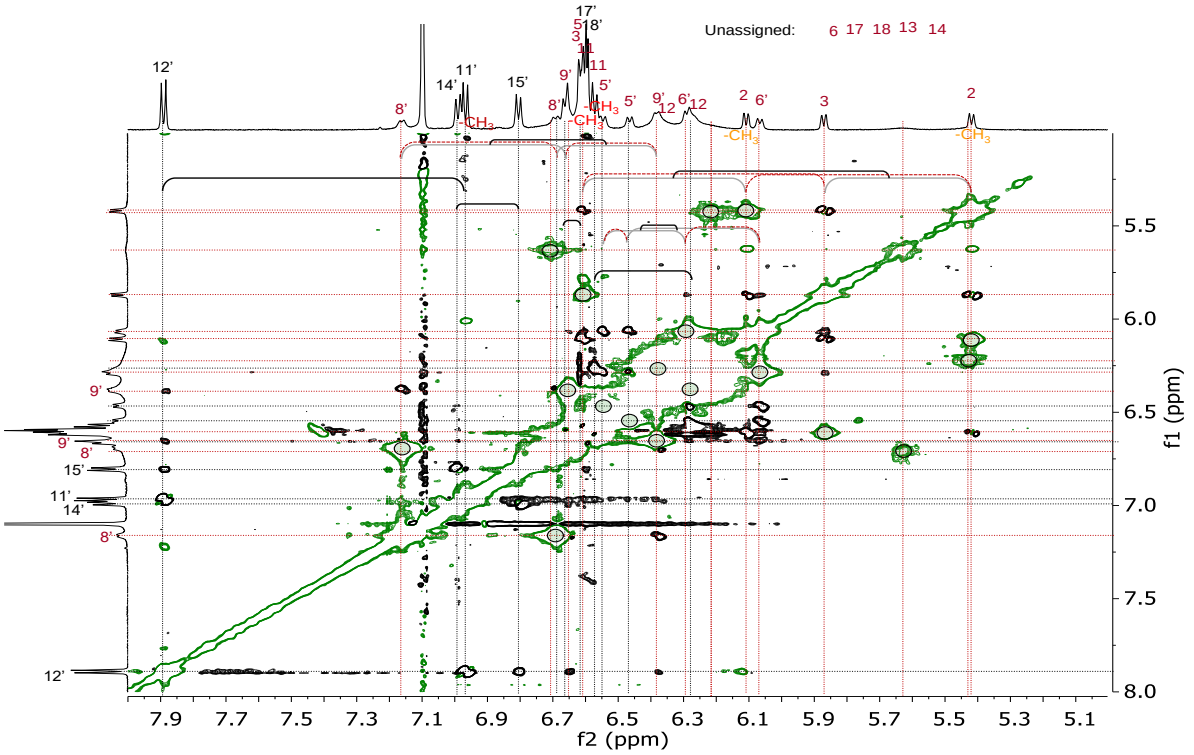

Figure S36. ^{1}H,^{1}H ROESY (300ms, benzene-d_6) of $H_2[(CF_3)_8Me_3(5\text{-}OH)]$ for the aromatic region.

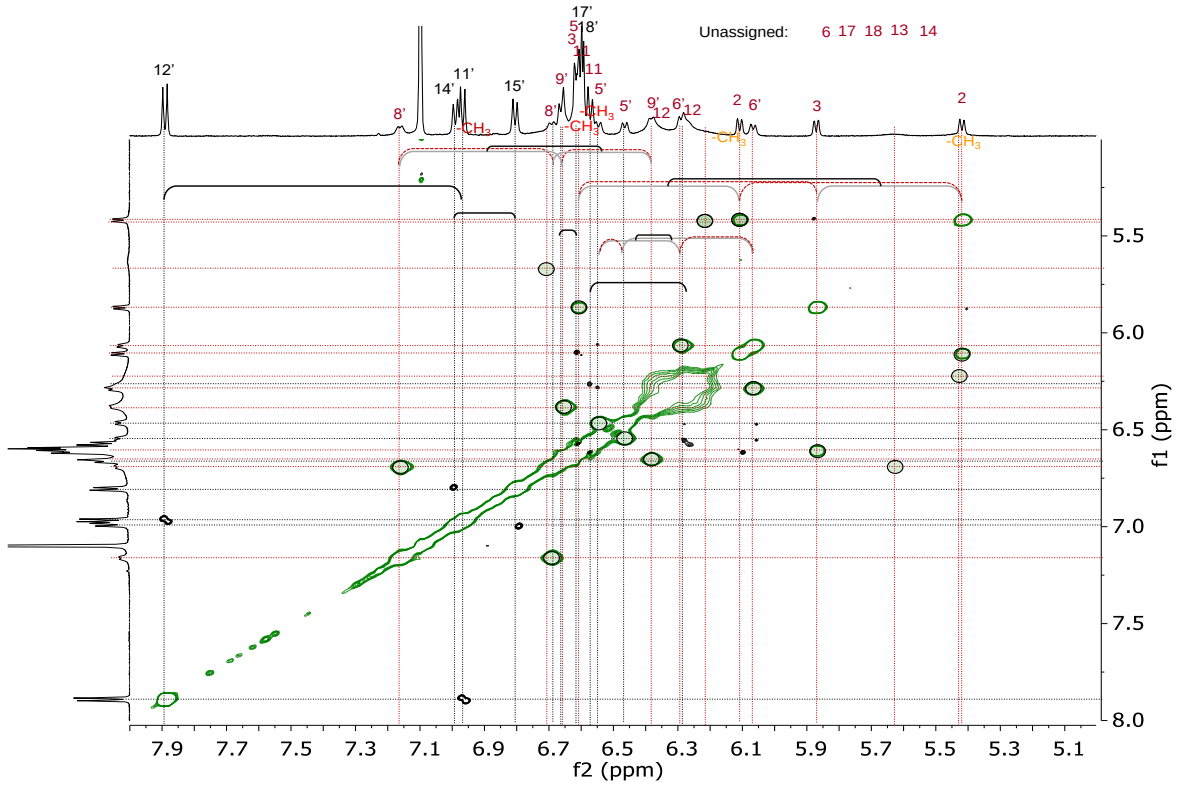

Figure S37. ^{1}H,^{1}H ROESY (300ms, benzene-d_6) of $H_2[(CF_3)_8Me_3(5\text{-}OH)]$ for the aromatic region. Conformational exchange peaks (same sign as diagonal) are shown as circles.

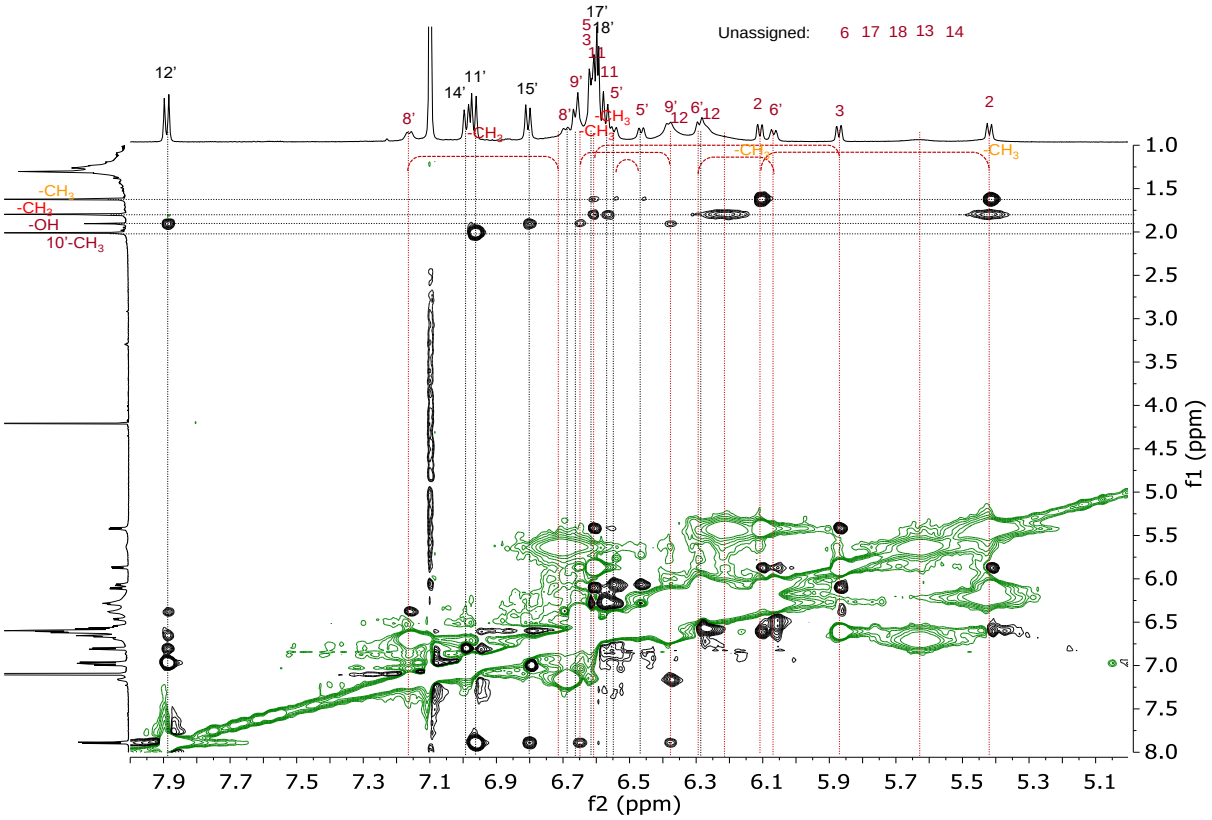

Figure S38. ^{1}H,^{1}H ROESY (300ms, benzene-d_6) of $H_2[(CF_3)_8Me_3(5\text{-}OH)]$ for the aromatic/methyl region.

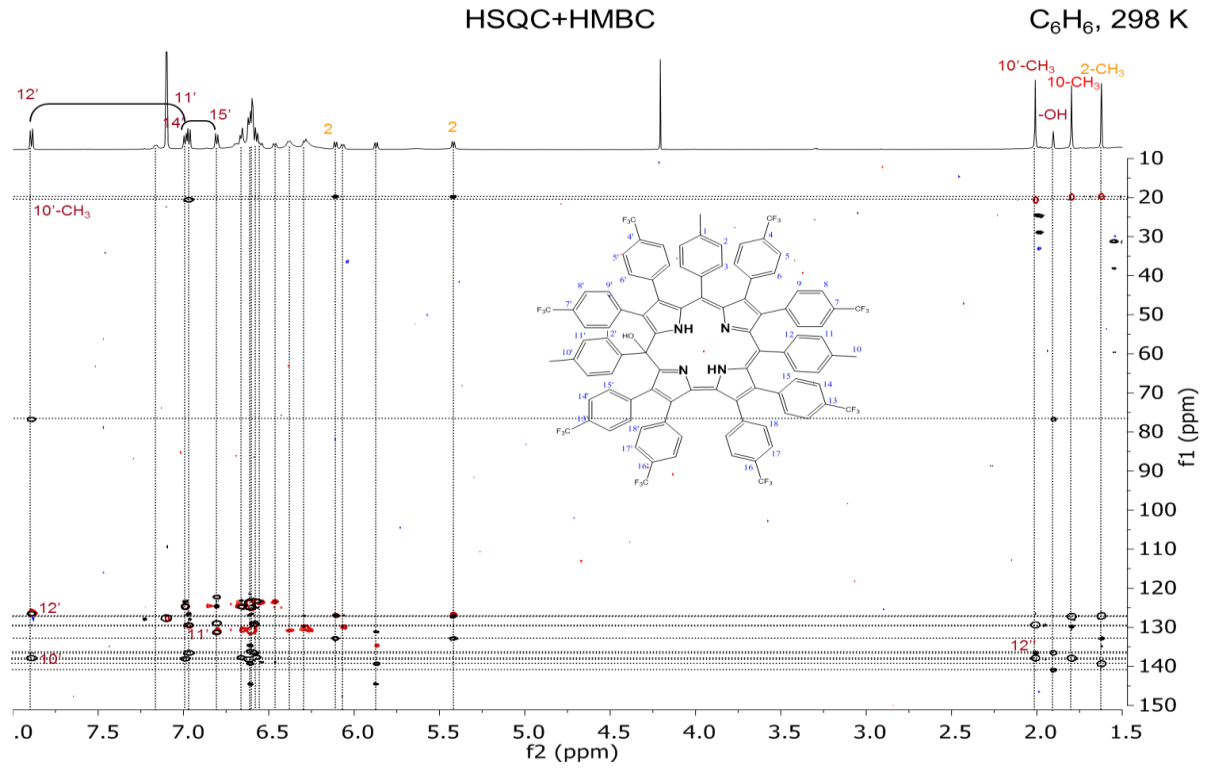

Figure S39. Superimposed ^{1}H,^{13}C HSQC and HMBC spectra (in benzene-d_6) of $H_2[(CF_3)_8Me_3(5\text{-}OH)]$.

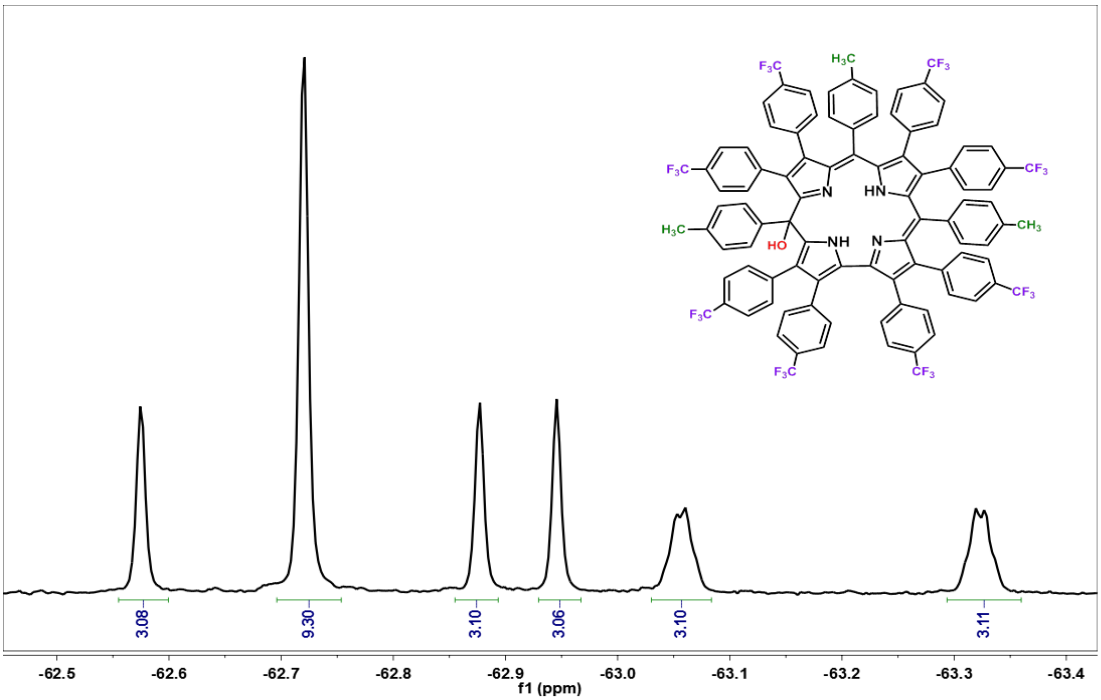

Figure S40. ^{19}F NMR spectrum of $H_2[(CF_3)_8Me_3(5\text{-}OH)]$ in benzene-d_6 at 333K.

NMR spectra of $H_2[(CF_3)_8Me_3(10\text{-}OH)]$

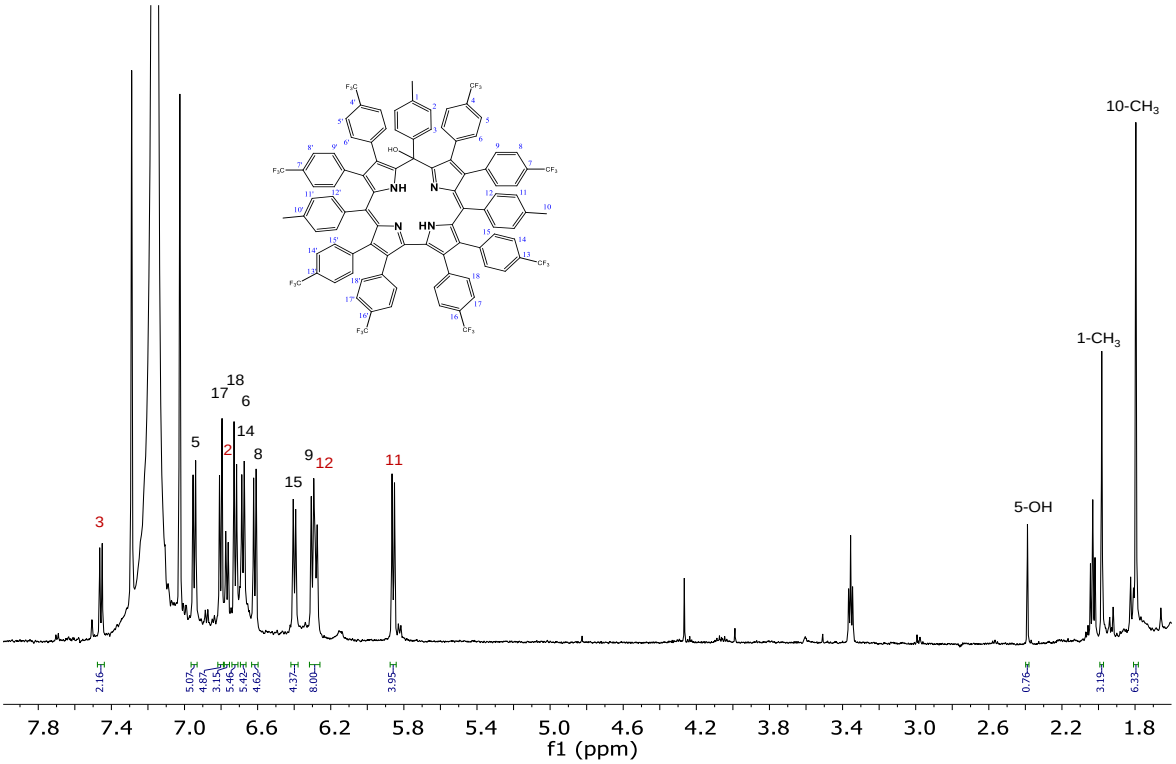

Figure S41. ^{1}H NMR spectrum of $H_2[(CF_3)_8Me_3(10\text{-}OH)]$ in benzene-d_6.

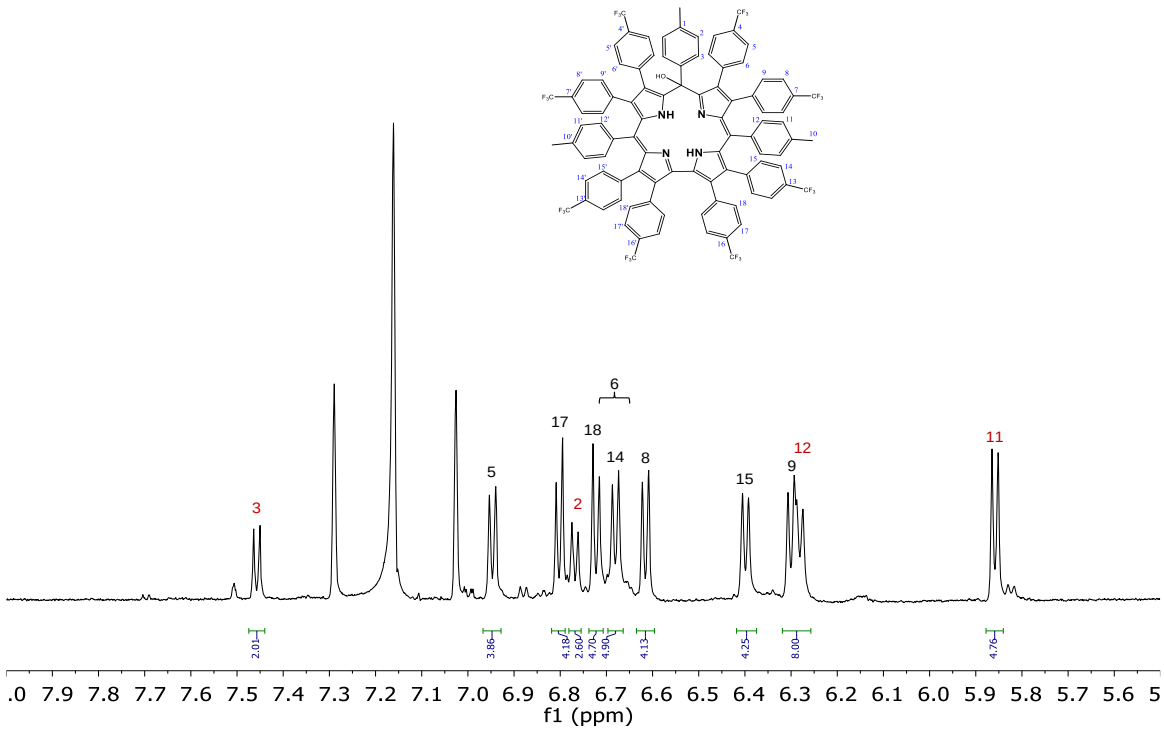

Figure S42. Aromatic region of the ^{1}H NMR spectrum of $H_2[(CF_3)_8Me_3(10\text{-}OH)]$ in benzene-d_6.

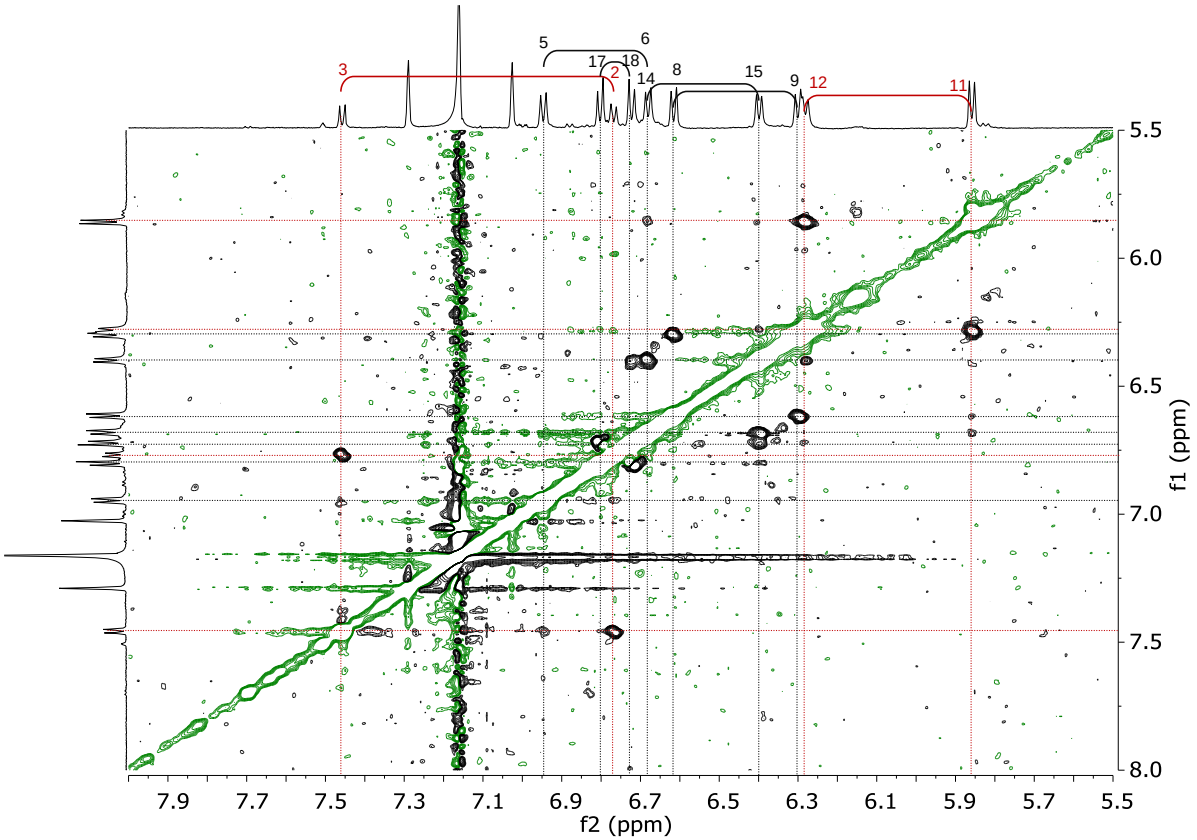

Figure S43. ^{1}H,^{1}H ROESY (300ms, benzene-d_6) of $H_2[(CF_3)_8Me_3(10\text{-}OH)]$ for the aromatic region.

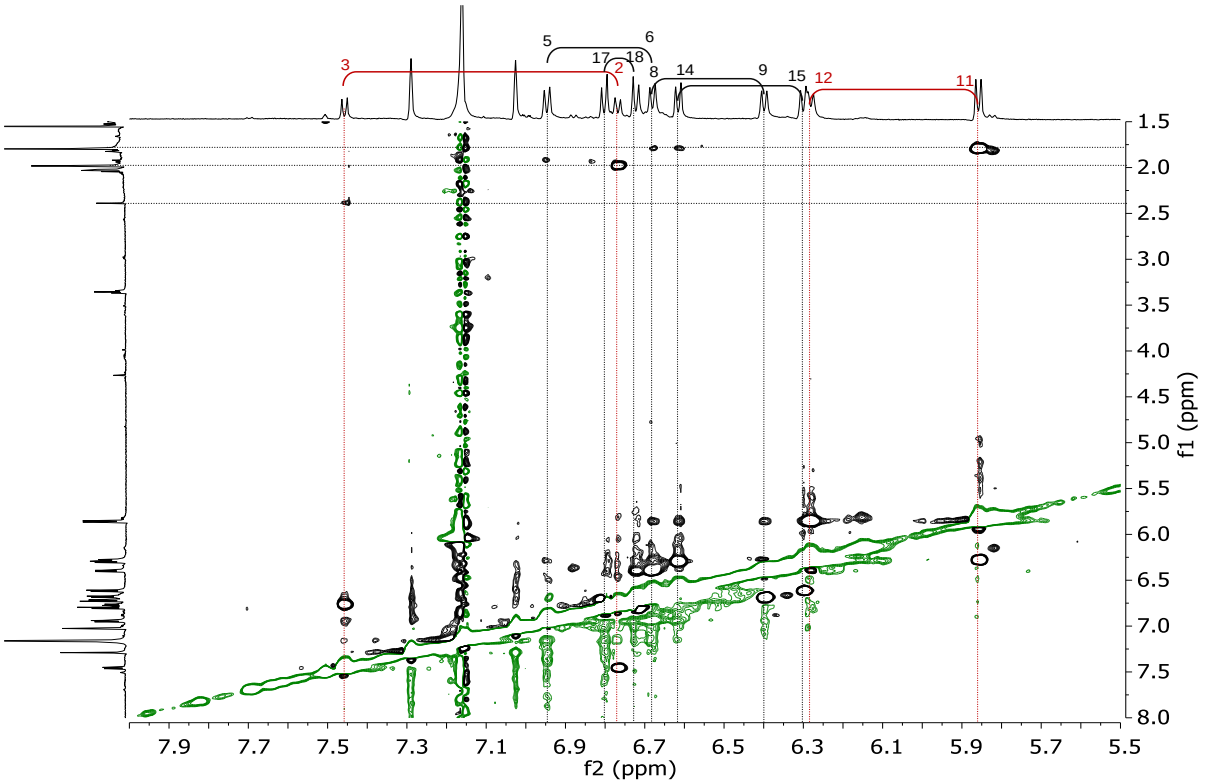

Figure S44. ^{1}H,^{1}H ROESY (300ms, benzene-*d*$_6$) of $H_2[(CF_3)_8Me_3(10\text{-}OH)]$ for the aromatic/methyl region.

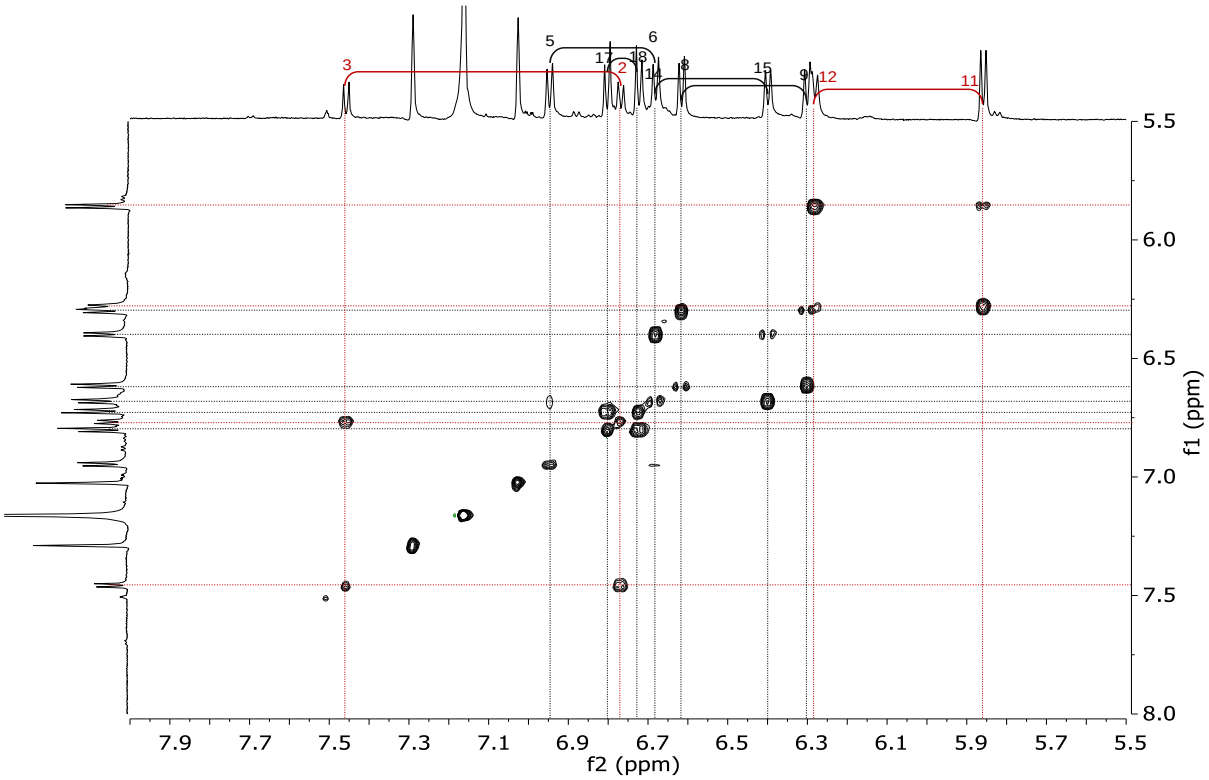

Figure S45. ^{1}H,^{1}H TOCSY (80ms, benzene-*d*$_6$) of $H_2[(CF_3)_8Me_3(10\text{-}OH)]$ for the aromatic region.

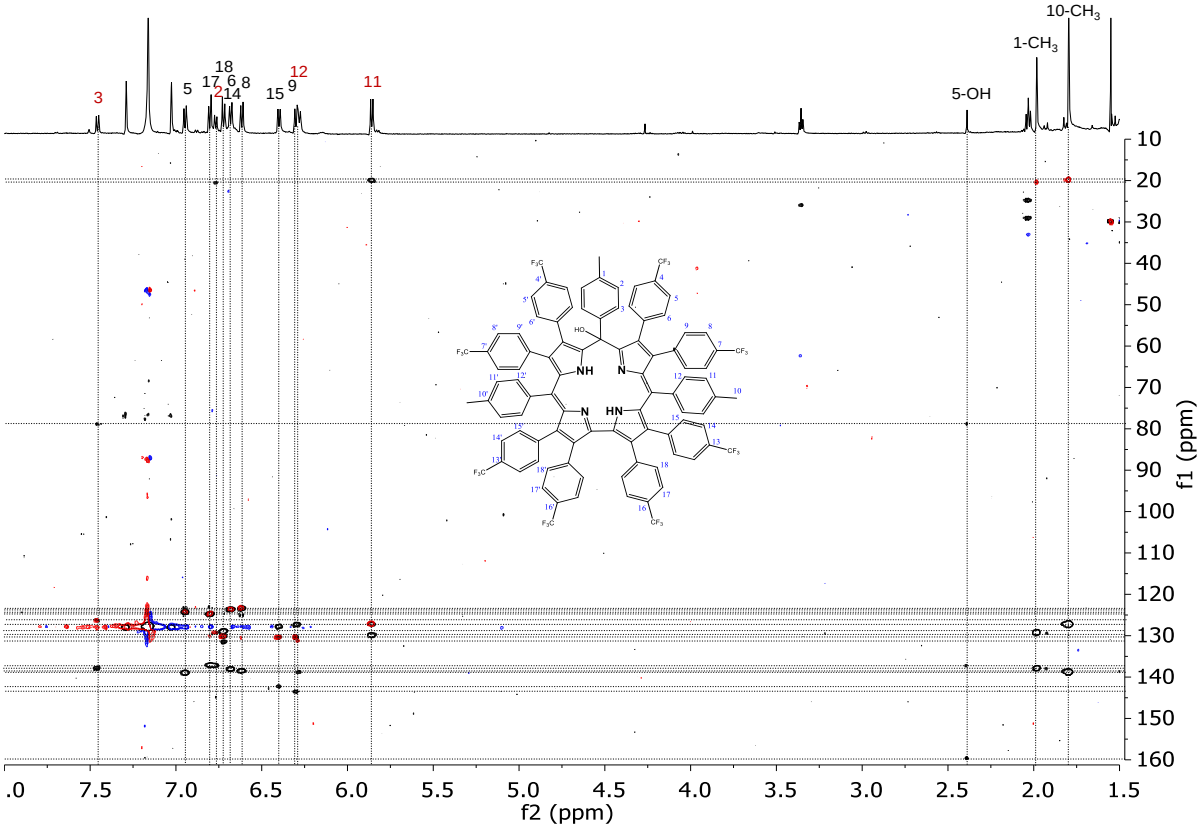

Figure S46. Superimposed ^{1}H,^{13}C HSQC and HMBC spectra (in benzene-d_6) of $H_2[(CF_3)_8Me_3(10\text{-}OH)]$.

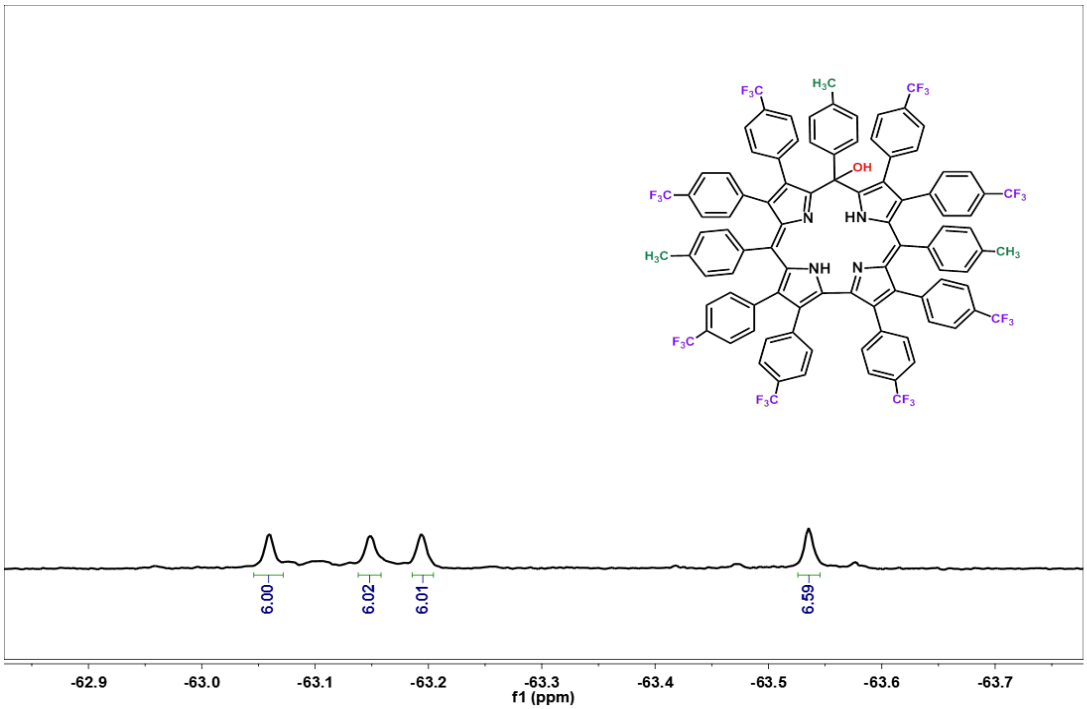

Figure S47. ^{19}F NMR spectrum of $H_2[(CF_3)_8Me_3(10\text{-}OH)]$ in $CDCl_3$ at 298 K.

NMR spectra of $H_2[H_8Me_3(5\text{-}OH)]$

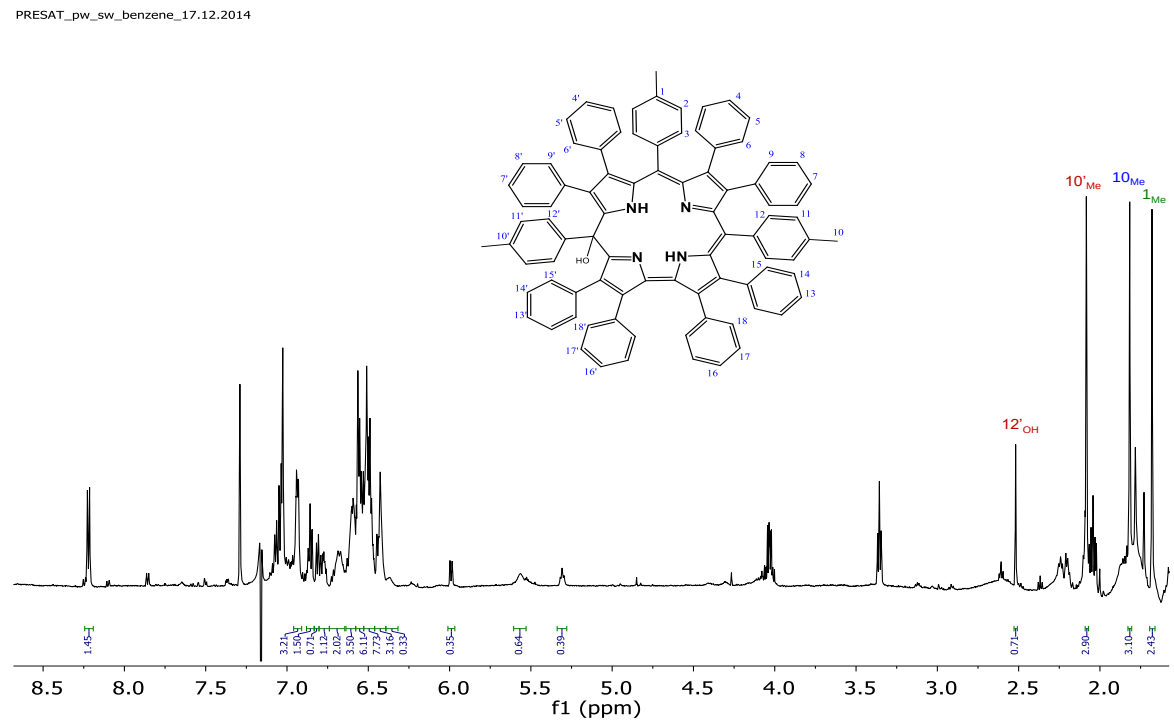

Figure S48. ^{1}H NMR spectrum of $H_2[H_8Me_3(5\text{-}OH)]$ in benzene-d_6.

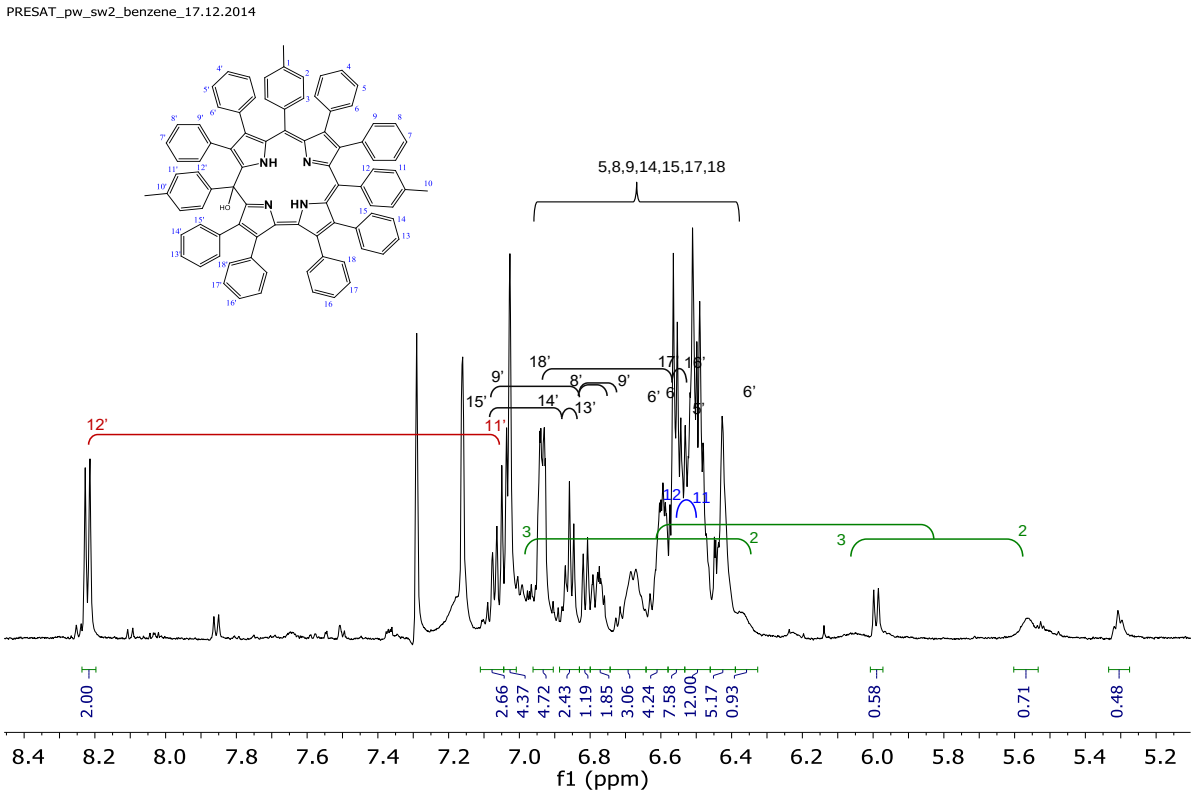

Figure S49. Aromatic region of the ^{1}H NMR spectrum of $H_2[H_8Me_3(5\text{-}OH)]$ in benzene-d_6.

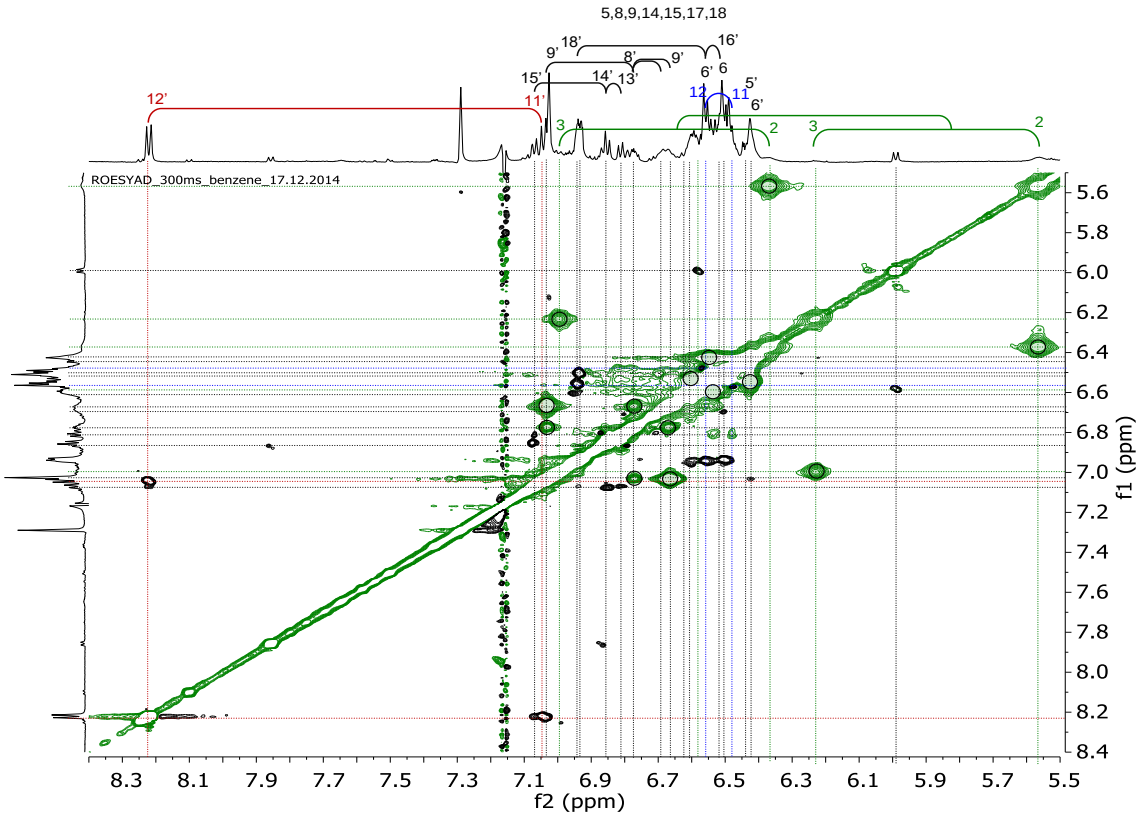

Figure S50. ^{1}H,^{1}H ROESY (300ms, benzene-d_6) of $H_2[H_8Me_3(5\text{-}OH)]$ for the aromatic region. Conformational exchange peaks (same sign as diagonal) are shown as circles.

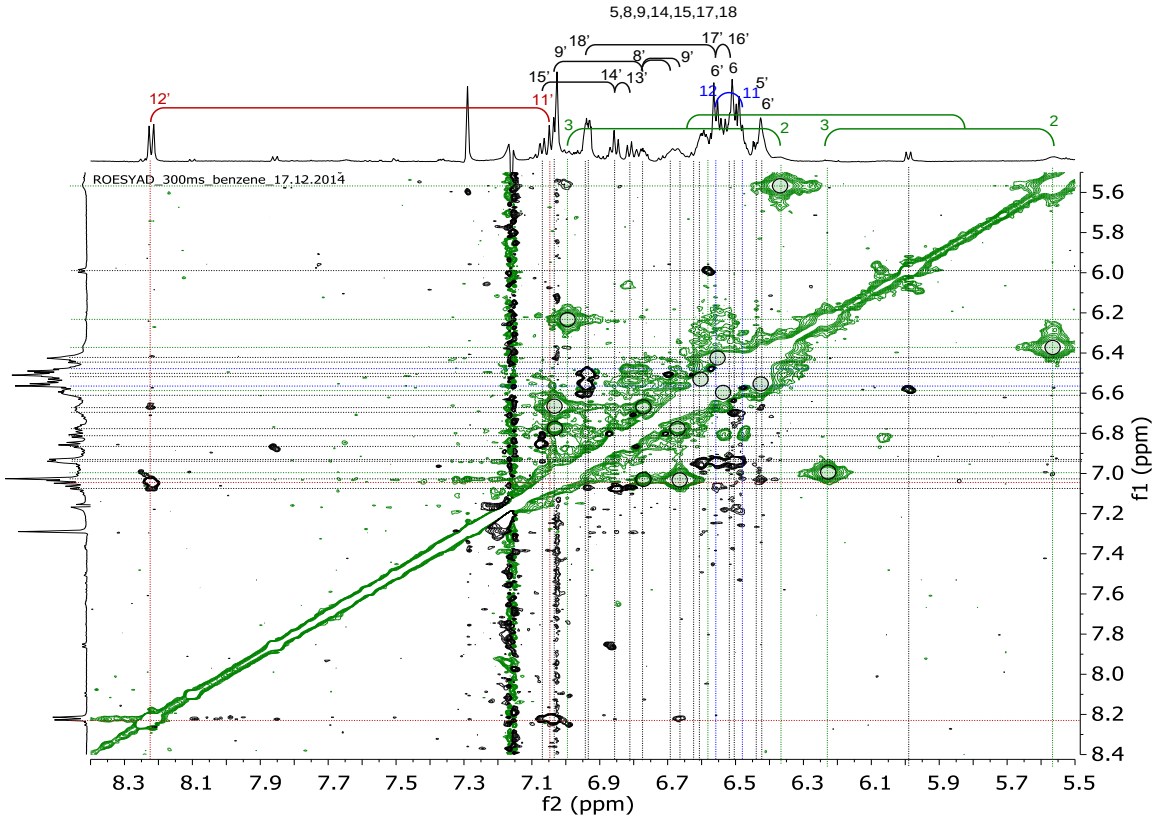

Figure S51.^{1}H,^{1}H ROESY (300ms, benzene-d_6) of $H_2[H_8Me_3(5\text{-}OH)]$. Conformational exchange peaks from ROESY are shown as circles.

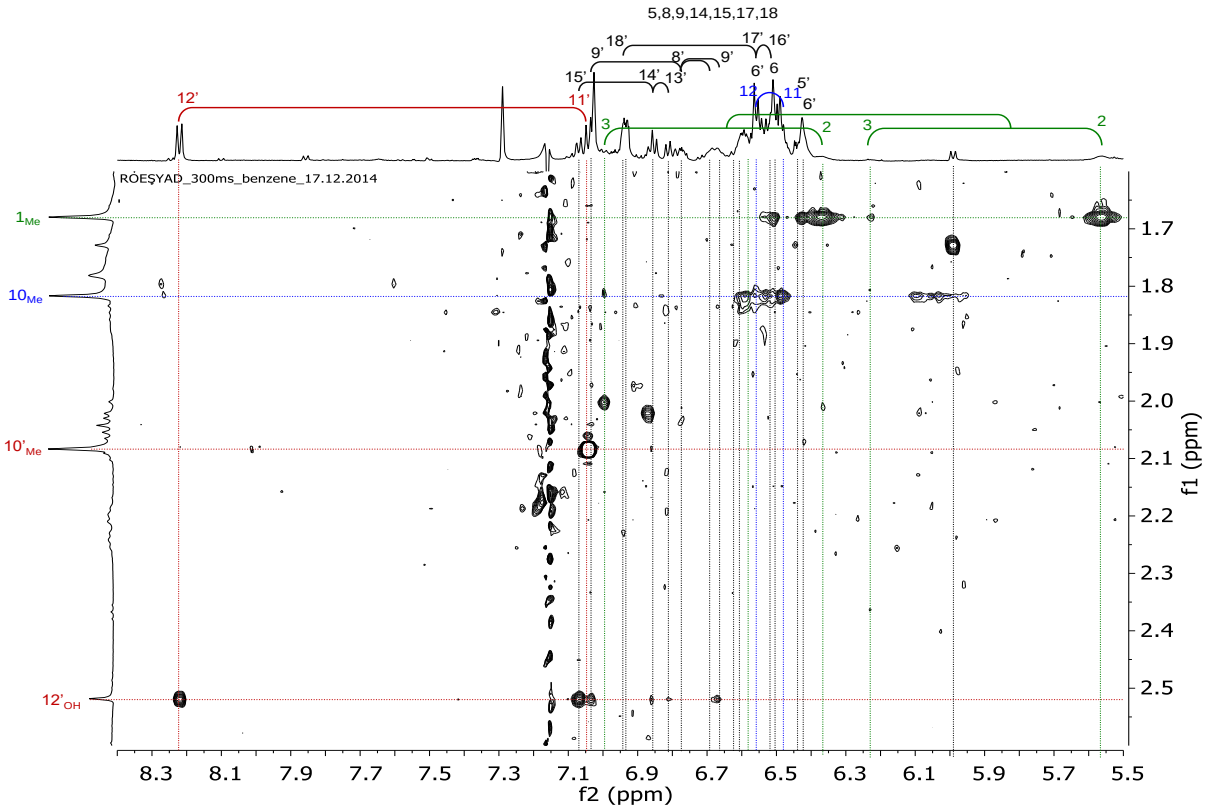

Figure S52. ^{1}H,^{1}H ROESY (300ms, benzene-d_6) of H_2[H_8Me_3(5-OH)] for the aromatic/methyl region.

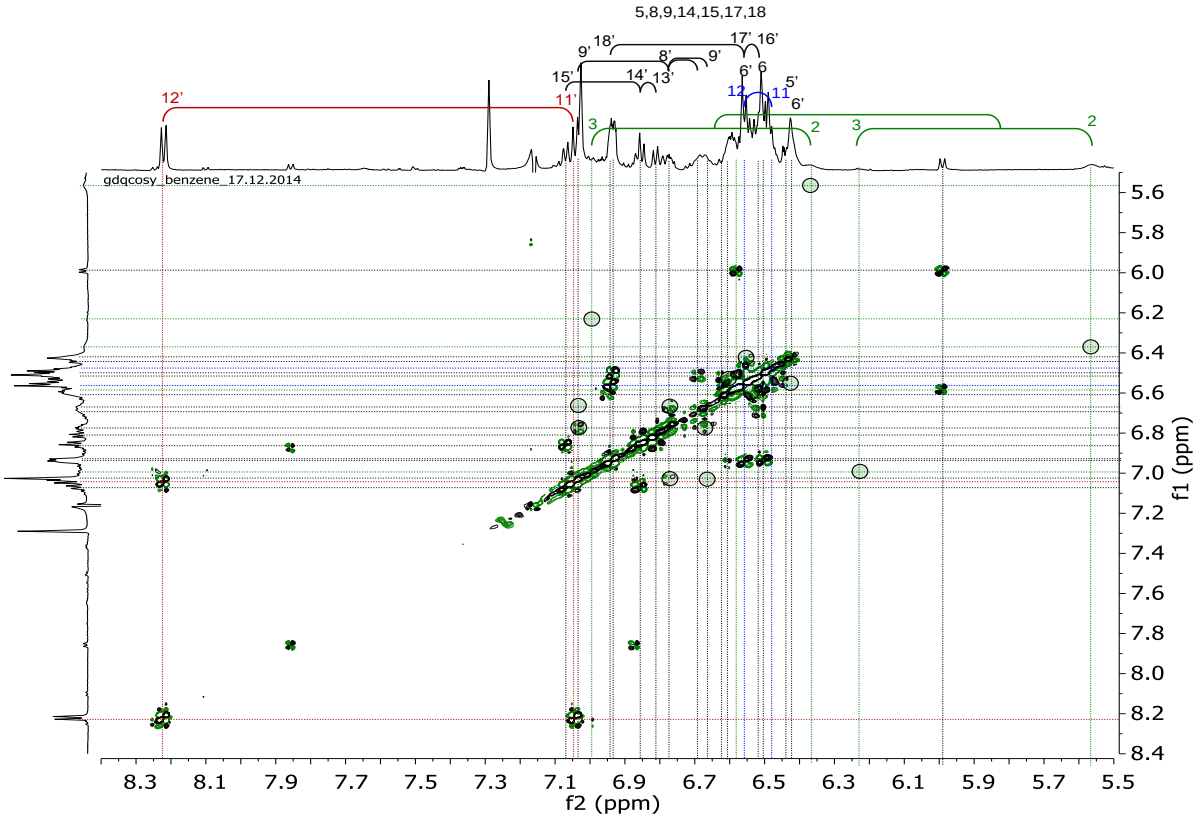

Figure S53 ^{1}H,^{1}H DQFCOSY (benzene-d_6) of H_2[H_8Me_3(5-OH)]. Conformational exchange peaks from ROESY are shown as circles.

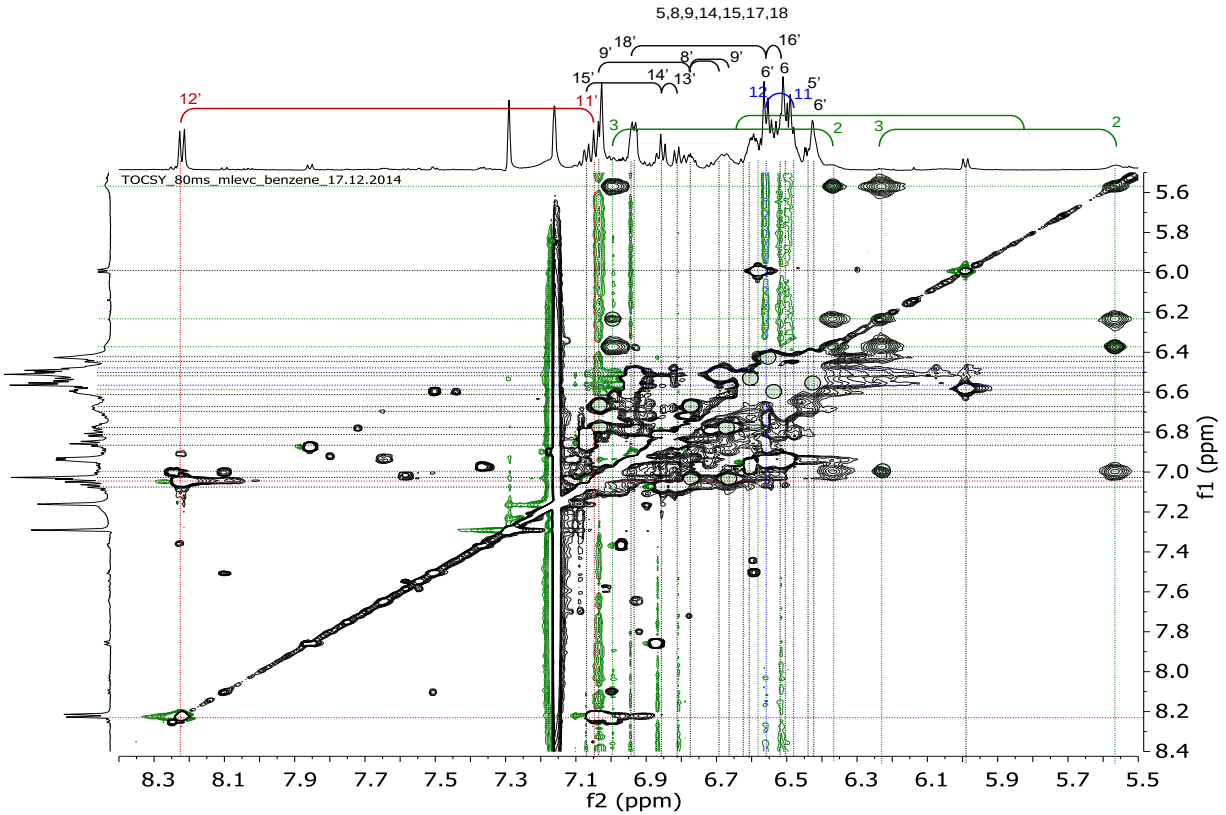

Figure S54. ^{1}H,^{1}H TOCSY (80ms, benzene-*d*$_6$) of $H_2[H_8Me_3(5\text{-}OH)]$. Conformational exchange peaks from ROESY are shown as circles.

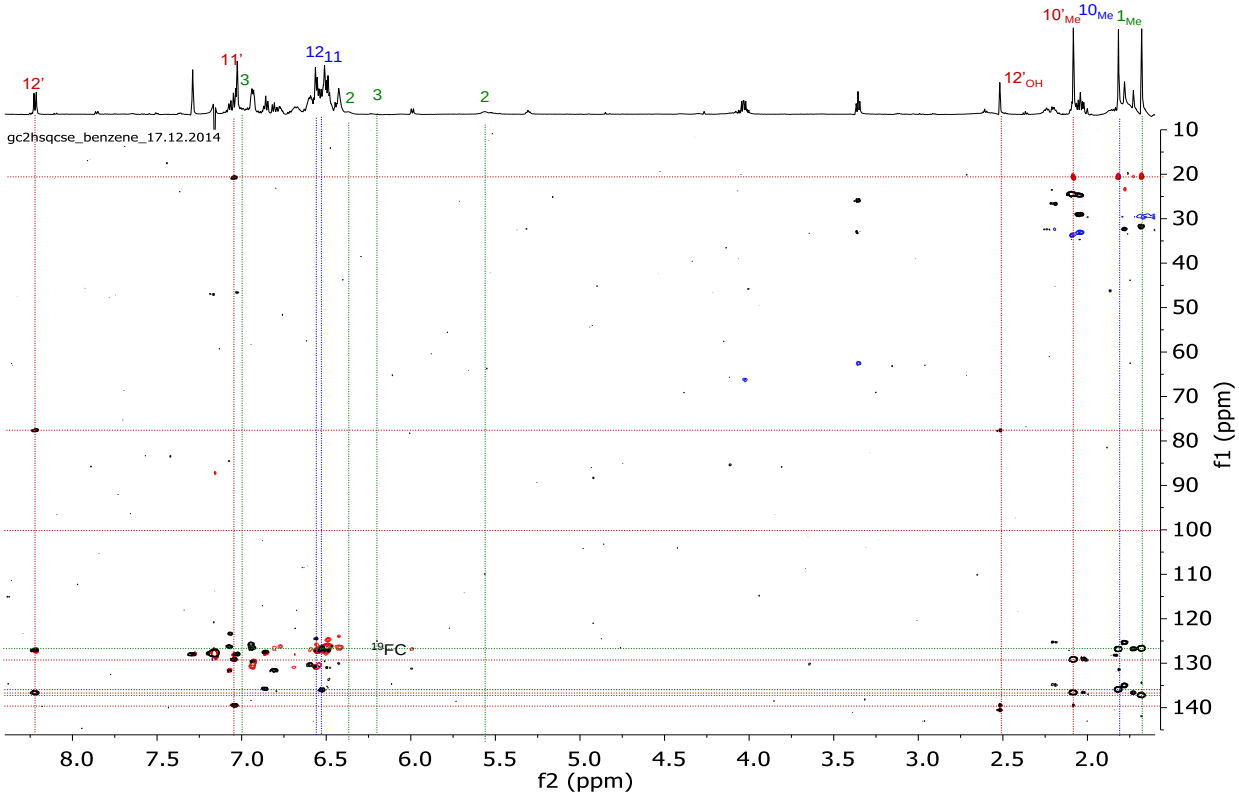

Figure S55. Superimposed ^{1}H,^{13}C HSQC and HMBC (in benzene-*d*$_6$) spectra of $H_2[H_8Me_3(5\text{-}OH)]$.

NMR spectra of $H_2[(CF_3)_8H_3(5\text{-}OH)]$

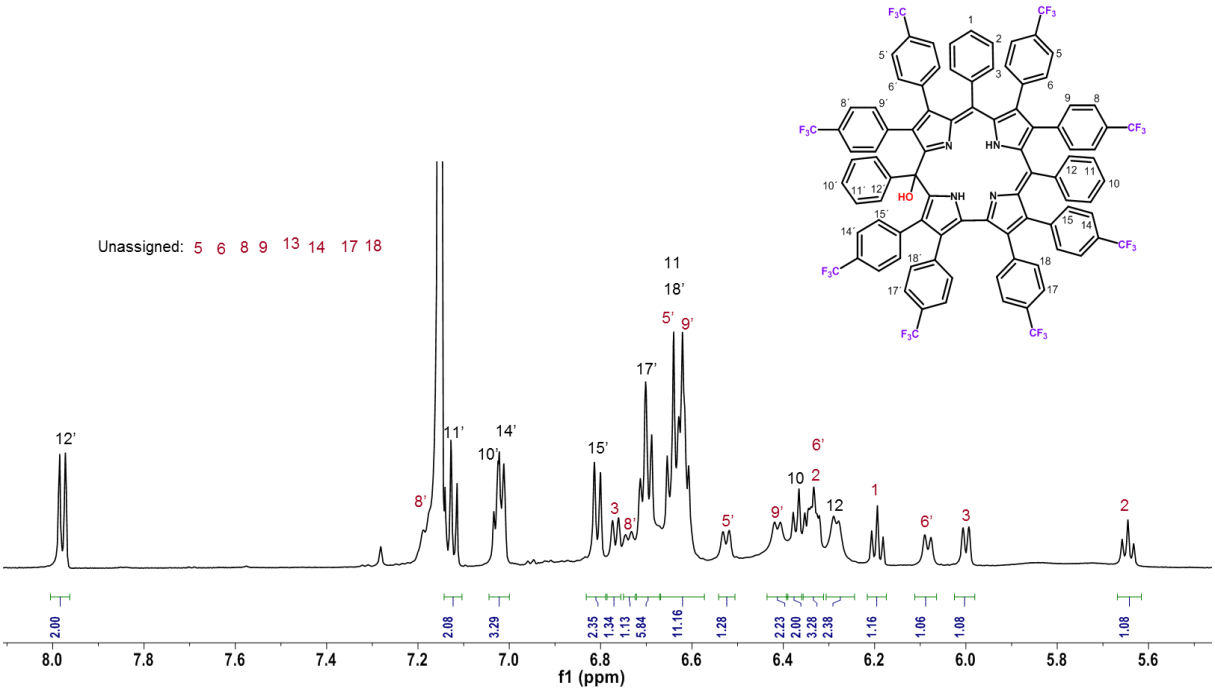

Figure S56. ^{1}H NMR spectrum of $H_2[(CF_3)_8H_3(5\text{-}OH)]$in benzene-$d_6$.

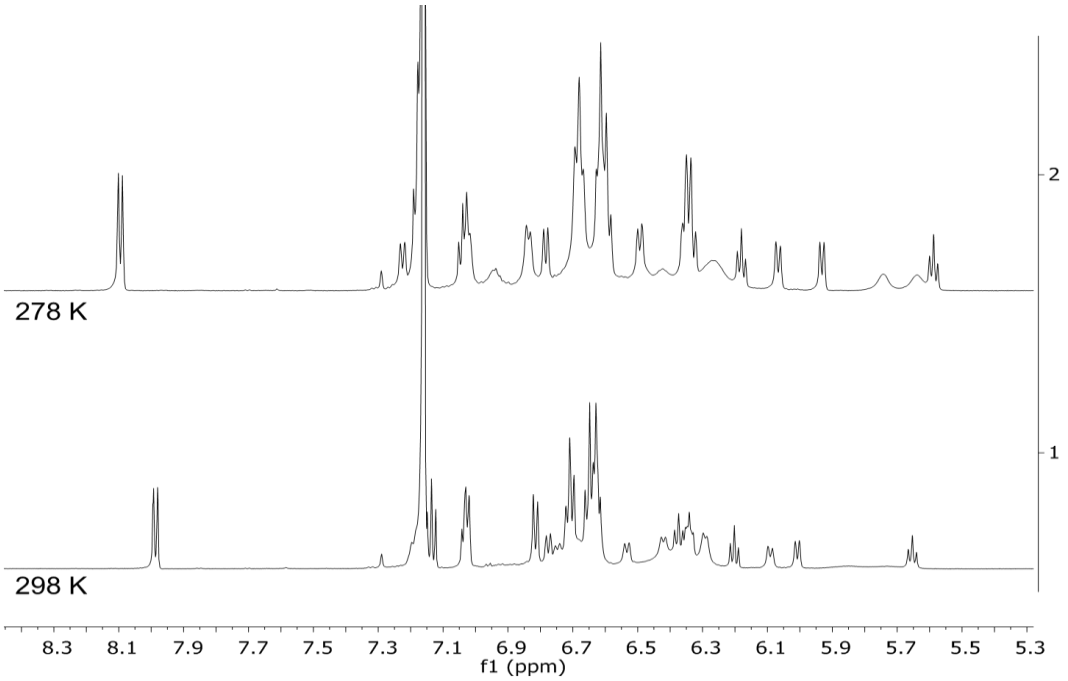

Figure S57. Variable temperature ^{1}H NMR spectra of $H_2[(CF_3)_8H_3(5\text{-}OH)]$in benzene-$d_6$.

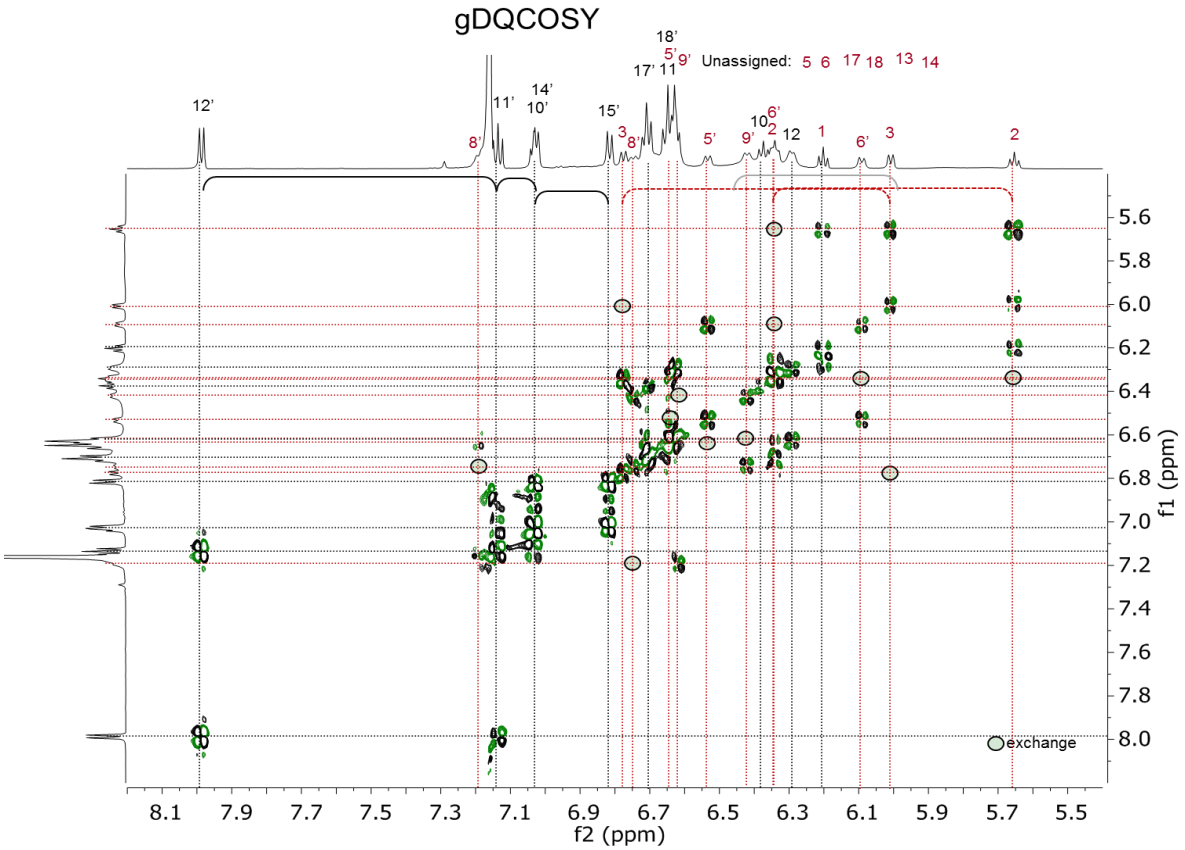

Figure S58. ^{1}H,^{1}H DQFCOSY (in benzene-*d*$_6$) of $H_2[(CF_3)_8H_3(5\text{-}OH)]$. Conformational exchange peaks from ROESY are shown as circles.

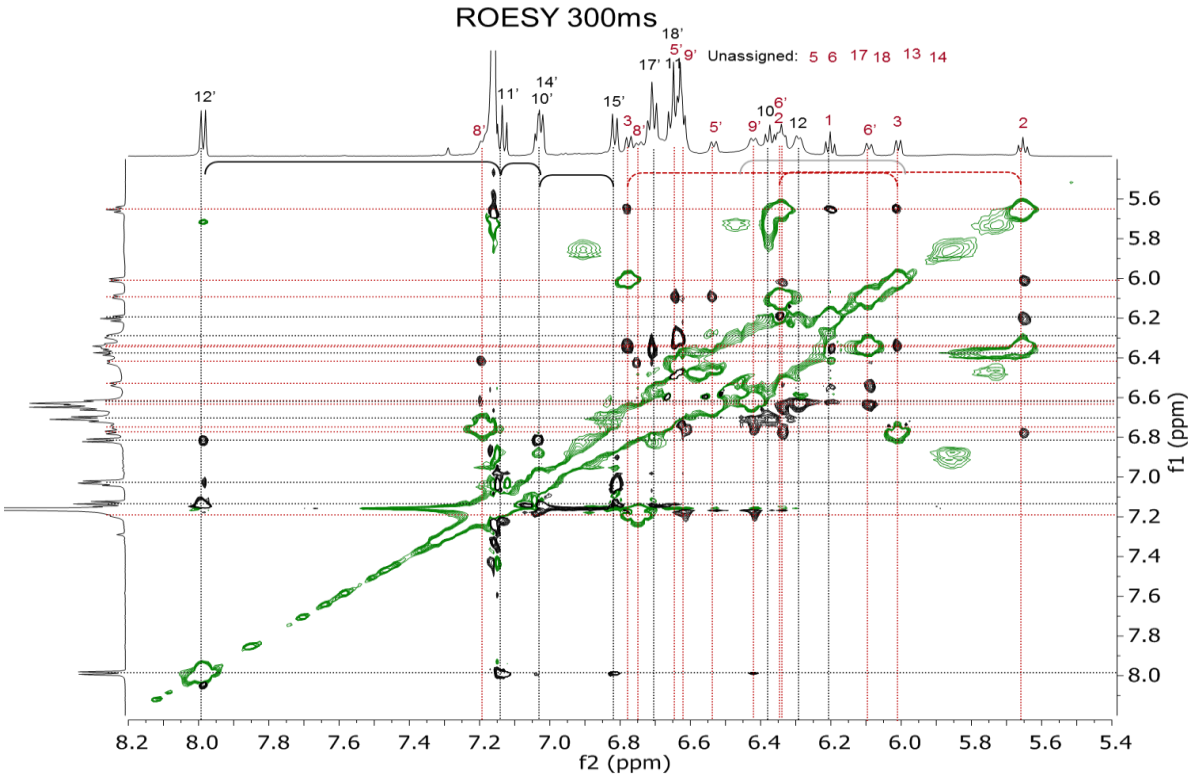

Figure S59. ^{1}H,^{1}H ROESY (300ms, benzene-*d*$_6$) of $H_2[(CF_3)_8H_3(5\text{-}OH)]$.

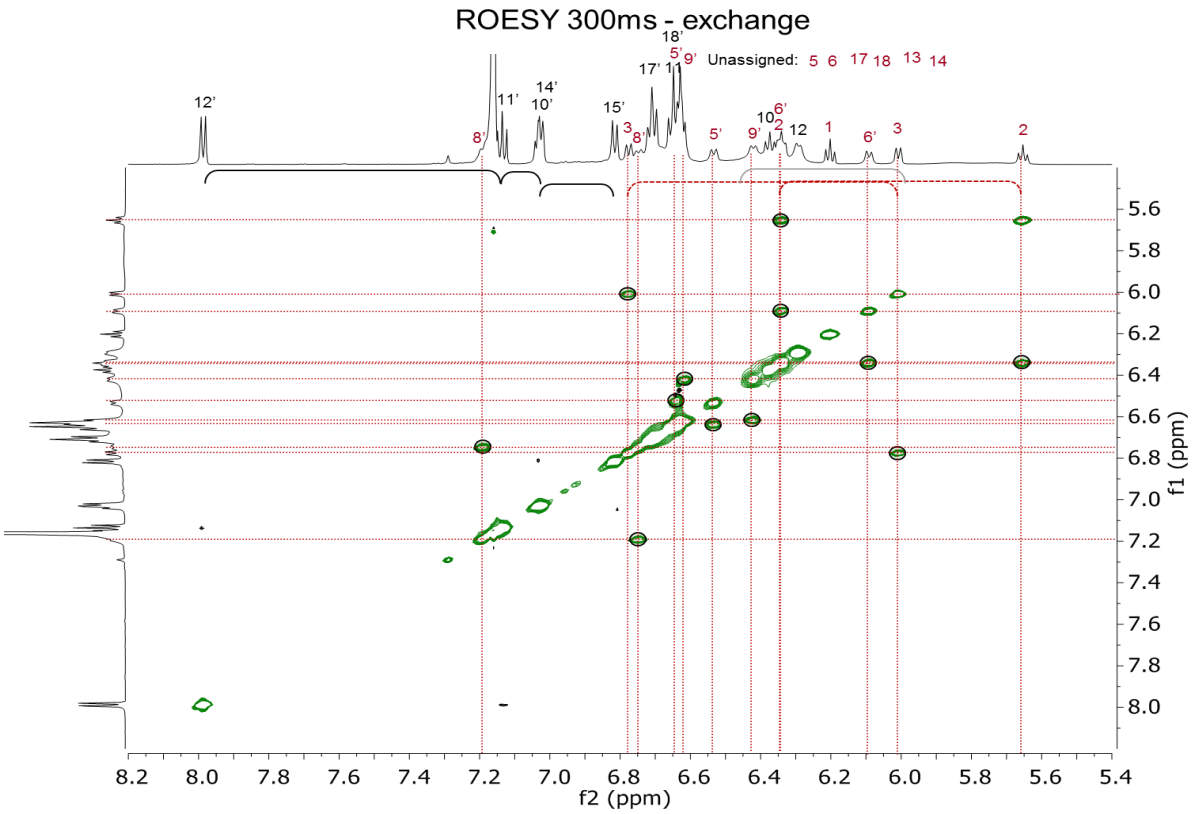

Figure S60. ^{1}H,^{1}H ROESY (300ms, benzene-d_6) of $H_2[(CF_3)_8H_3(5\text{-}OH)]$. Conformational exchange peaks are shown in circles.

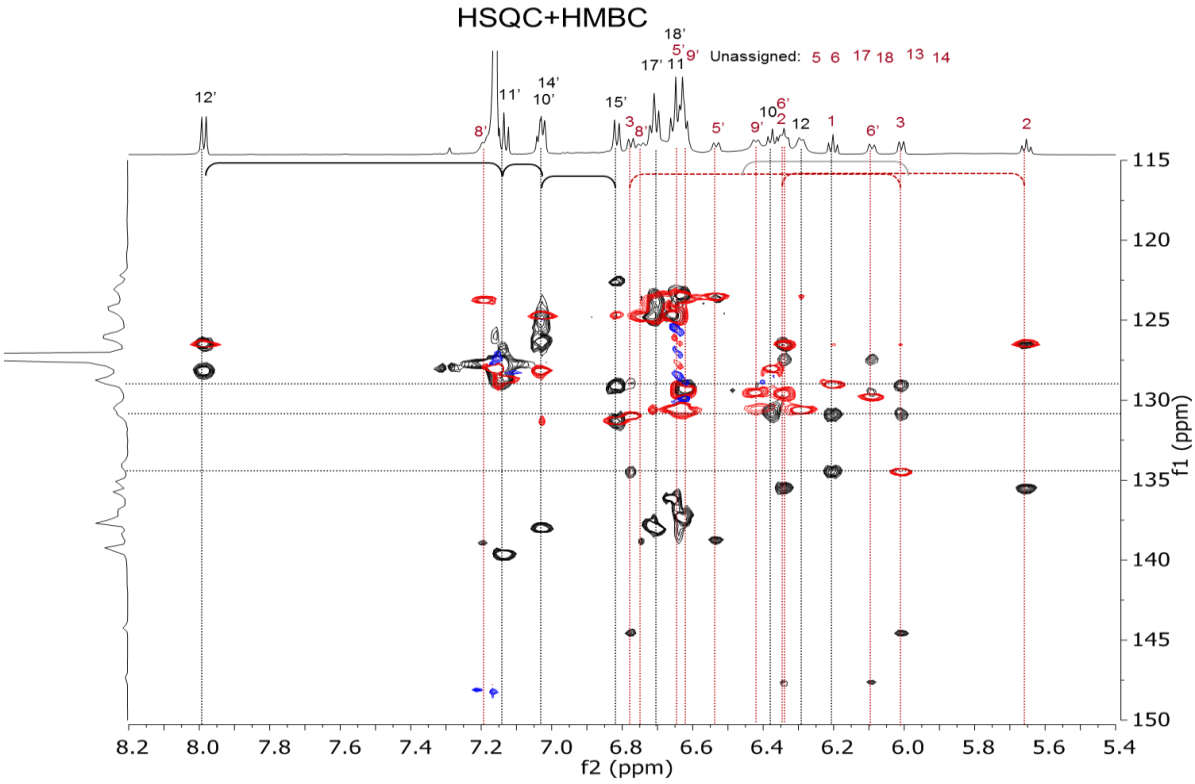

Figure S61. Superimposed ^{1}H,^{13}C HSQC and HMBC spectra (in benzene-d_6) of $H_2[(CF_3)_8H_3(5\text{-}OH)]$.

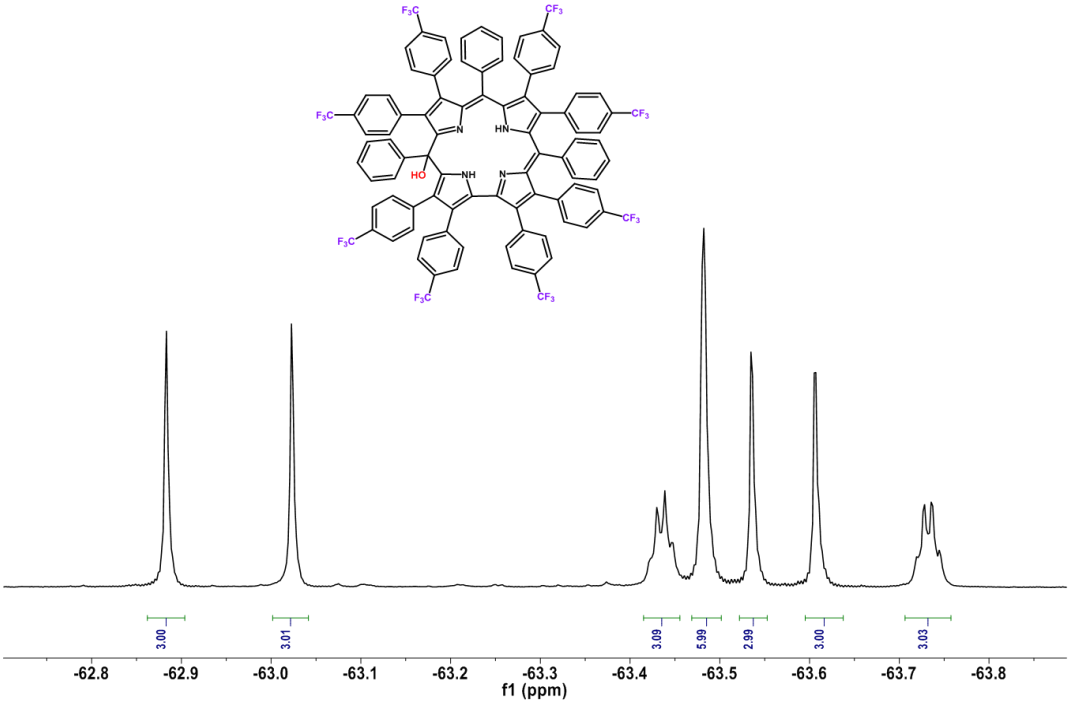

Figure S62. ^{19}F NMR spectrum of $H_2[(CF_3)_8H_3(5\text{-}OH)]$in benzene-$d_6$.

(c) HR-MS of free base undecaarylisocorroles

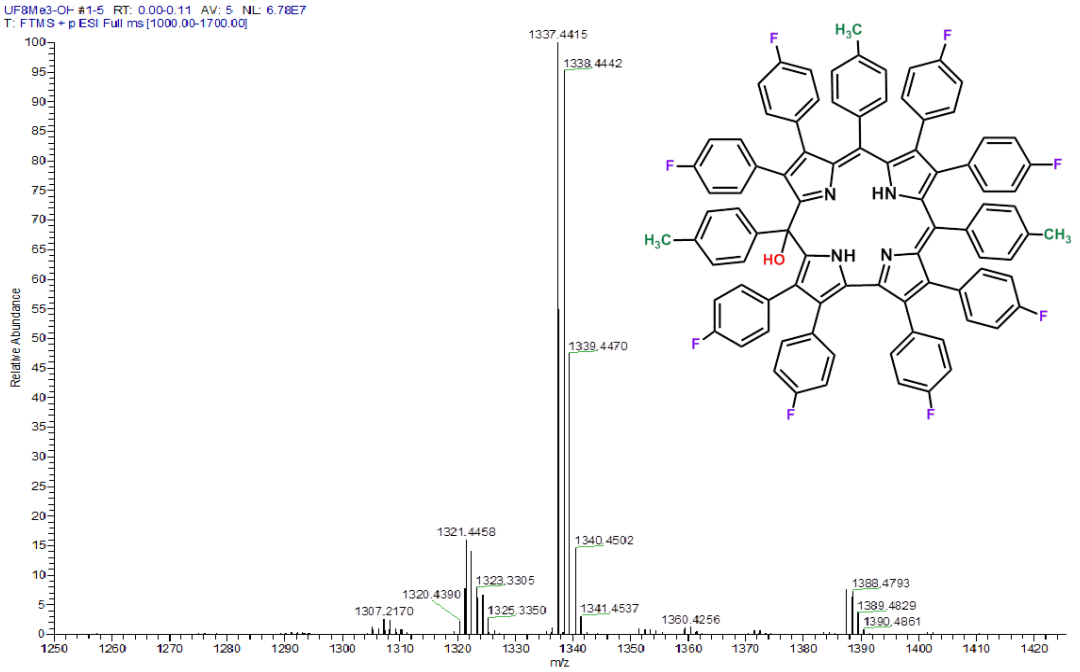

Figure S63. HR-ESI mass spectrum of $H_2[F_8Me_3(5\text{-}OH)]$.

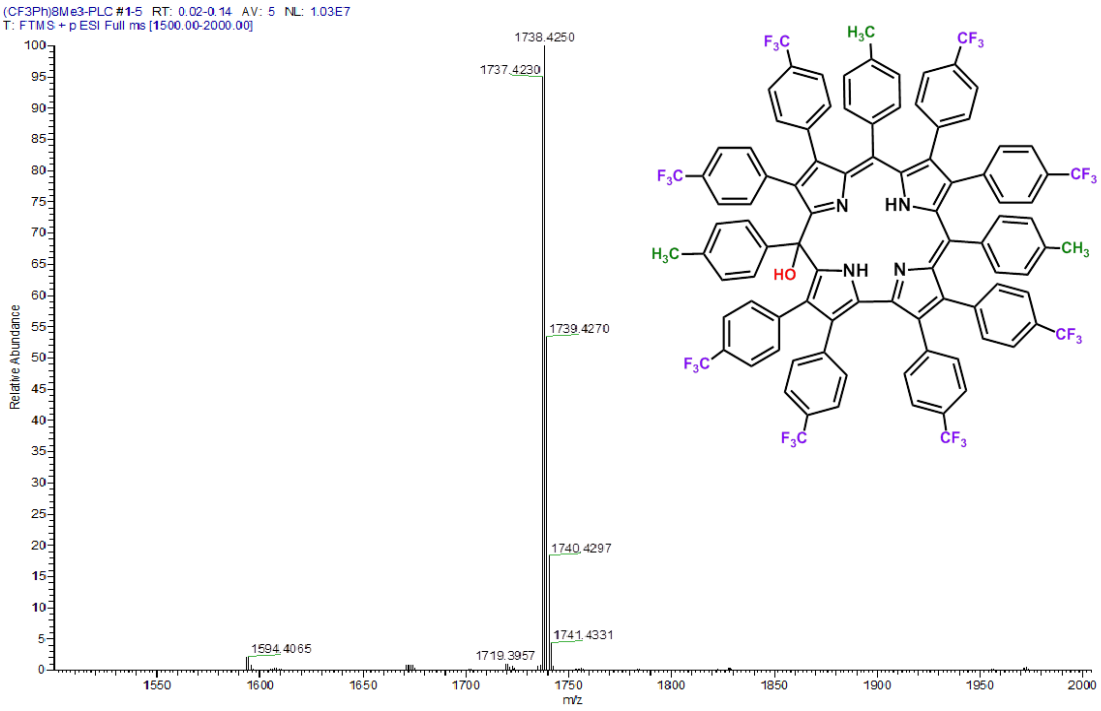

Figure S64. HR-ESI mass spectrum of $H_2[(CF_3)_8Me_3(5\text{-}OH)]$.

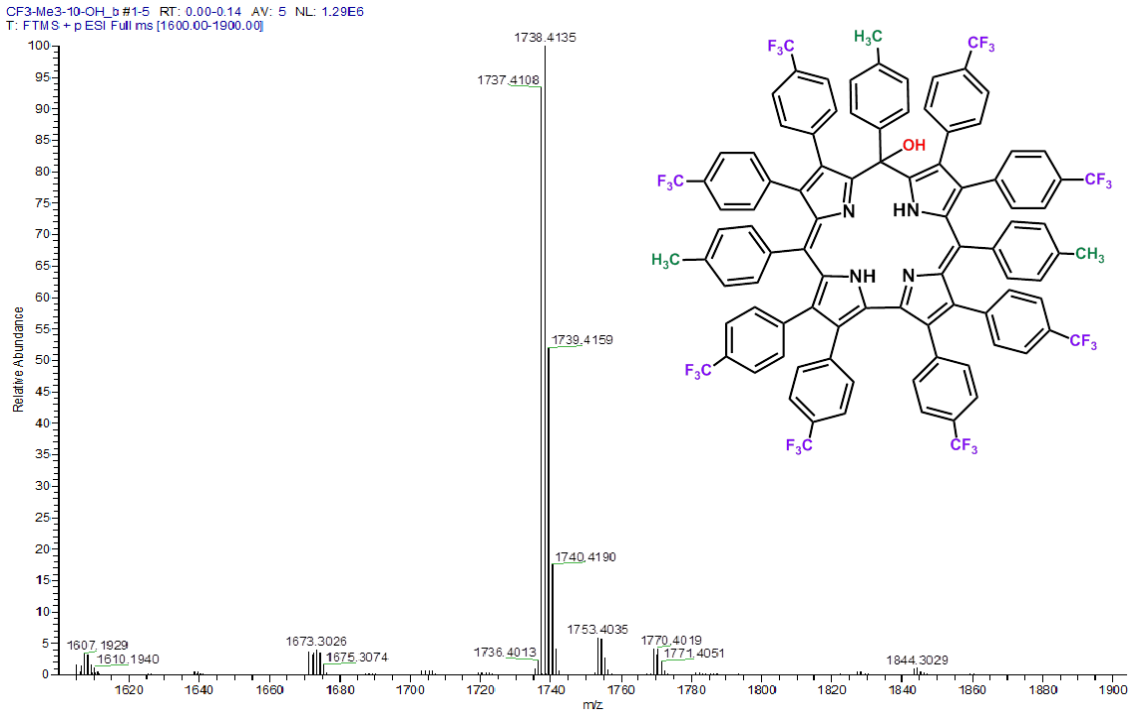

Figure S65. HR-ESI mass spectrum of $H_2[(CF_3)_8Me_3(10\text{-}OH)]$.

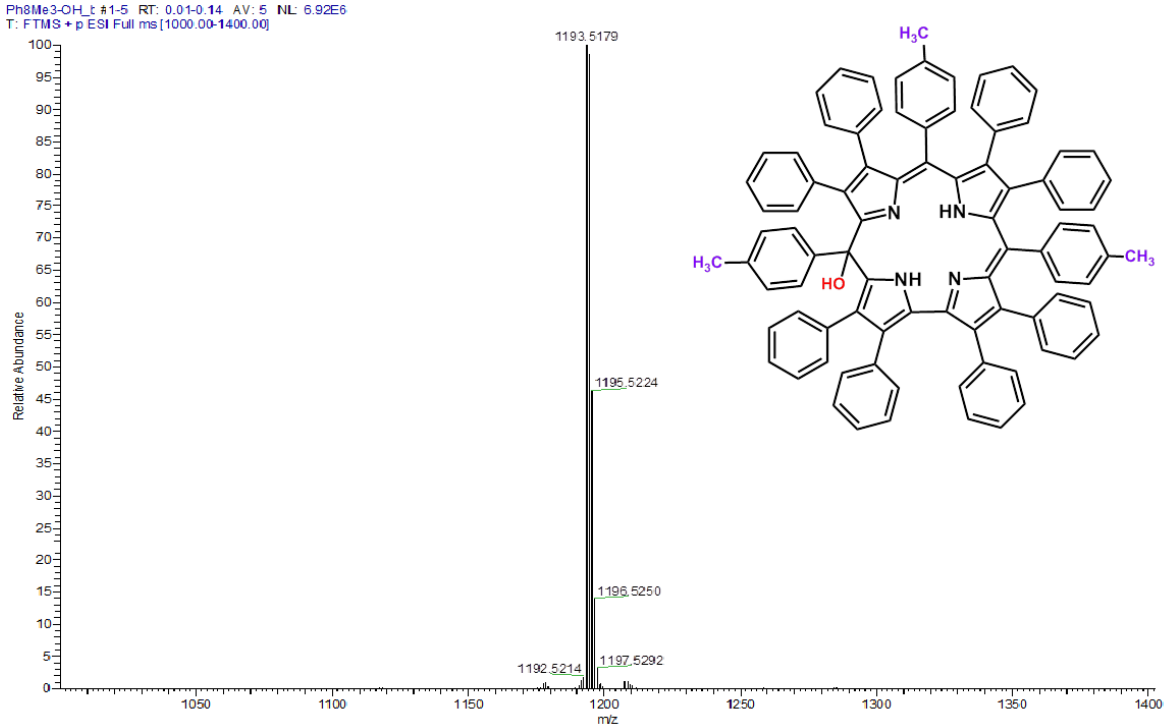

Figure S66. HR-ESI mass spectrum of $H_2[H_8Me_3(5\text{-}OH)]$.

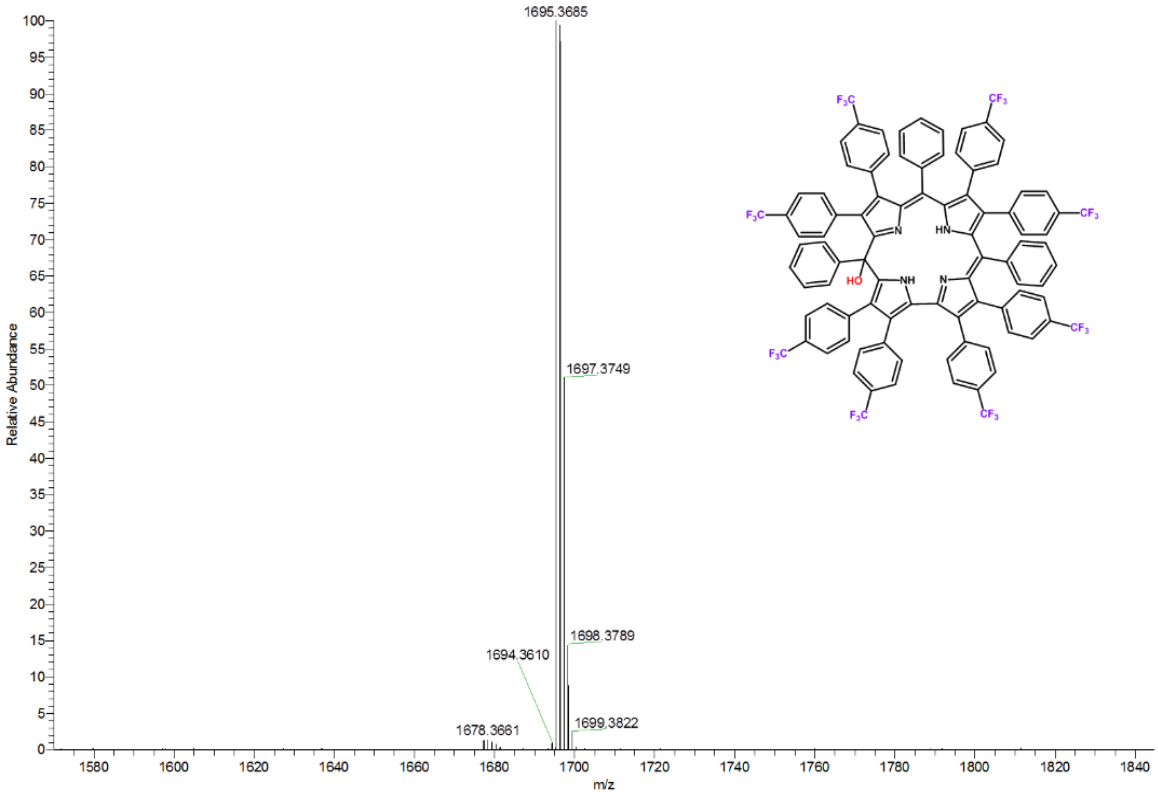

Figure S67. HR-ESI mass spectrum of $H_2[(CF_3)_8H_3(5\text{-}OH)]$**.**

Free base undecaarylcorroles

(a) UV-vis spectra of free base undecaarylcorroles

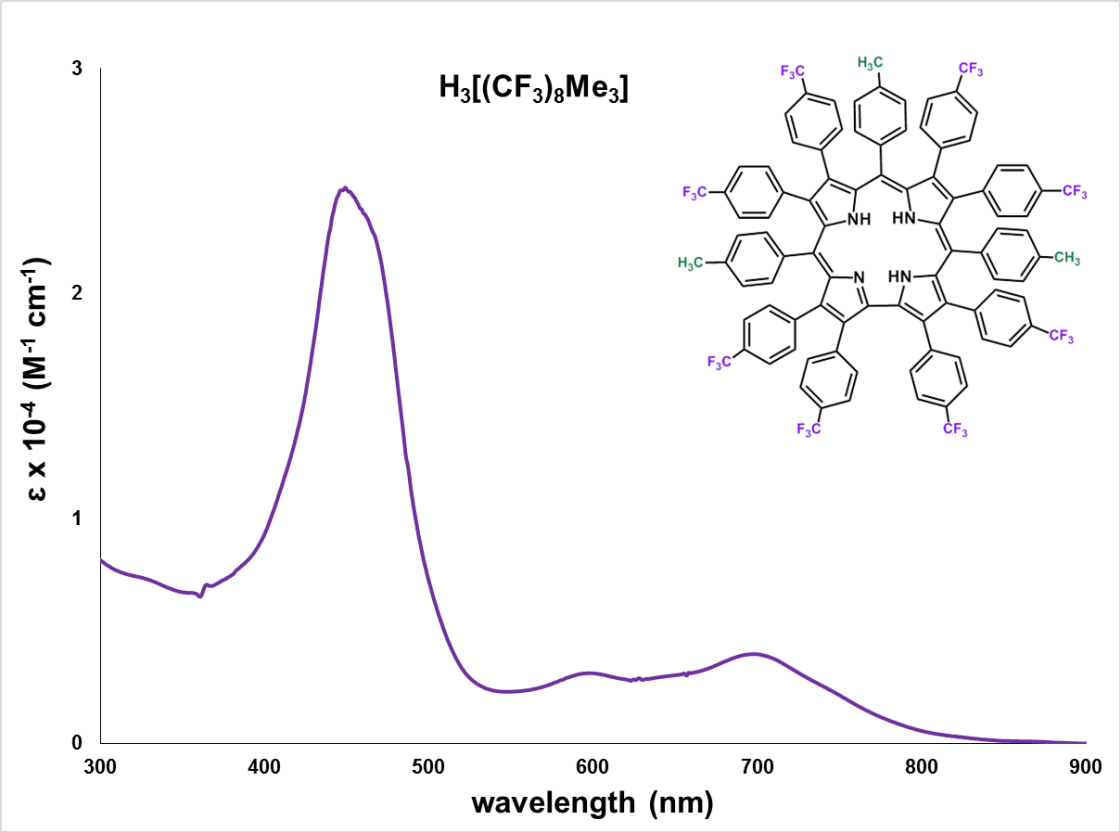

Figure S68. UV-vis spectrum of $H_3[(CF_3)_8Me_3]$.

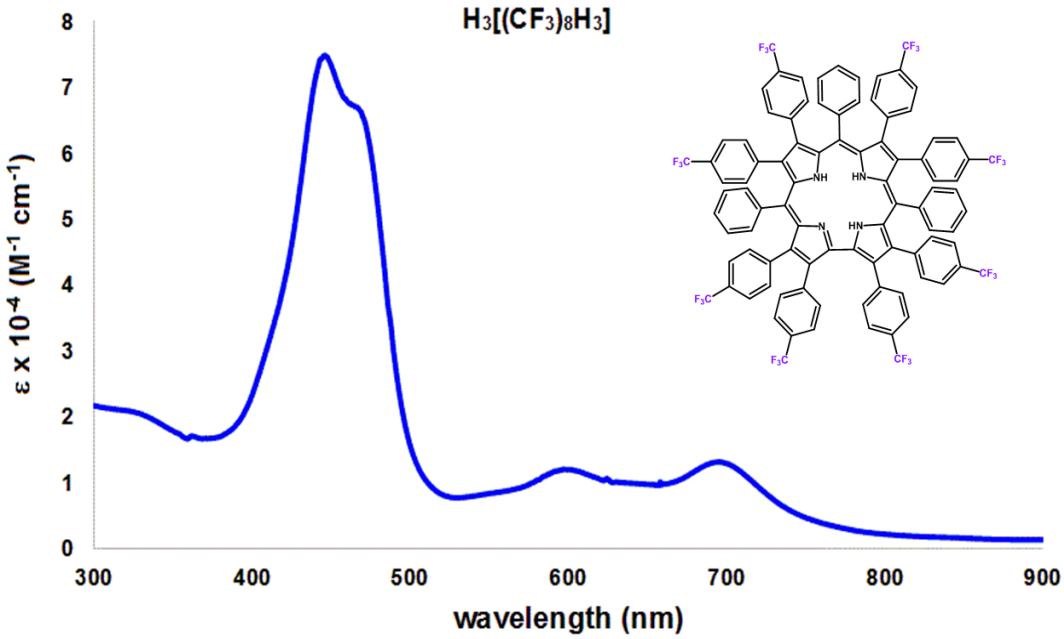

Figure S69. UV-vis spectrum of $H_3[(CF_3)_8H_3]$.

HR-MS of free base undecaarylcorroles

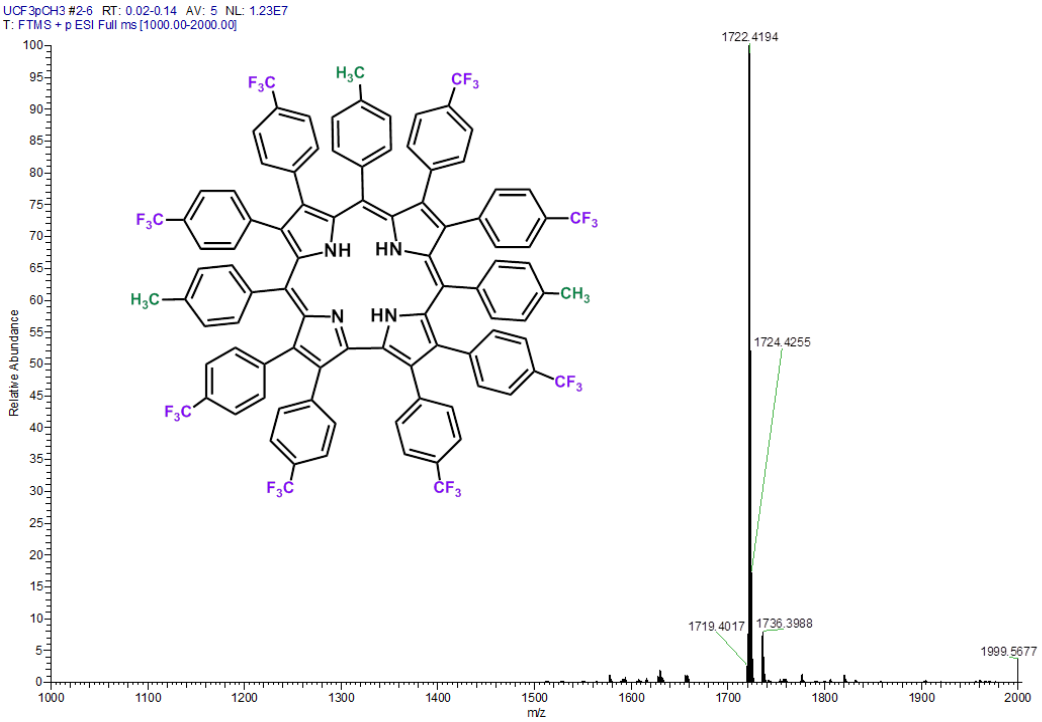

Figure S70. HR-ESI mass spectrum of $H_3[(CF_3)_8Me_3]$.

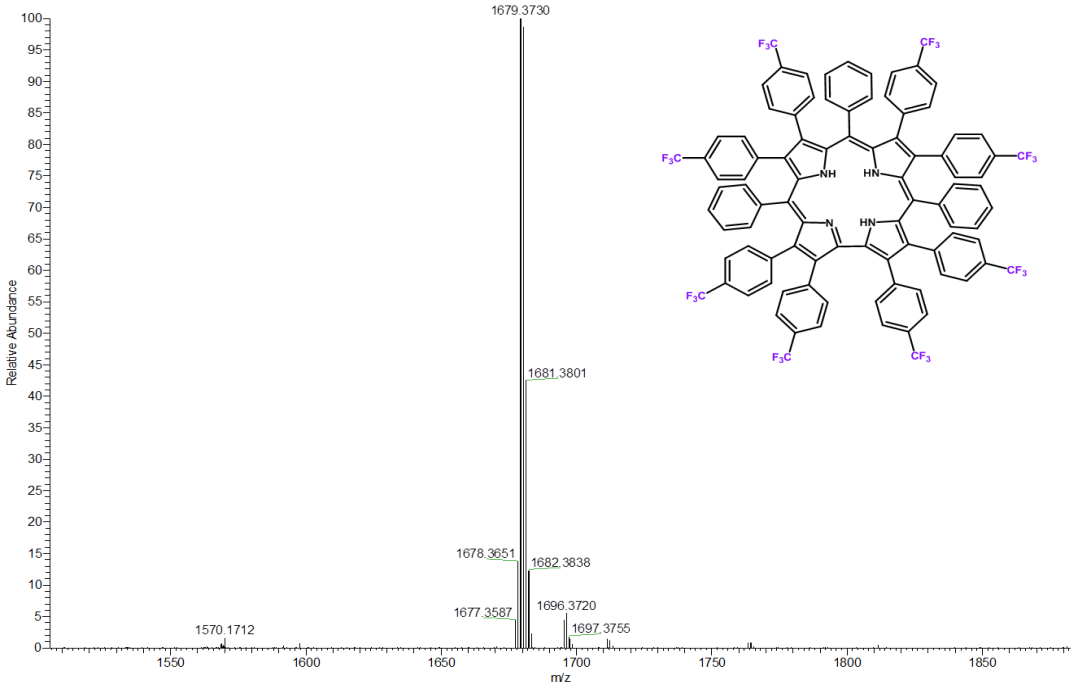

Figure S71. HR-ESI mass spectrum of $H_3[(CF_3)_8H_3]$.

Gold Corrole

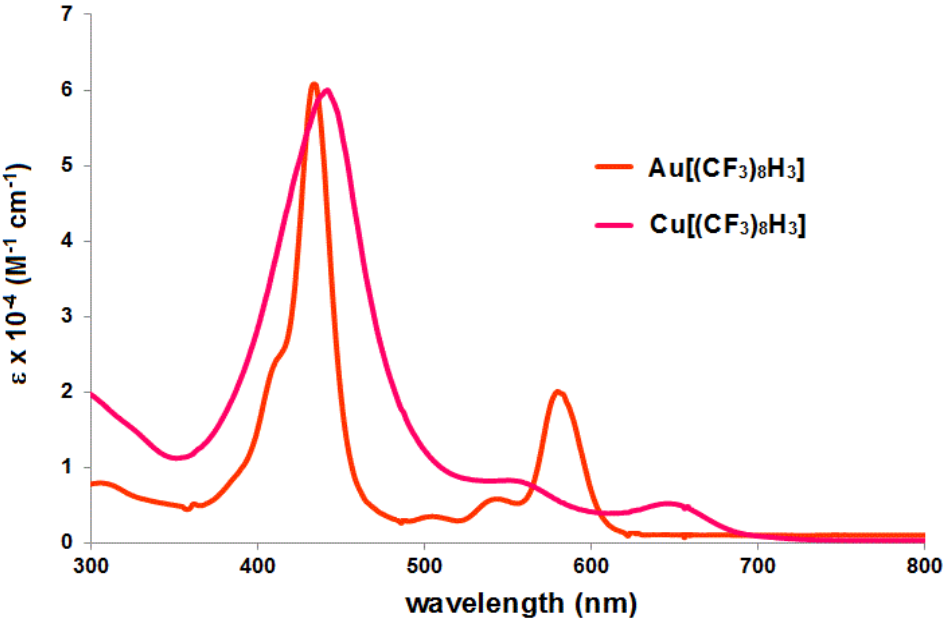

Figure S72. Overlayed UV-vis spectra of copper and gold undecaarycorroles.

NMR spectra of Au[$(CF_3P)_8H_3$]

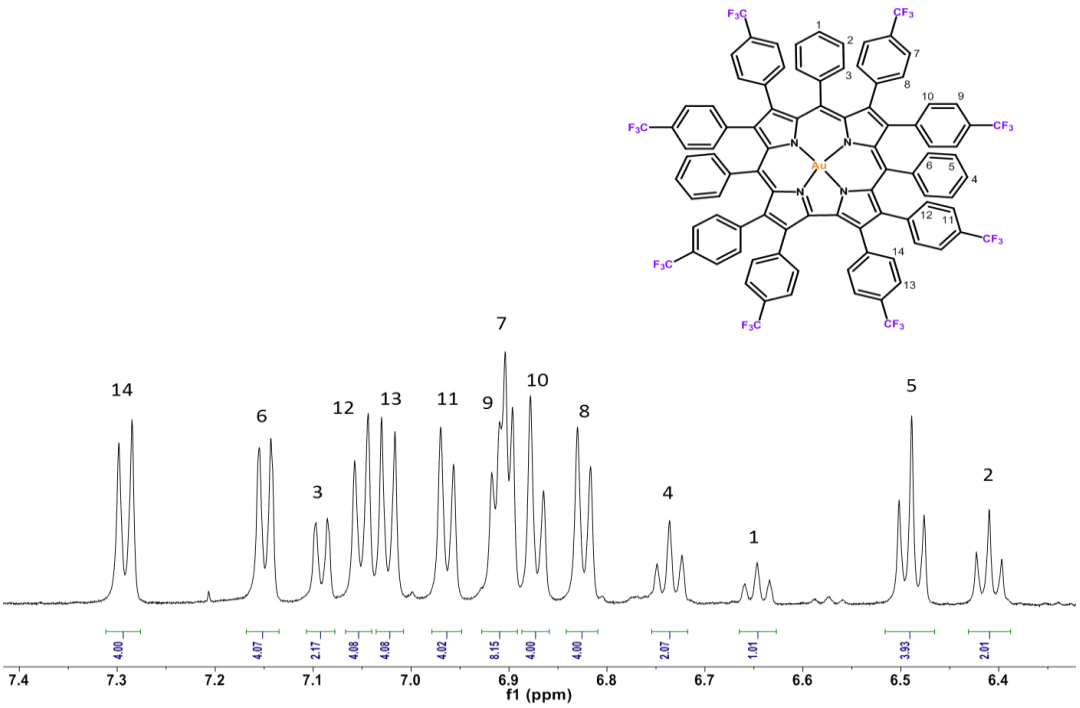

Figure S73. ^{1}H NMR spectrum of Au[$(CF_3)_8H_3$] in tetrachloroethane-d_2.

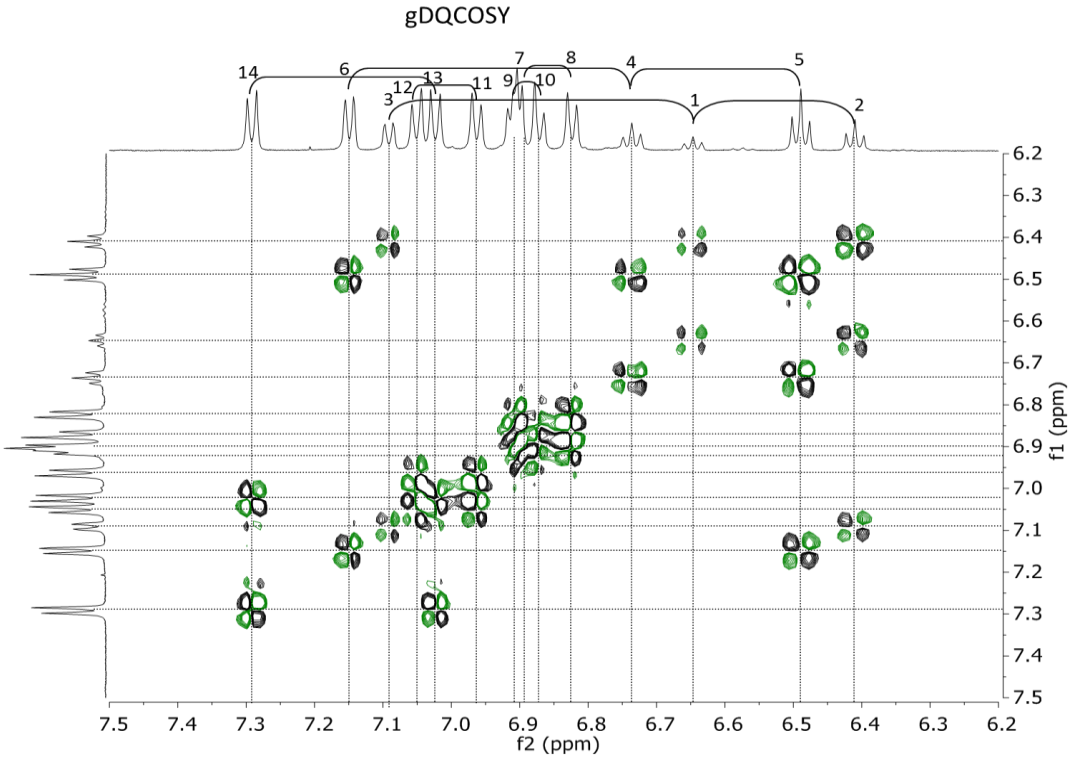

Figure S74. $^{1}H,^{1}H$ DQFCOSY spectrum of $Au[(CF_3)_8H_3]$ in $(CDCl_2)_2$.

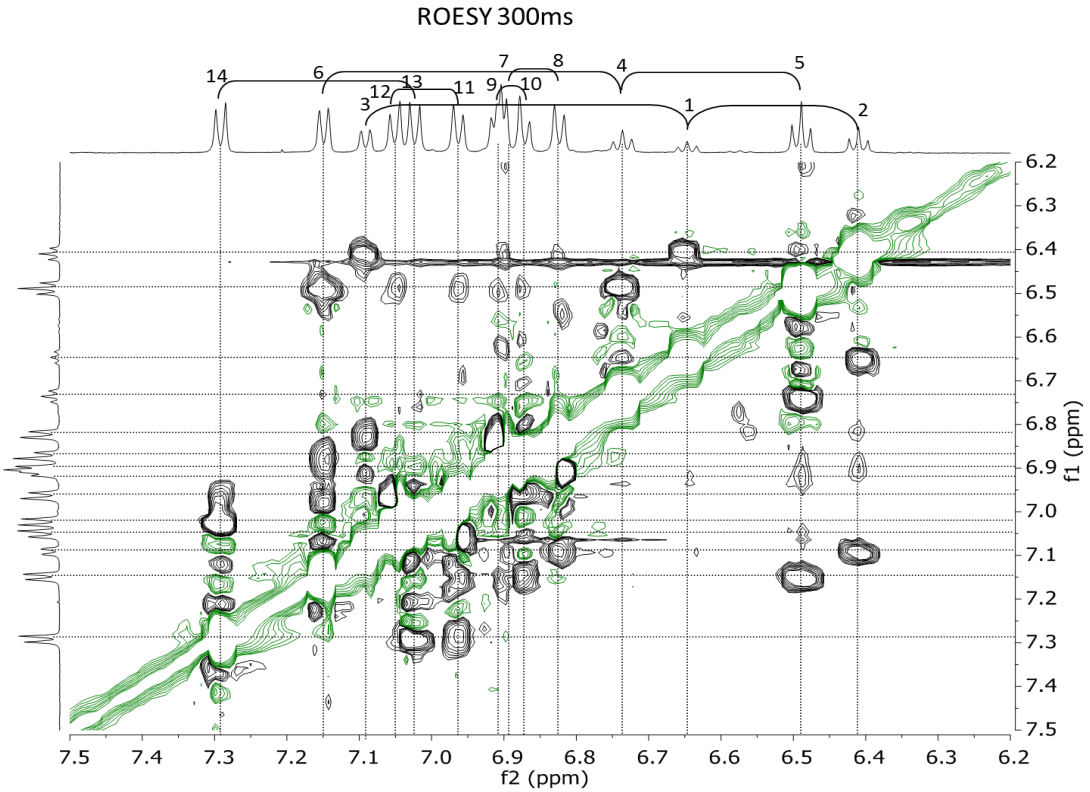

Figure S75. $^{1}H,^{1}H$ ROESY {300ms, $(CDCl_2)_2$} spectrum of $Au[(CF_3)_8H_3]$.

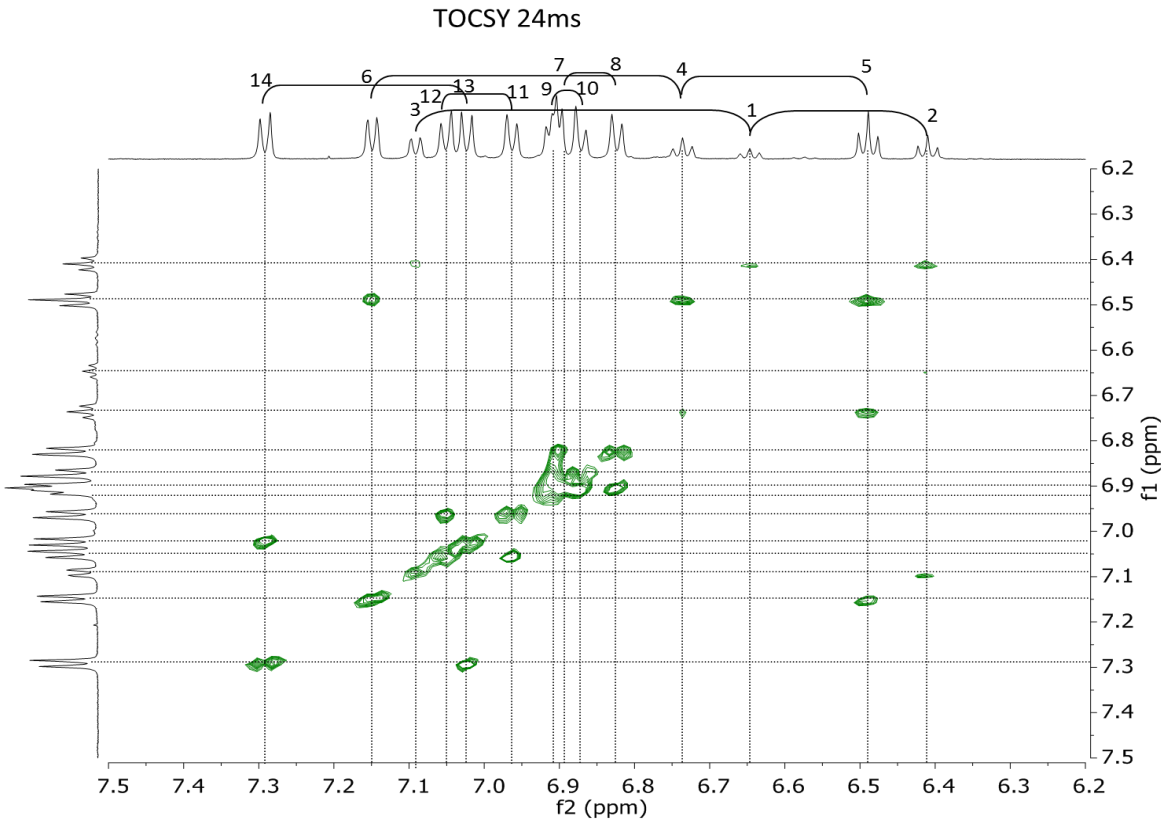

Figure S76. $^{1}H,^{1}H$ TOCSY{24ms, $(CDCl_2)_2$} spectrum of $Au[(CF_3)_8H_3]$.

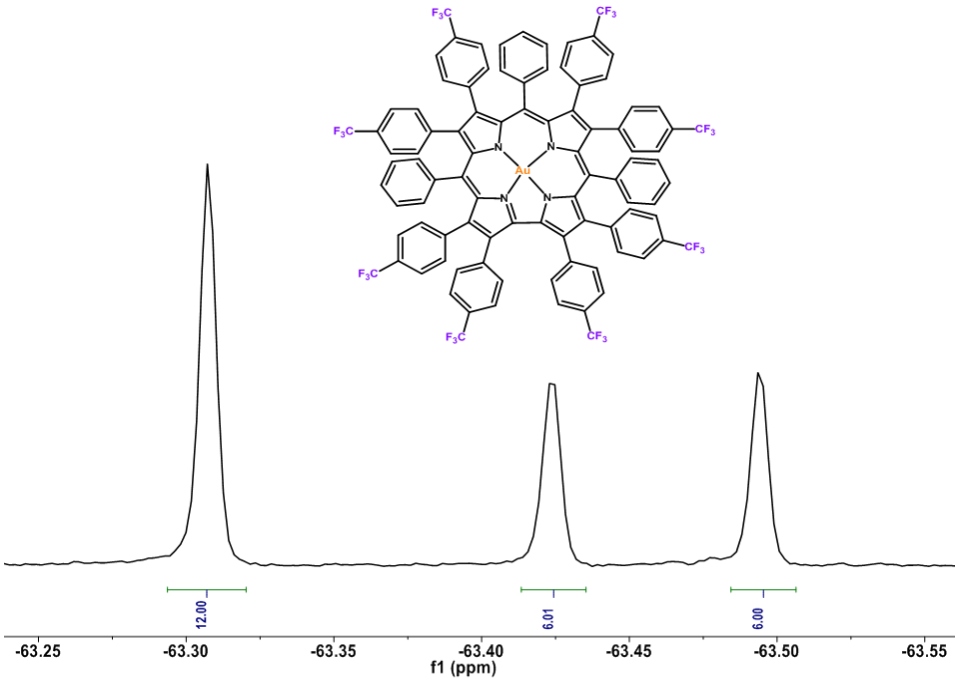

Figure S77. ^{19}F NMR spectrum of $Au[(CF_3)_8H_3]$ in $CDCl_3$.

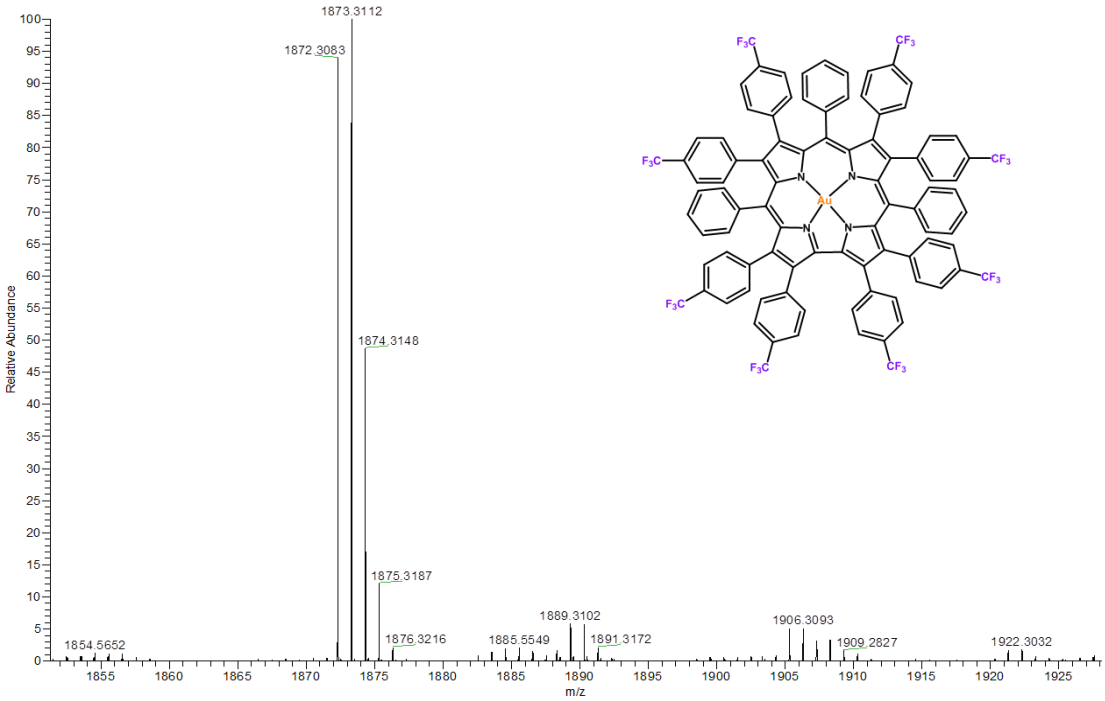

Figure S78. HR-ESI mass spectrum of Au[$(CF_3)_8H_3$].

Supporting Information

Table of Contents

A. Free-base Octabromocorroles

(a) UV-vis spectra of free-base octabromocorroles

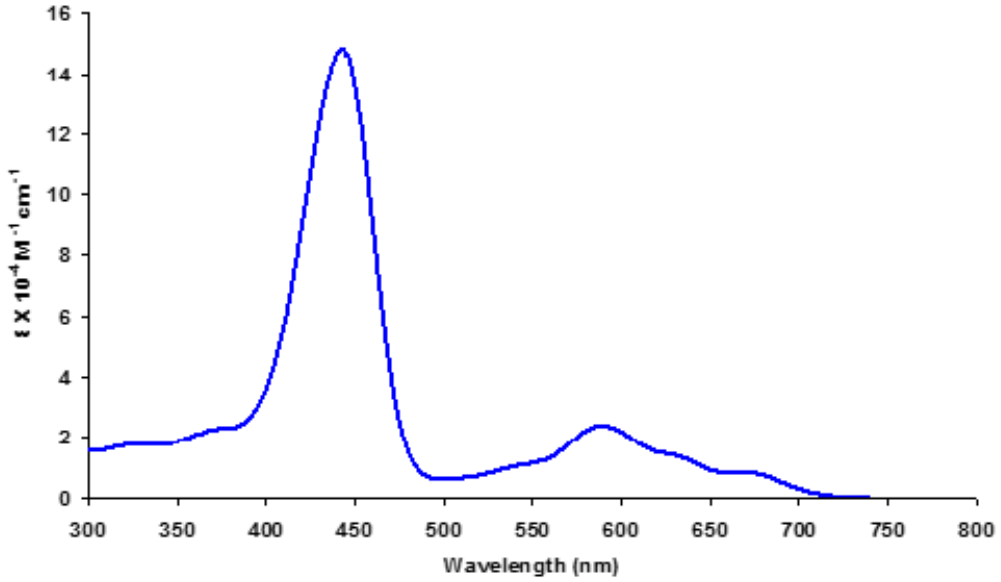

Figure S1. UV-vis spectrum of $H_3[Br_8TPFPC]$.

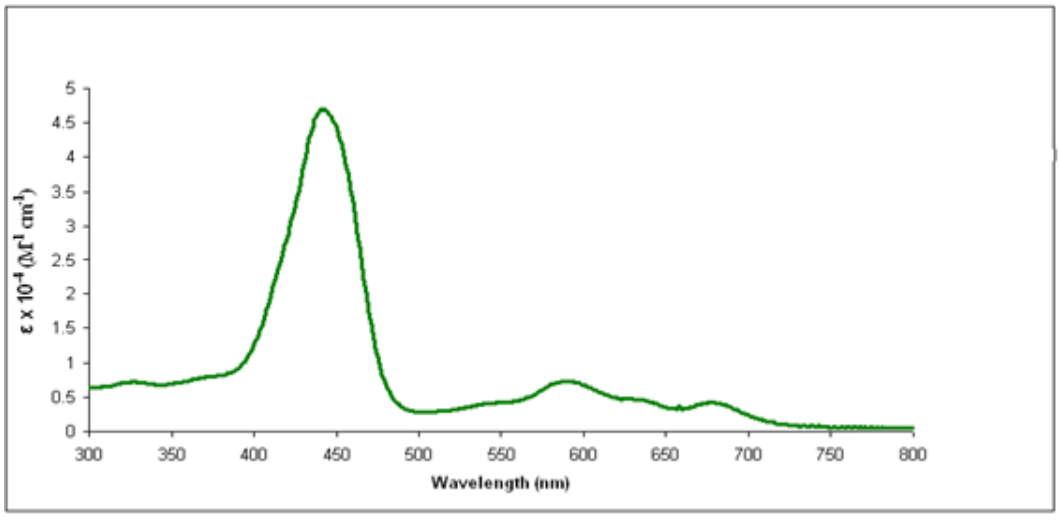

Figure S2. UV-vis spectrum of $H_3[Br_8TDCPC]$.

(b) NMR spectra of free-base octabromocorroles

NMR spectra of $H_3[Br_8TPFPC]$

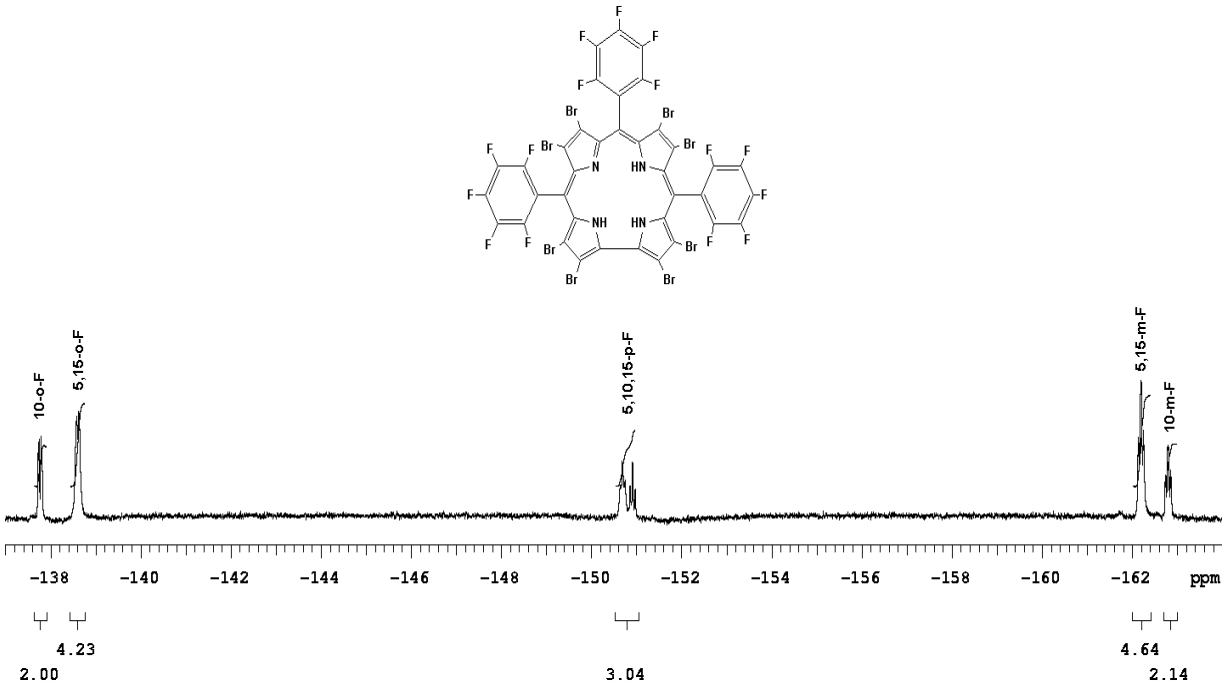

Figure S3. ^{19}F NMR spectrum of $H_3[Br_8TPFPC]$ in $CDCl_3$.

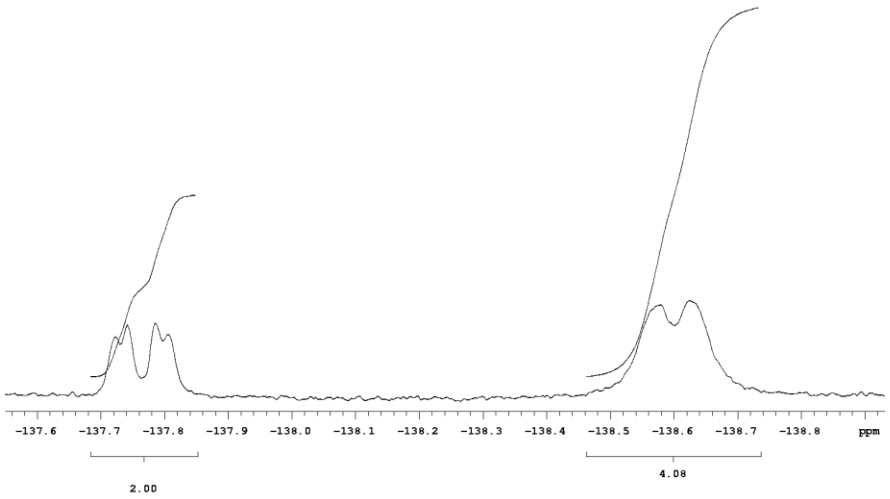

Figure S4. ^{19}F NMR spectrum of $H_3[Br_8TPFPC]$ in $CDCl_3$ **(**expanded views of the peaks).

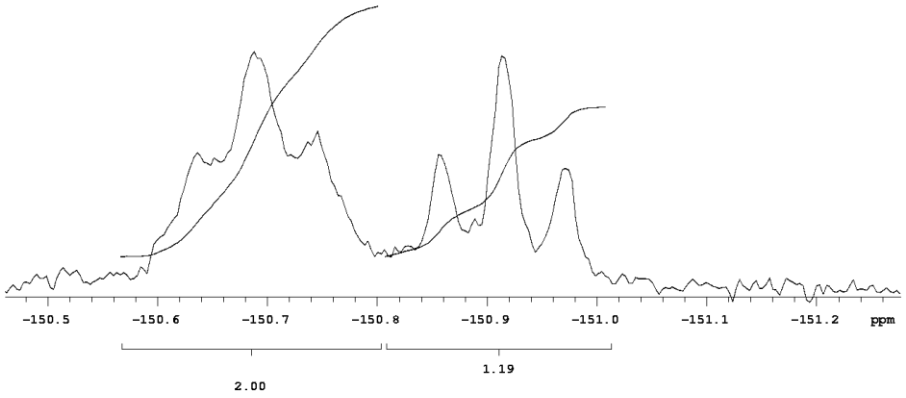

Figure S5. ^{19}F NMR spectrum of $H_3[Br_8TPFPC]$ in $CDCl_3$ **(**expanded views of the peaks).

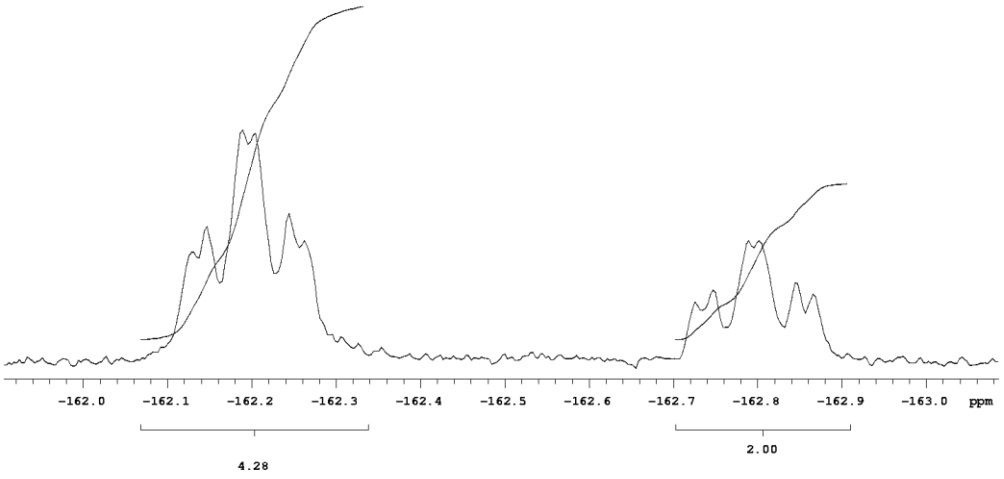

Figure S6. ^{19}F NMR spectrum of $H_3[Br_8TPFPC]$ in $CDCl_3$ **(**expanded views of the peaks).

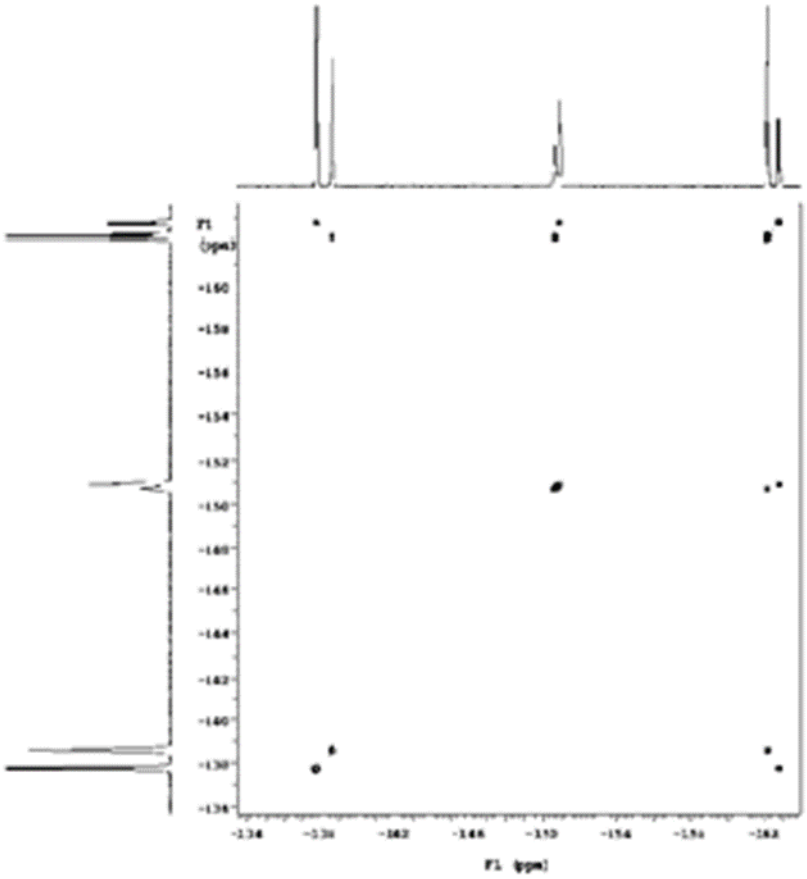

Figure S7. $^{19}F,^{19}F$ COSY spectrum of $H_3[Br_8TPFPC]$ in $CDCl_3$.

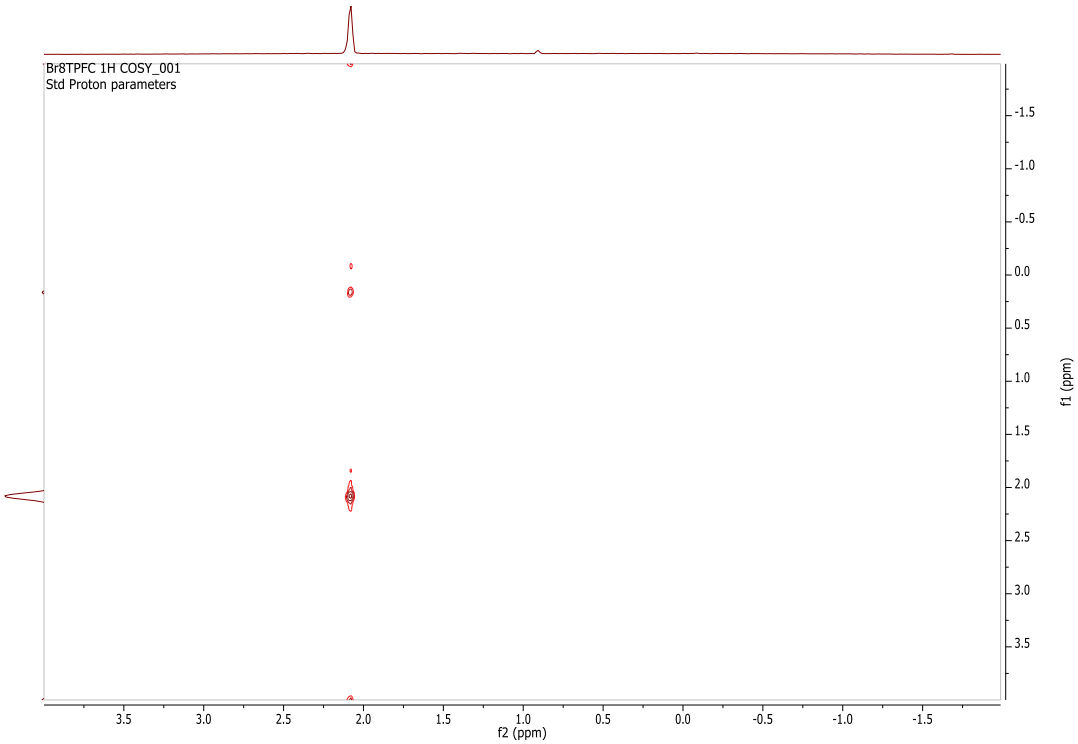

Figure S8. $^{1}H,^{1}H$ COSY spectrum of $H_3[Br_8TPFPC]$ in $CDCl_3$.

NMR spectra of $H_3[Br_8TDCPC]$

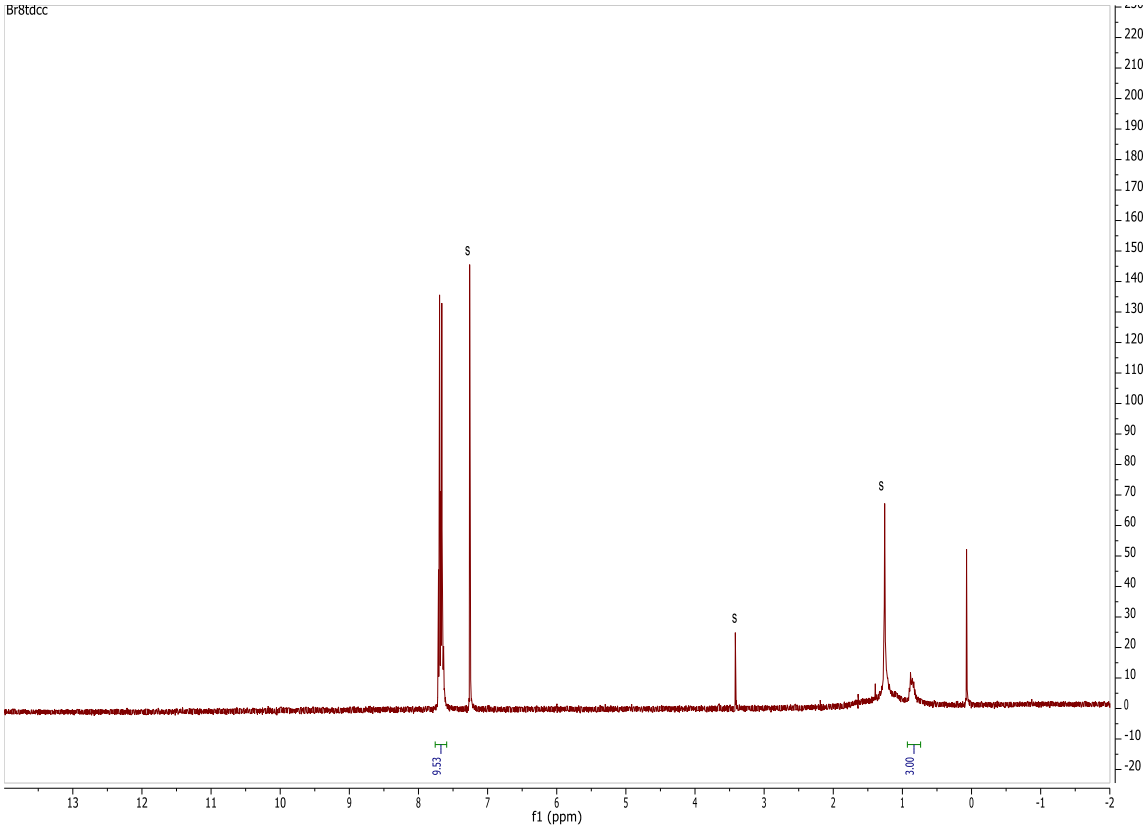

Figure S9. ^1H NMR spectrum of $H_3[Br_8TDCPC]$ in $CDCl_3$.

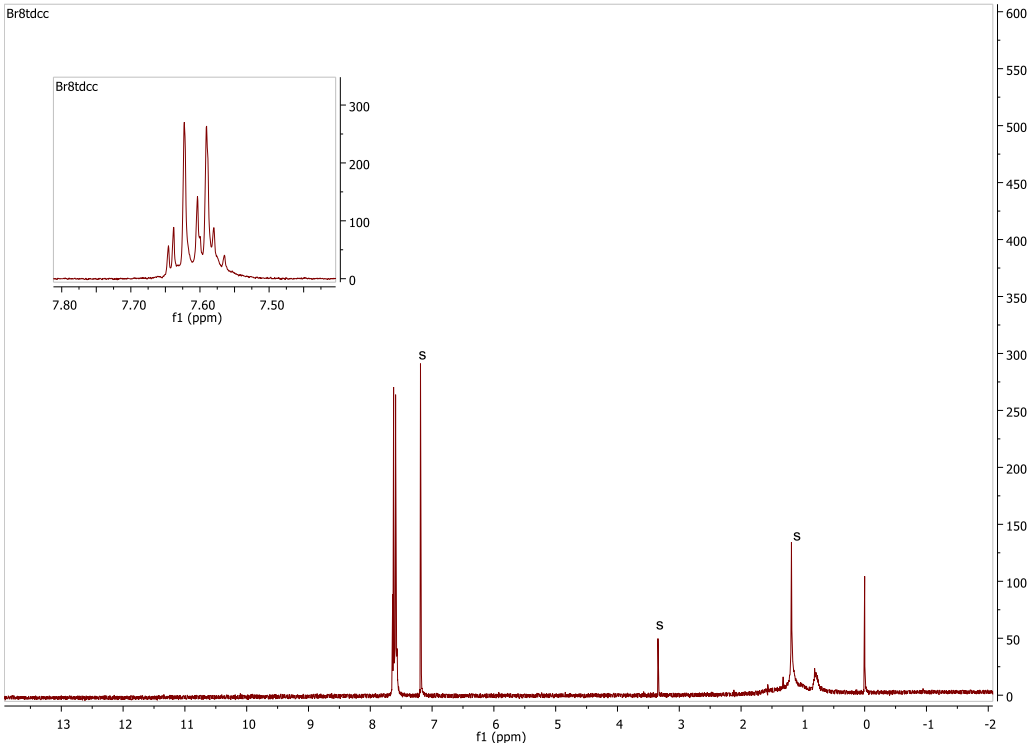

Figure S10. ^1H NMR spectrum of $H_3[Br_8TDCPC]$ in $CDCl_3$.

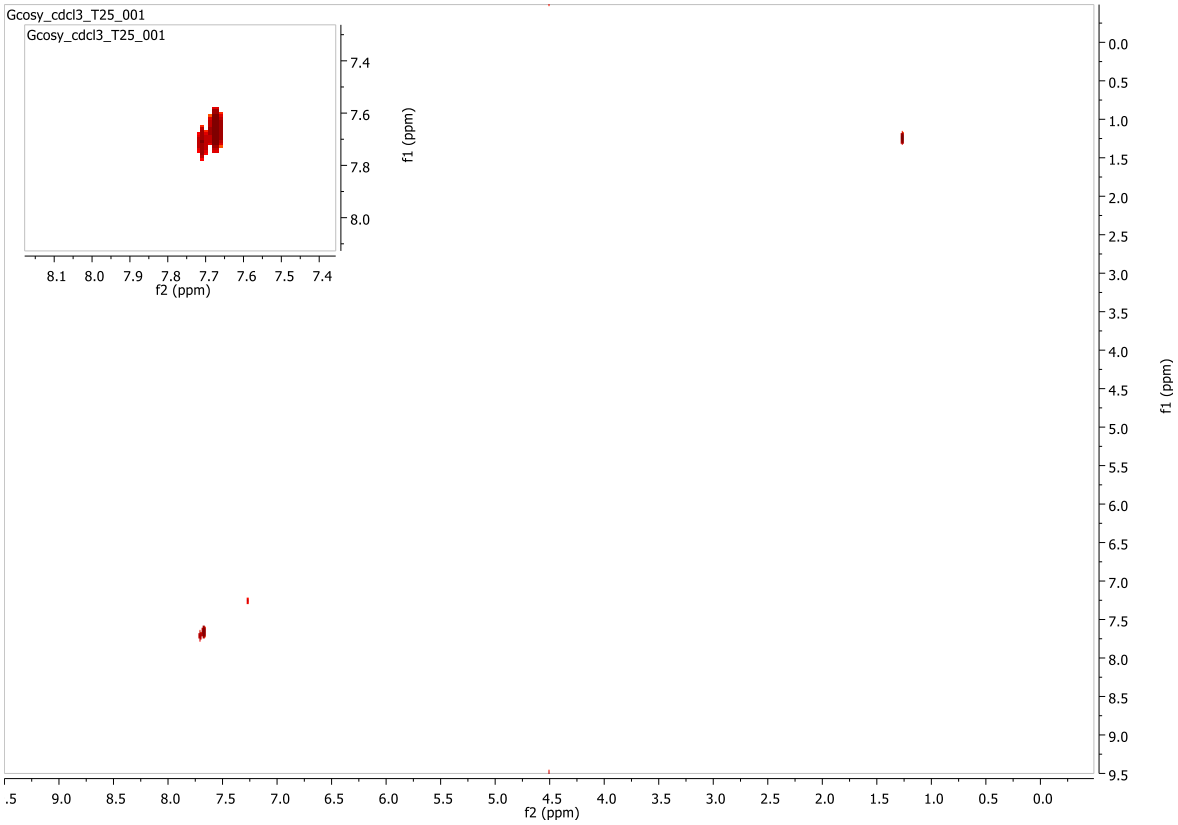

Figure S11. $^{1}H,^{1}H$ COSY of $H_3[Br_8TDCPC]$ in $CDCl_3$.

(c) HR-MS spectra of free-base octabromocorroles

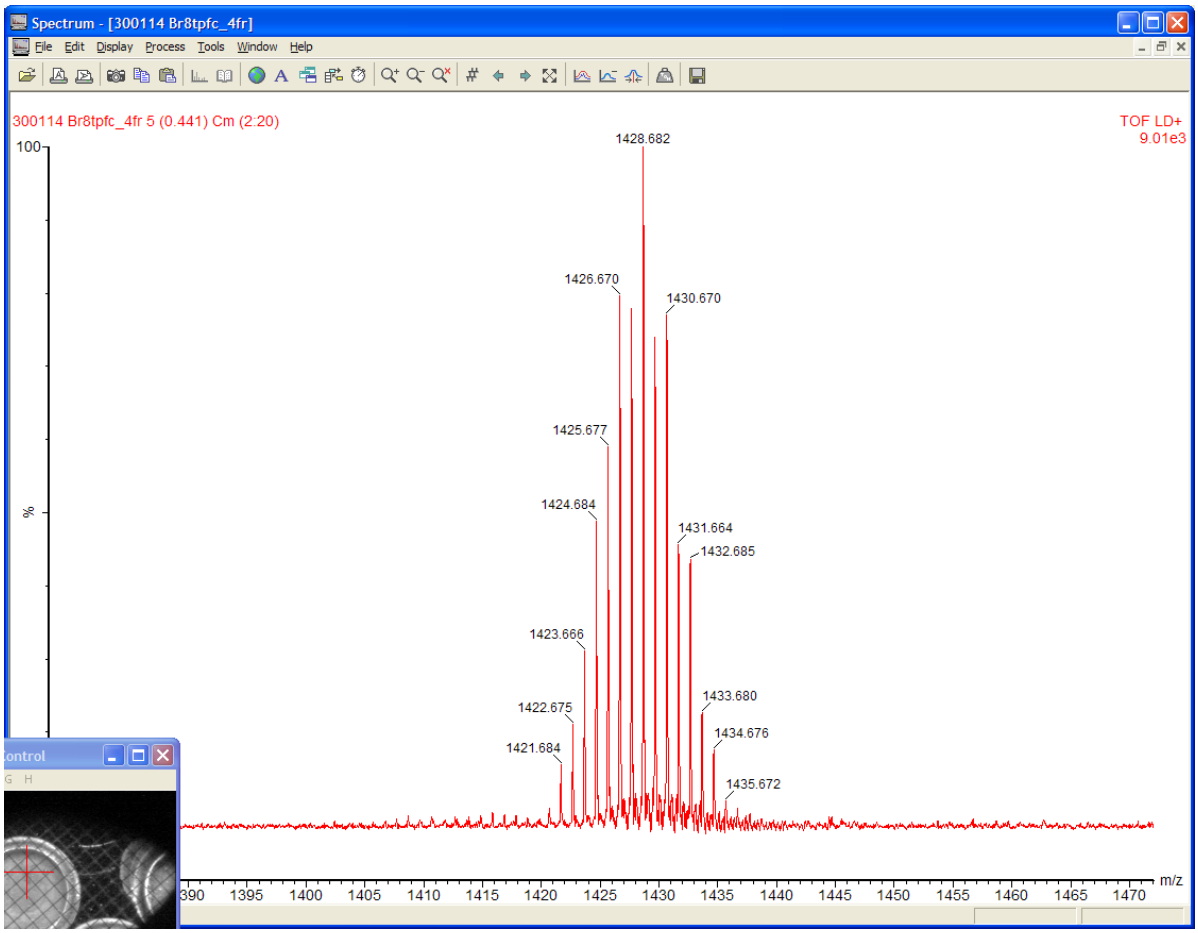

Figure S12. MS (MALDI-TOF) mass spectrum of $H_3[Br_8TPFPC]$.

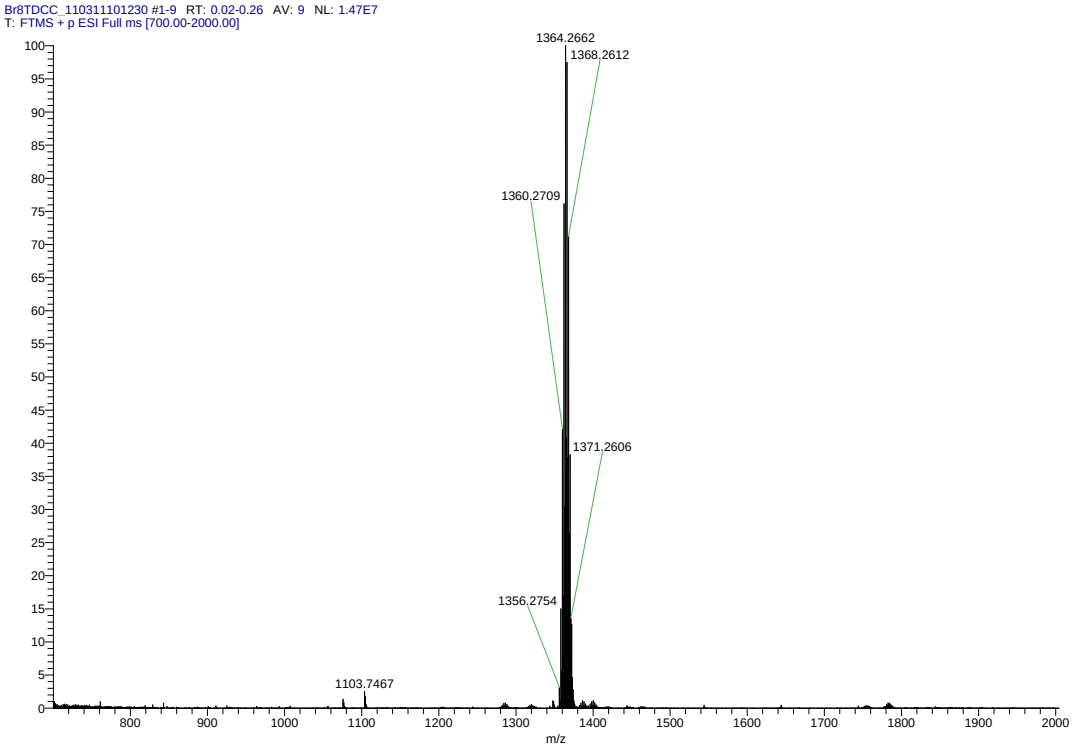

Figure S13. HR-ESI mass spectrum of H_3[Br_8TDCPC].

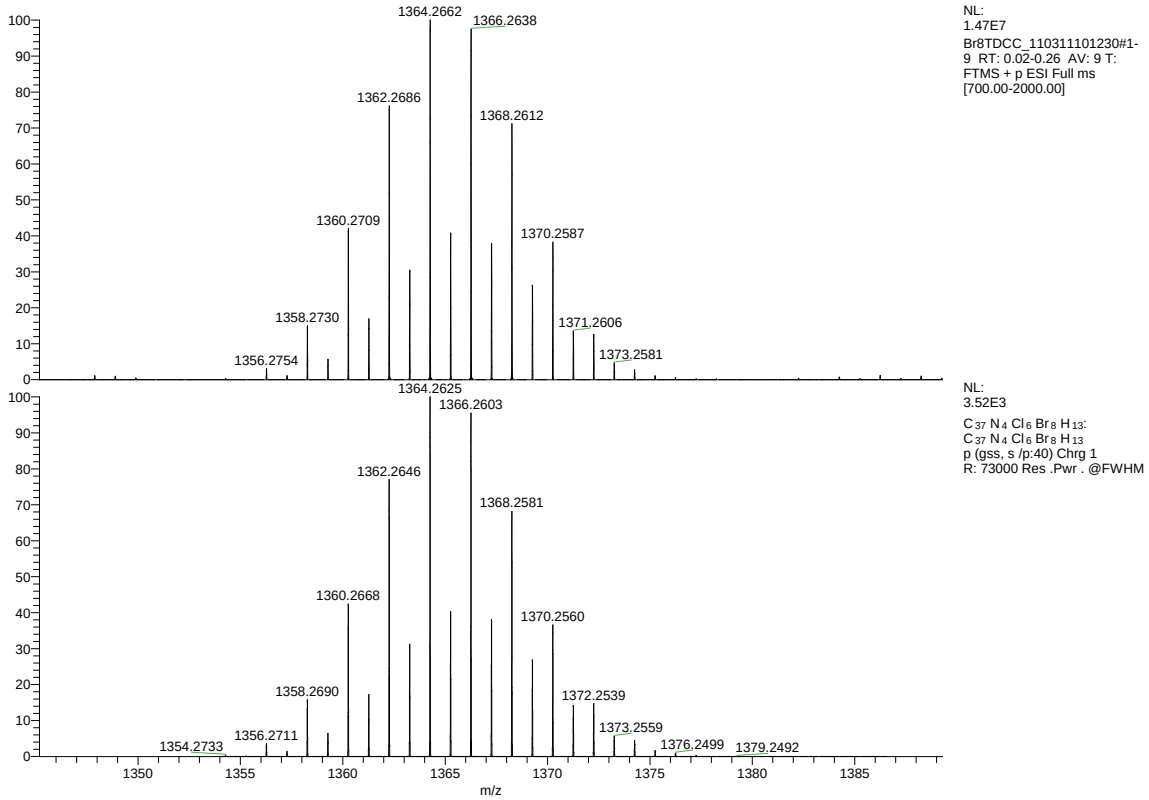

Figure S14. HR-ESI mass spectrum of H_3[Br_8TDCPC] (bottom: theoritical value).

B. Iron Octabromocorroles

(a) UV-vis spectra of iron octabromocorroles

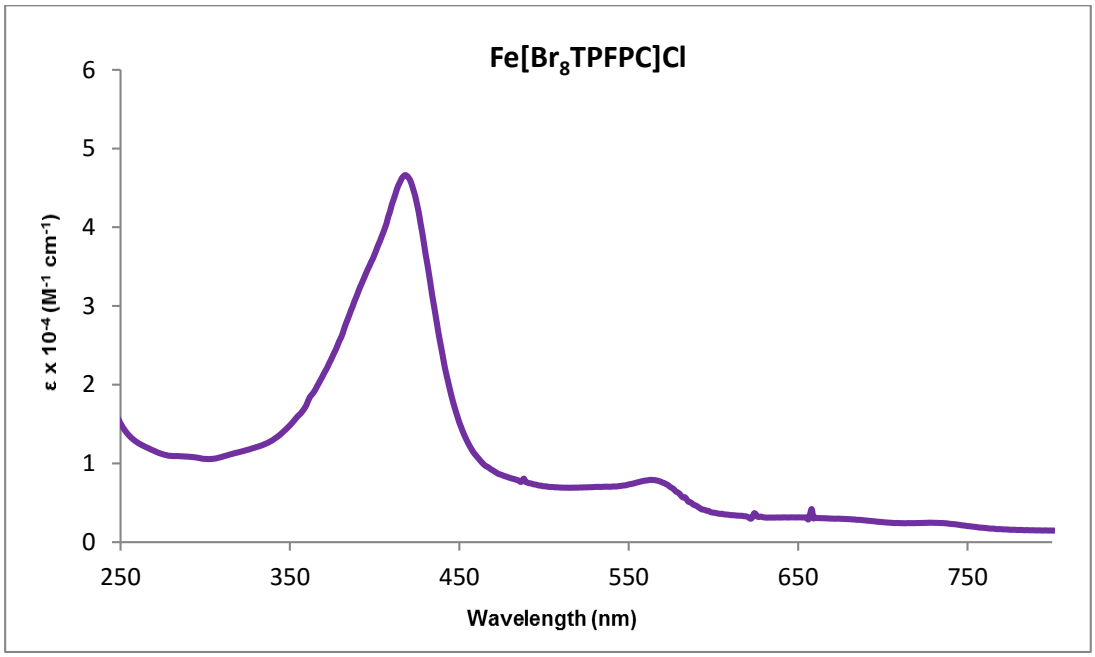

Figure S15. UV-vis spectrum of Fe[Br$_8$TPFPC]Cl.

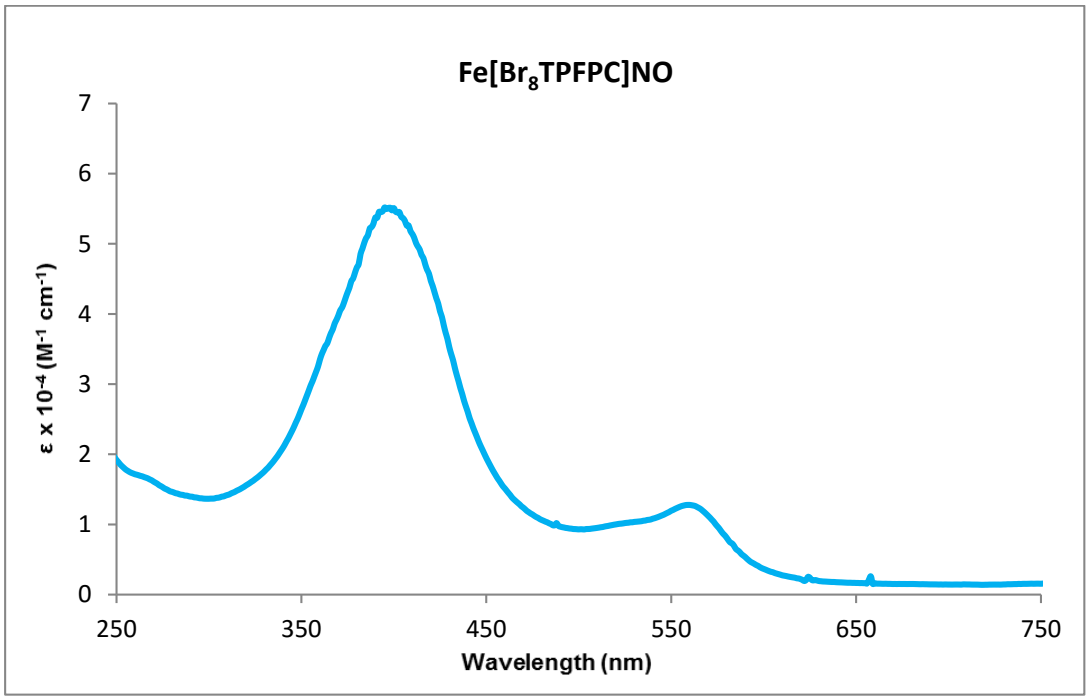

Figure S16. UV-vis spectrum of Fe[Br$_8$TPFPC]NO.

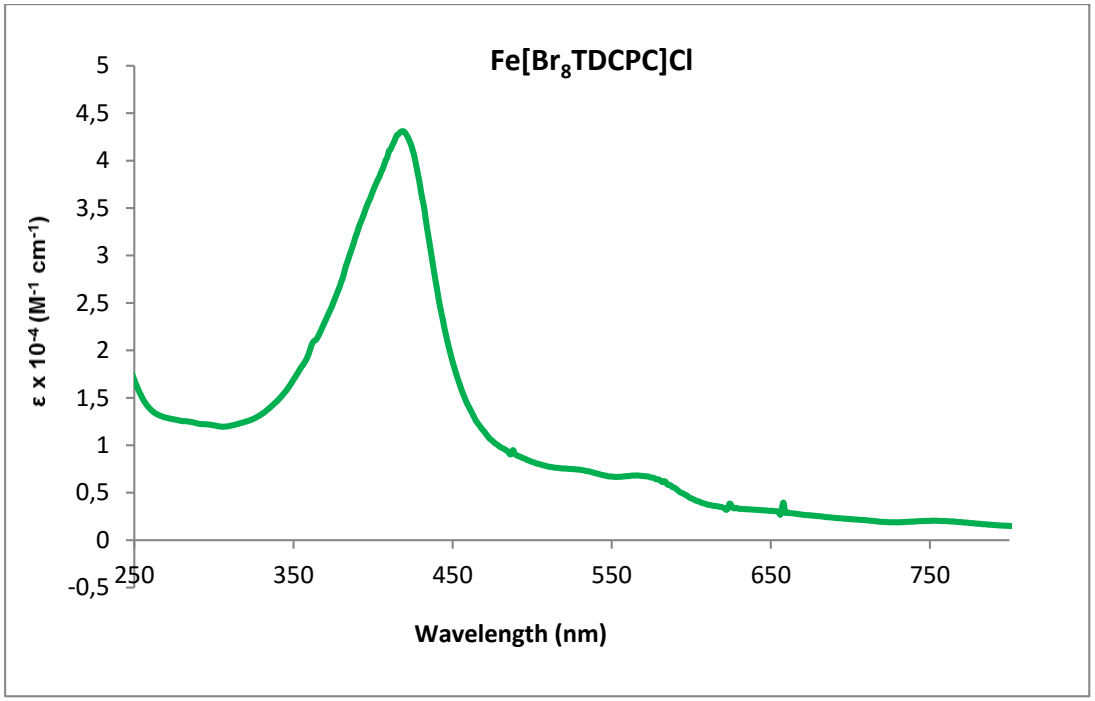

Figure S17. UV-vis spectrum of Fe[Br8TDCPC]Cl.

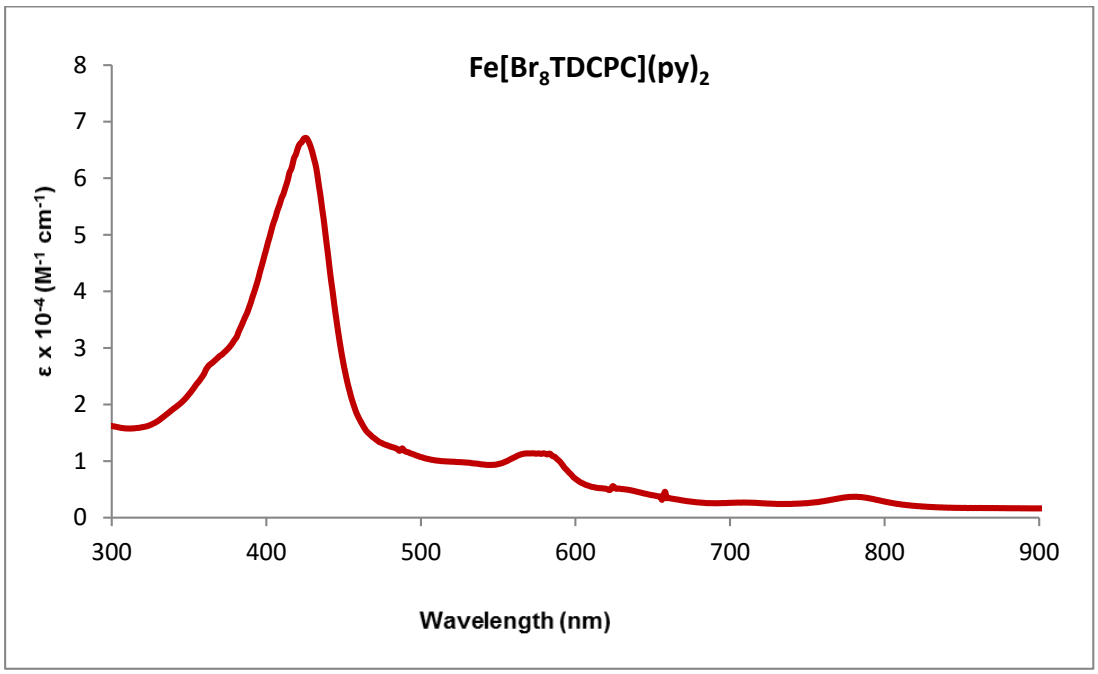

Figure S18. UV-vis spectrum of Fe[Br8TDCPC](py)2.

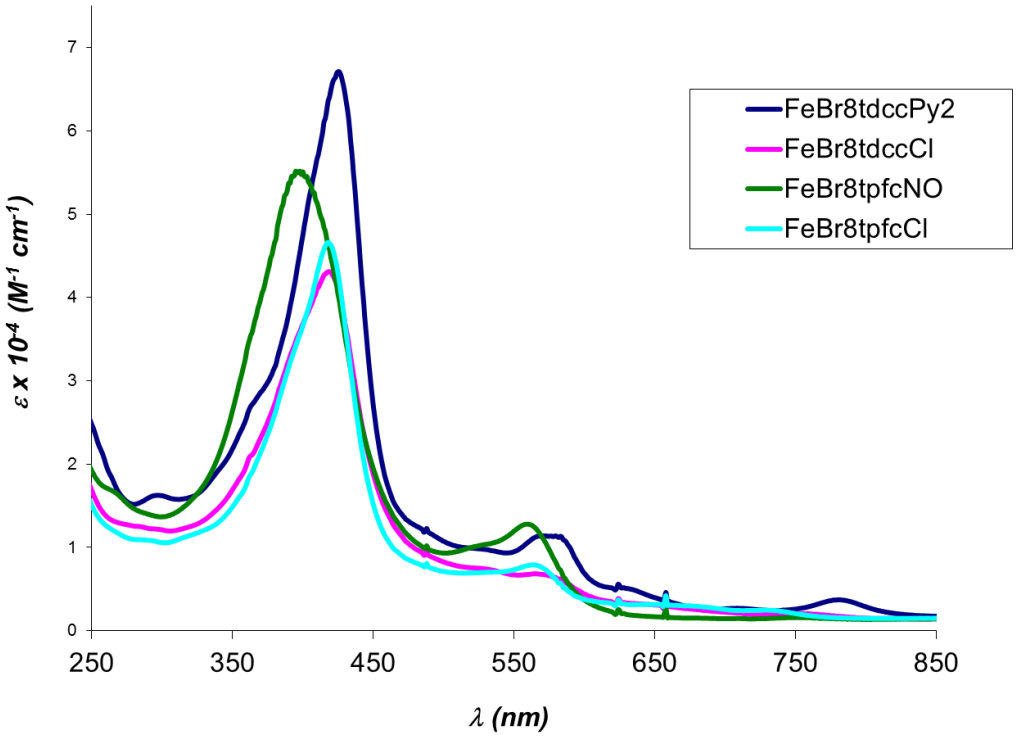

Figure S19. UV-vis spectra of Fe[Br$_8$TDCPC](py)$_2$, Fe[Br$_8$TDCPC]Cl, Fe[Br$_8$TPFPC]NO, FeBr$_8$[TPFPC]Cl.

(b) NMR spectra of iron octabromocorroles

NMR spectra of Fe[Br_8TPFPC]Cl

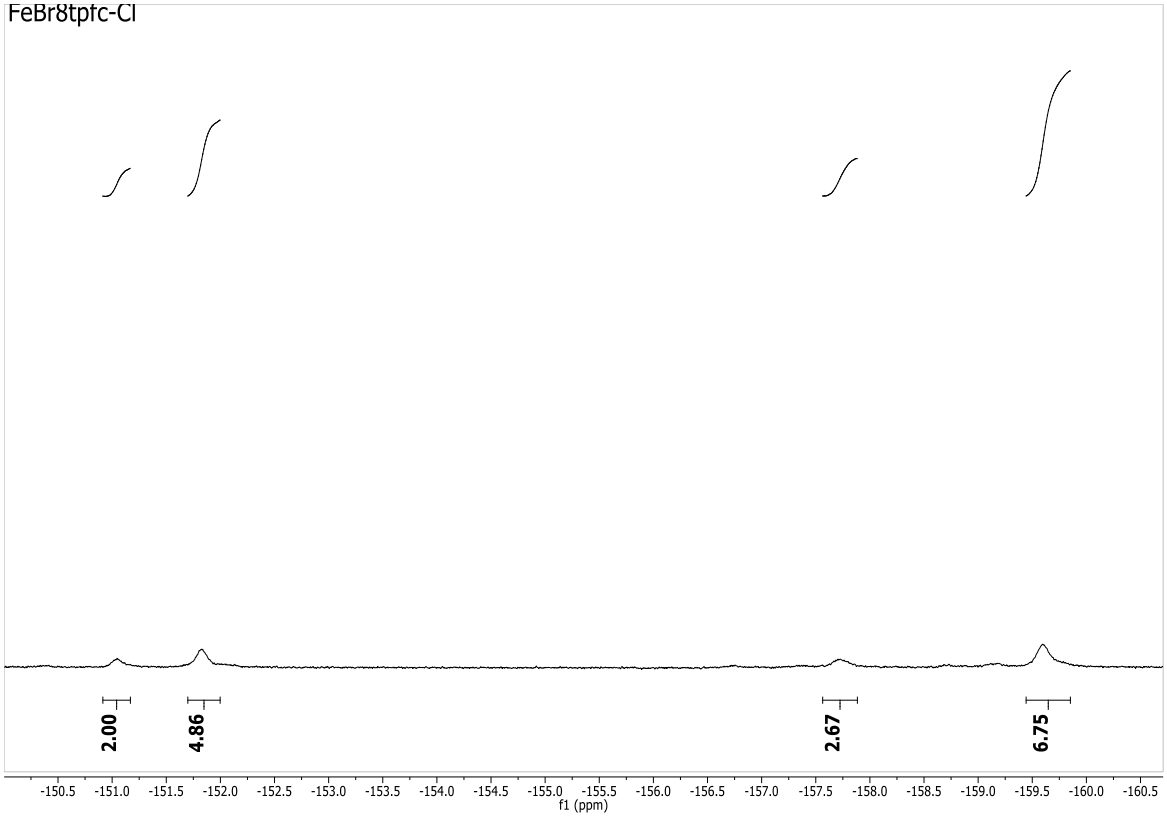

Figure S20. ^{19}F NMR spectrum of Fe[Br_8TPFPC]Cl in $CDCl_3$.

NMR spectra of Fe[Br_8TPFPC]NO

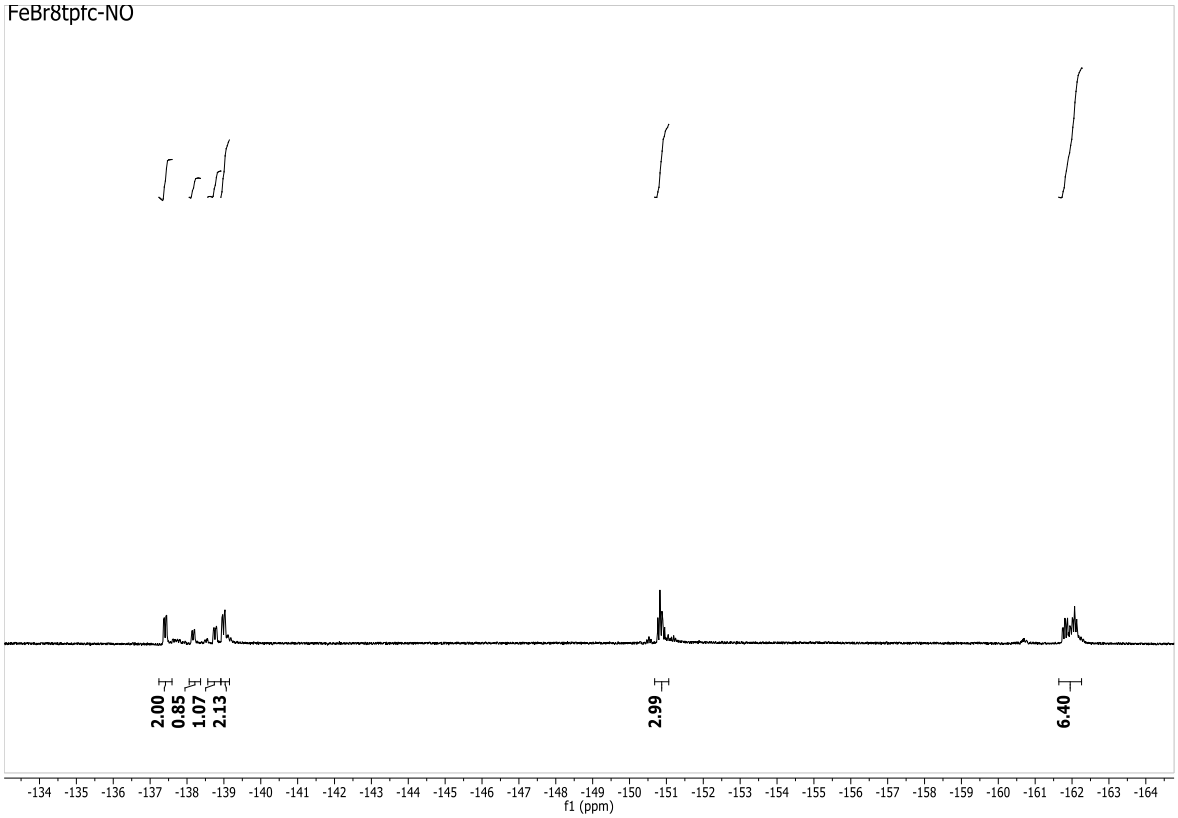

Figure S21. ^{19}F NMR spectrum of Fe[Br_8TPFPC]NO in $CDCl_3$.

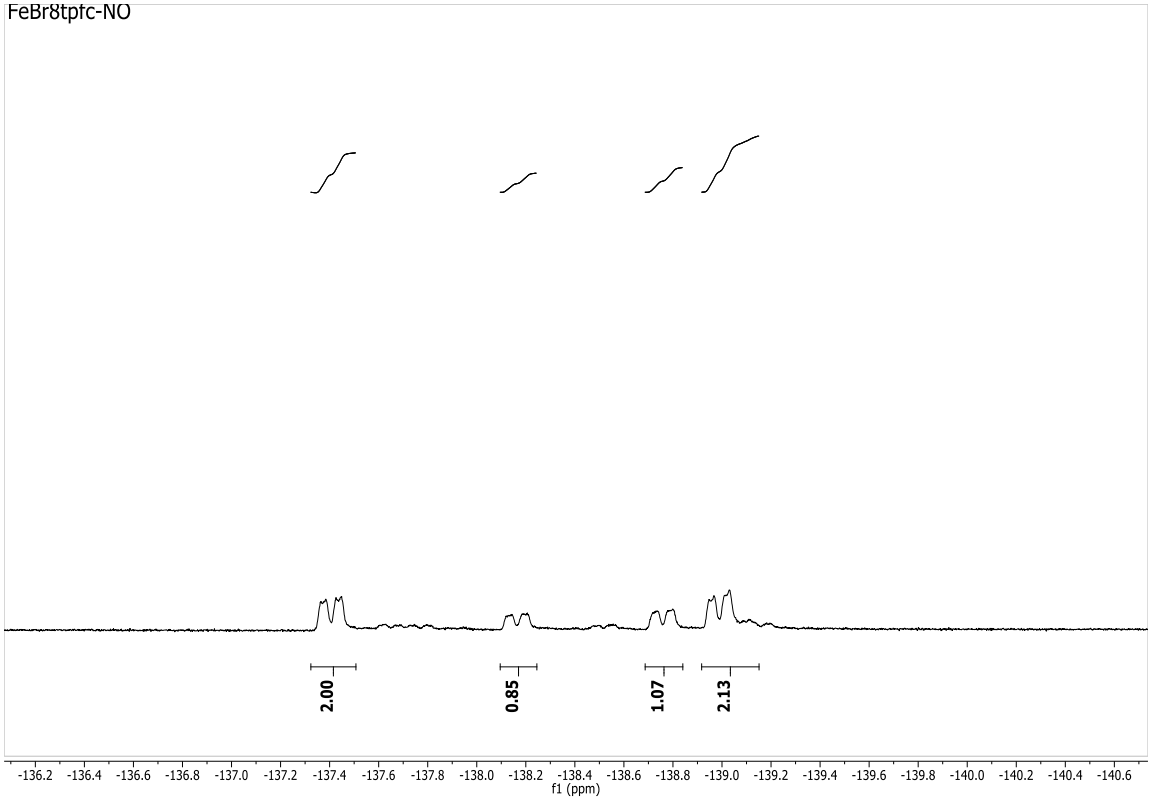

Figure S22. ^{19}F NMR spectrum of Fe[Br_8TPFPC]NO in $CDCl_3$.

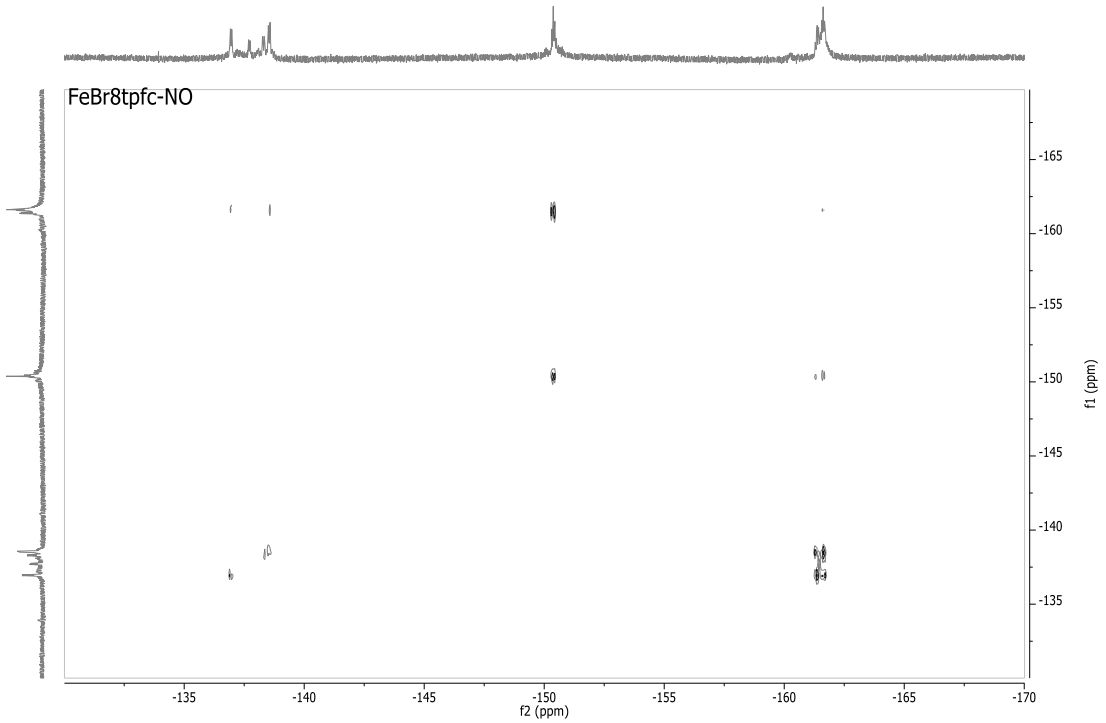

Figure S23. $^{19}F,^{19}F$ COSY spectrum of Fe[Br_8TPFPC]NO in $CDCl_3$**.**

NMR spectra of Fe[Br_8TDCPC]Cl

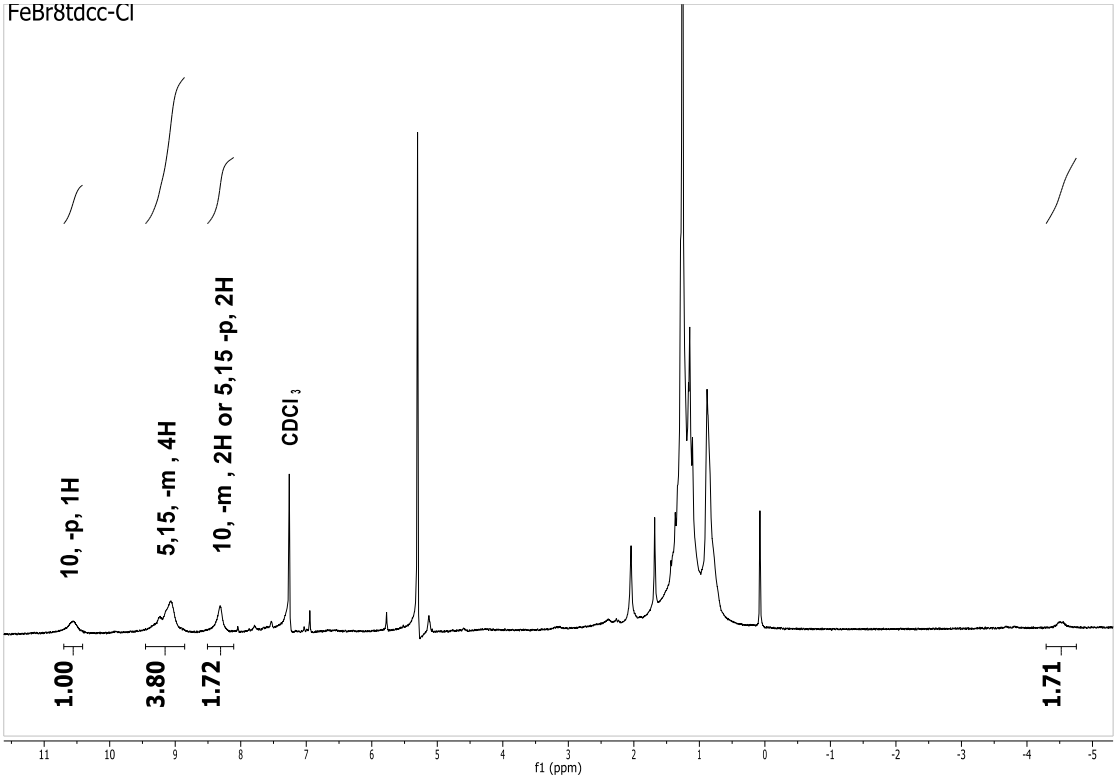

Figure S24. ^{1}H NMR spectrum of Fe[Br_8TDCPC]Cl in $CDCl_3$.

NMR spectra of Fe[Br_8TDCPC](py)$_2$

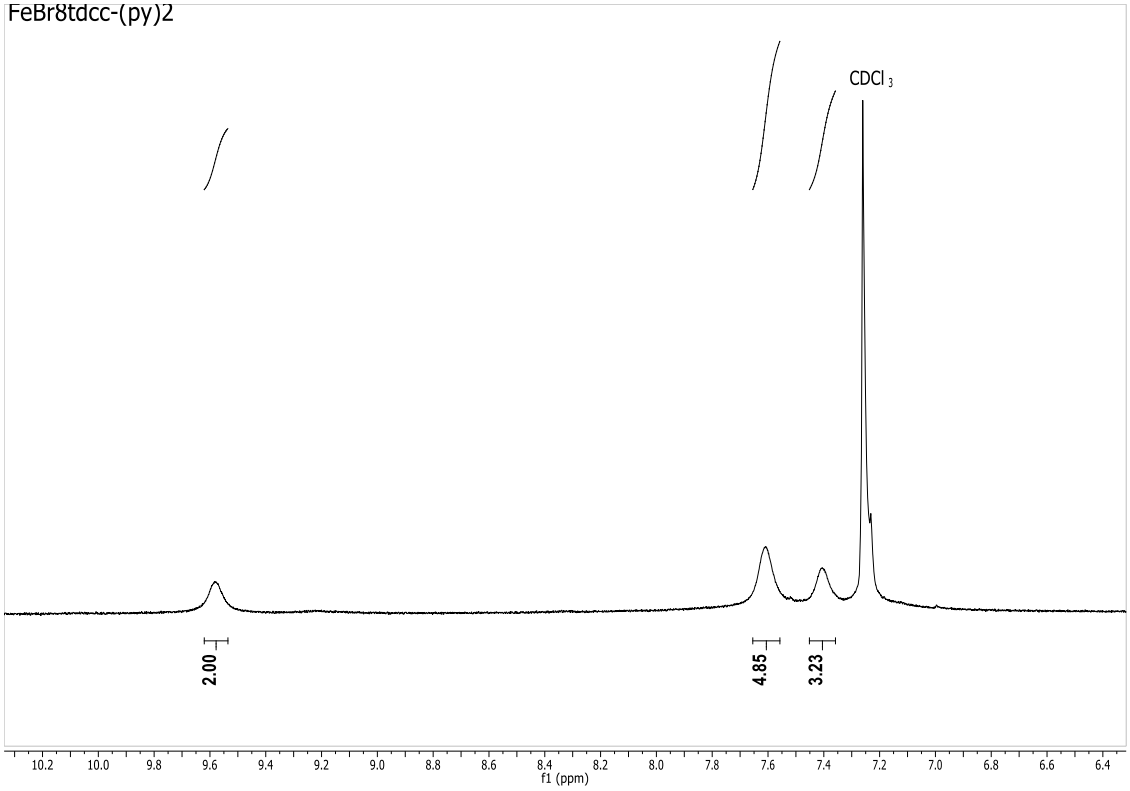

Figure S25. ^{1}H NMR spectrum of Fe[Br_8TDCPC](py)$_2$ in $CDCl_3$.

(c) HR-MS spectra of iron octabromocorroles

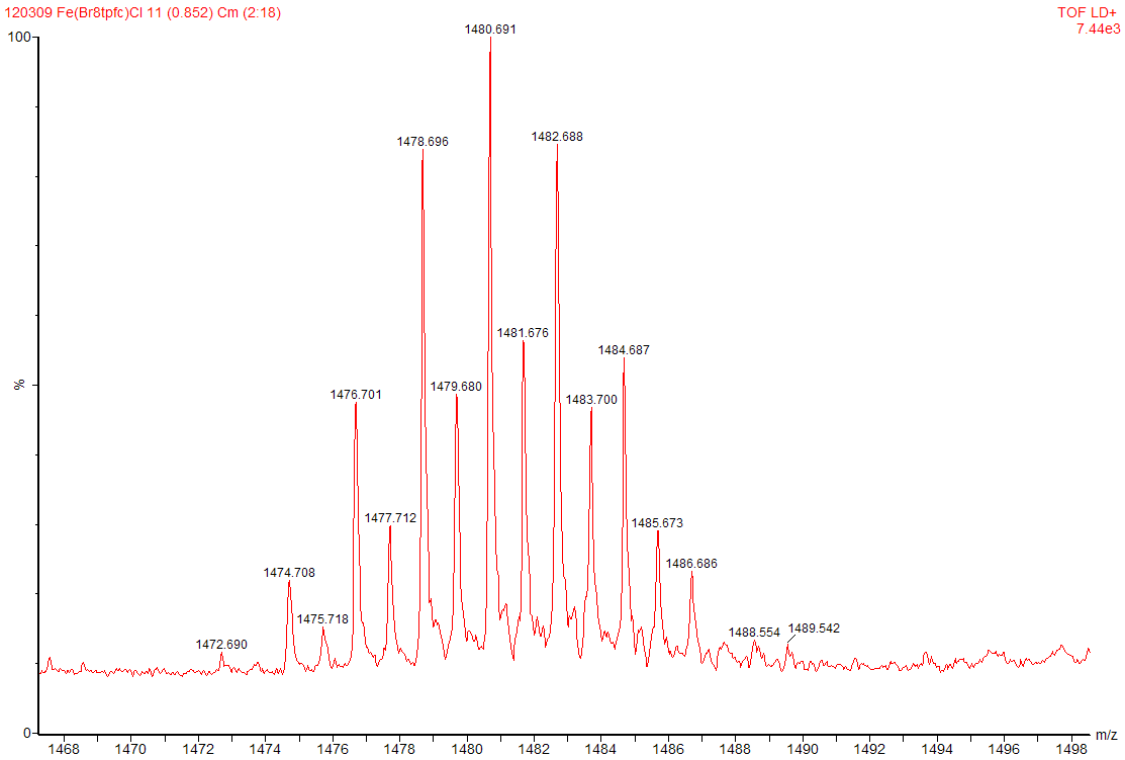

Figure S26. MS **(**MALDI-TOF) mass spectrum of Fe[Br_8TPFPC]Cl (M - Cl^-).

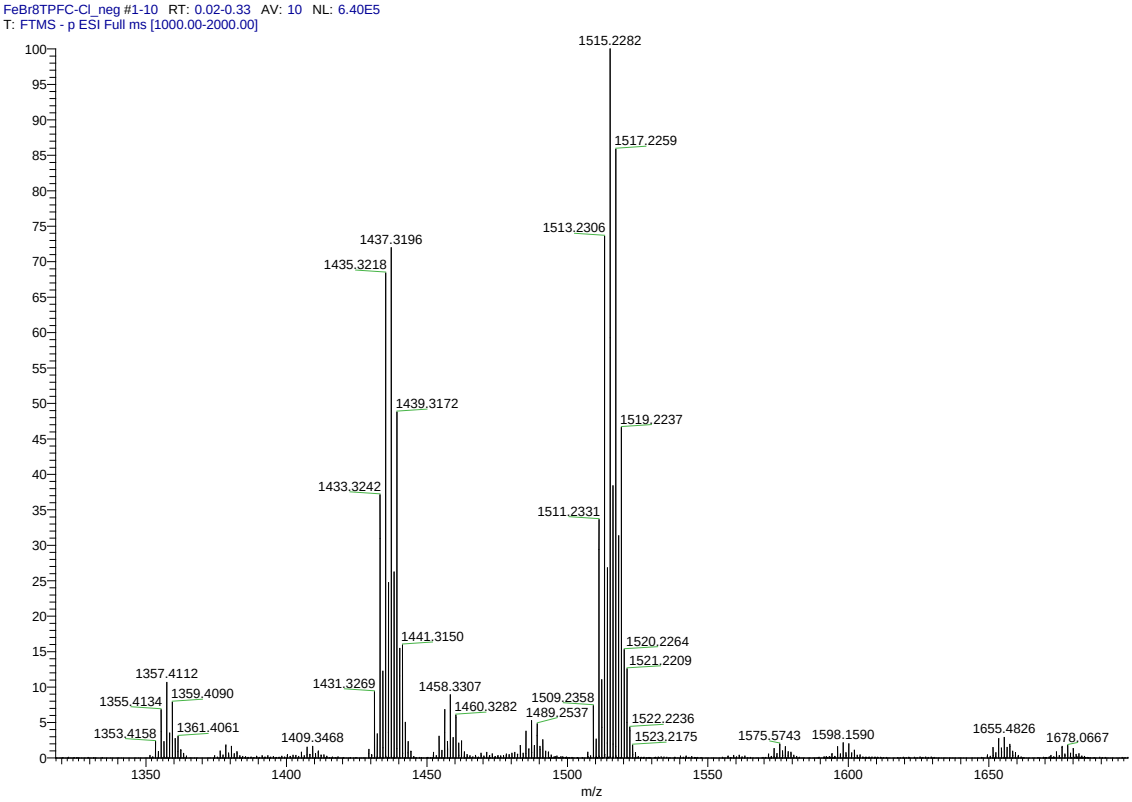

Figure S27. HR-ESI mass spectrum of Fe[Br_8TPFPC]Cl.

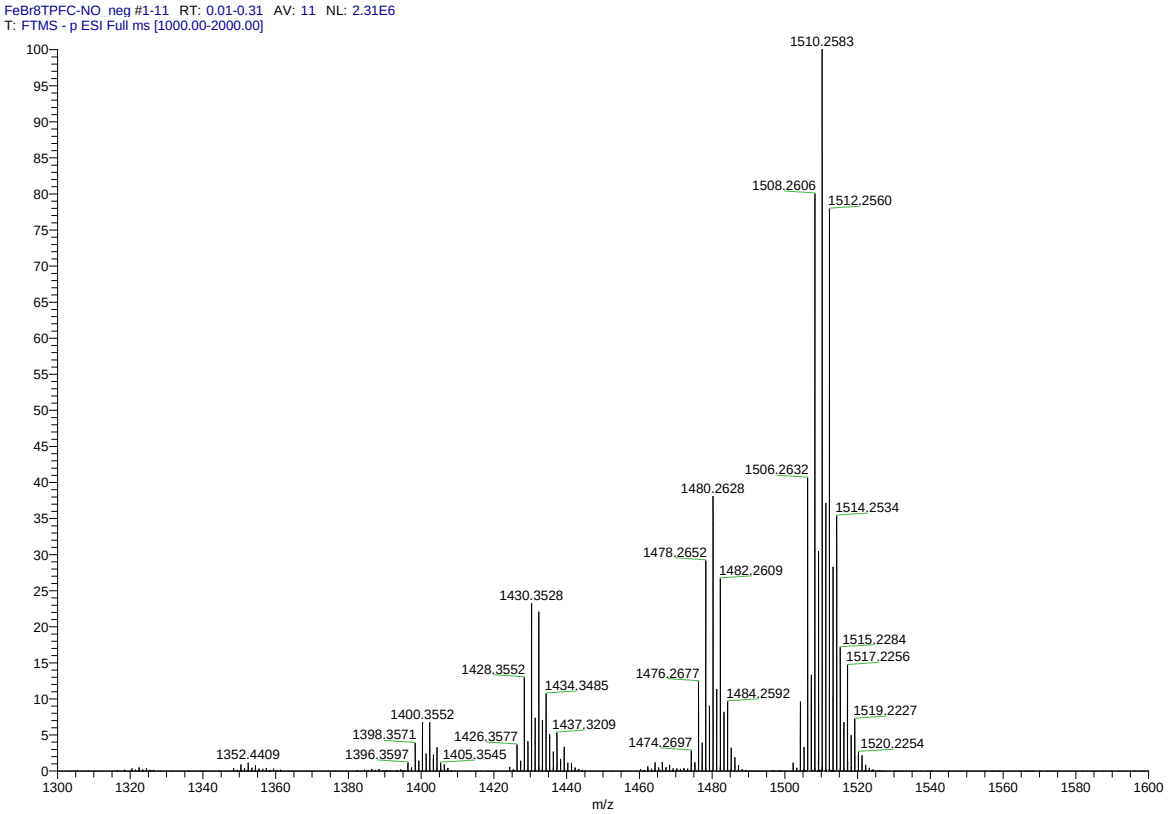

Figure S28. HR-ESI mass spectrum of Fe[Br$_8$TPFPC]NO.

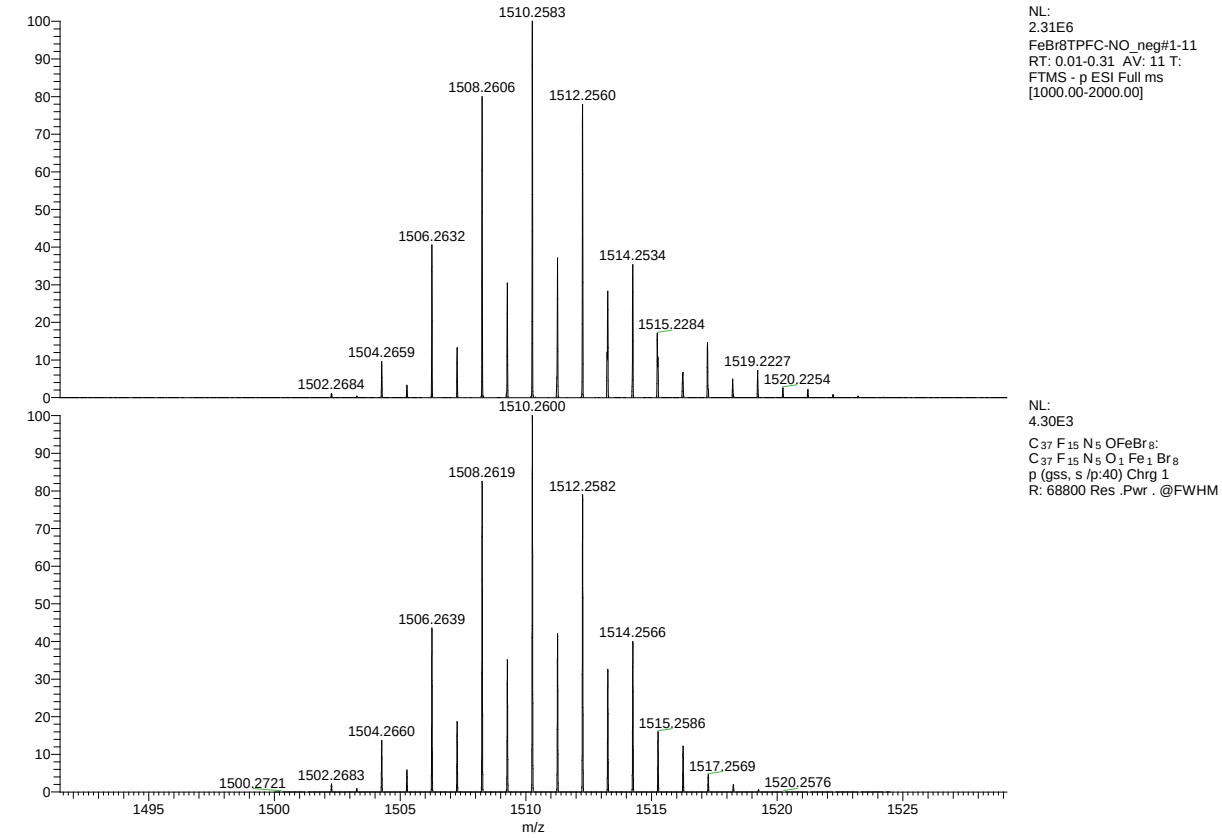

Figure S29. HR-ESI mass spectrum of Fe[Br$_8$TPFPC]NO (bottom: theoritical value).

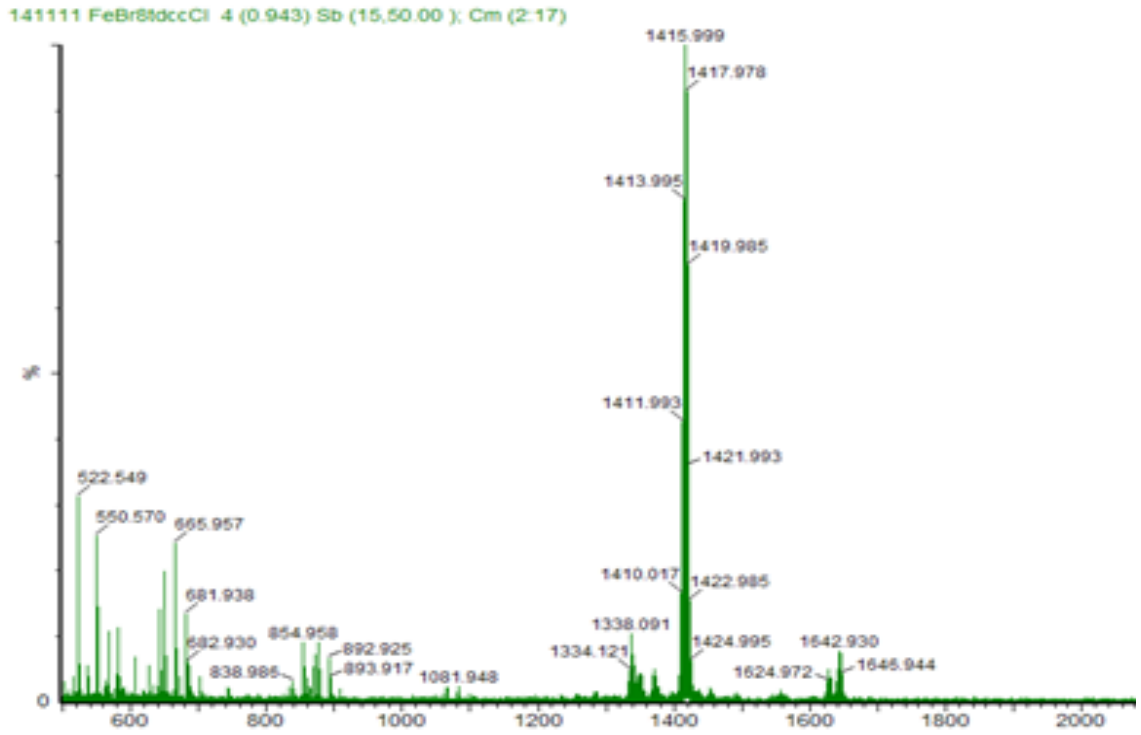

Figure S30. MS **(**MALDI-TOF) mass spectrum of Fe[Br_8TDCPC]Cl (M - Cl^-).

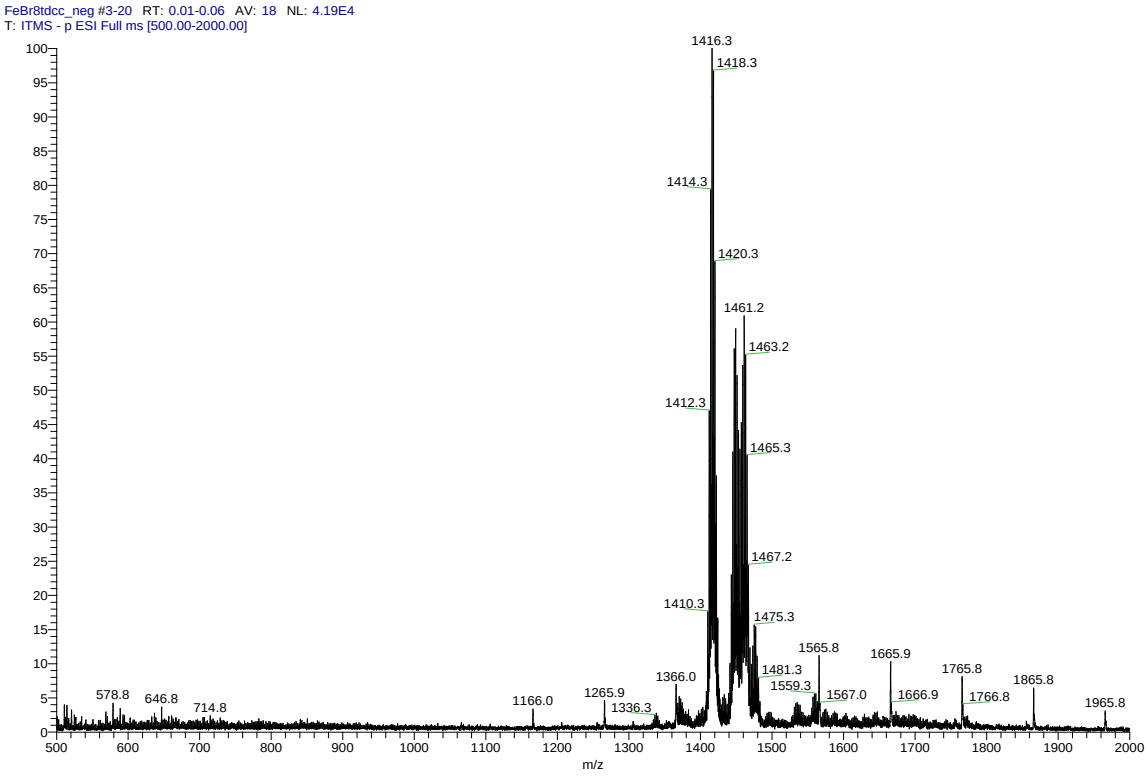

Figure S31. HR-ESI mass spectrum of Fe[Br_8TDCPC]Cl (M - Cl^-).

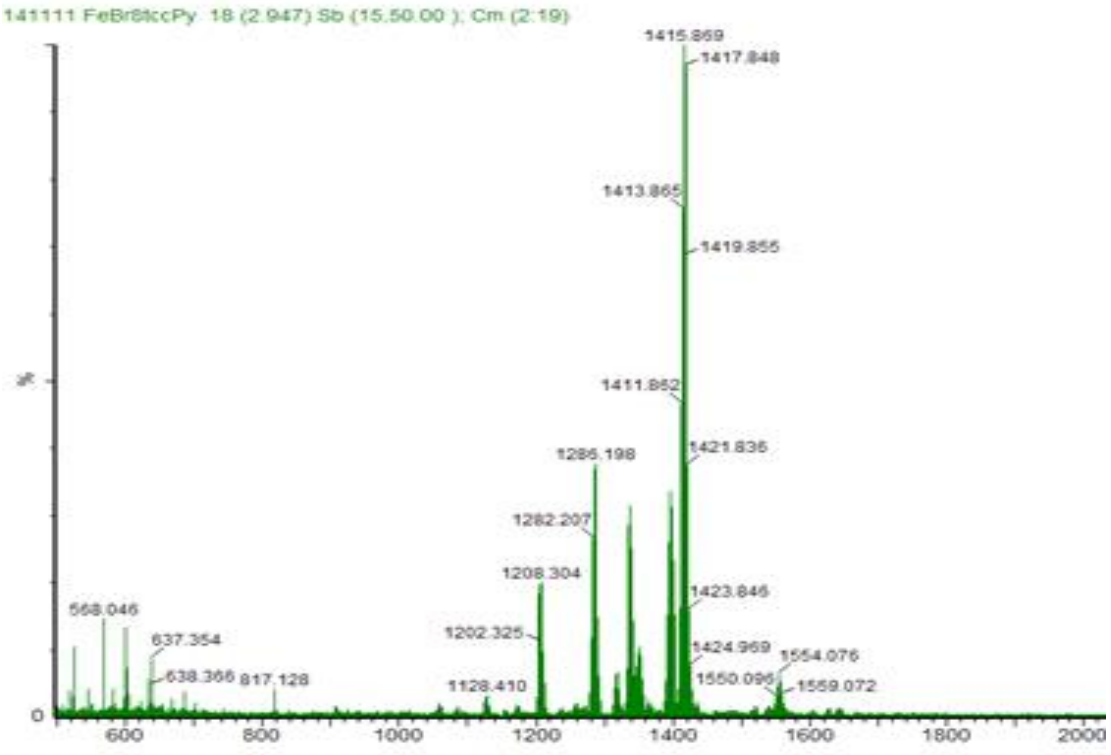

Figure S32. MS (MALDI-TOF) mass spectrum of Fe[Br_8TDCPC](py)$_2$ (M - 2py).

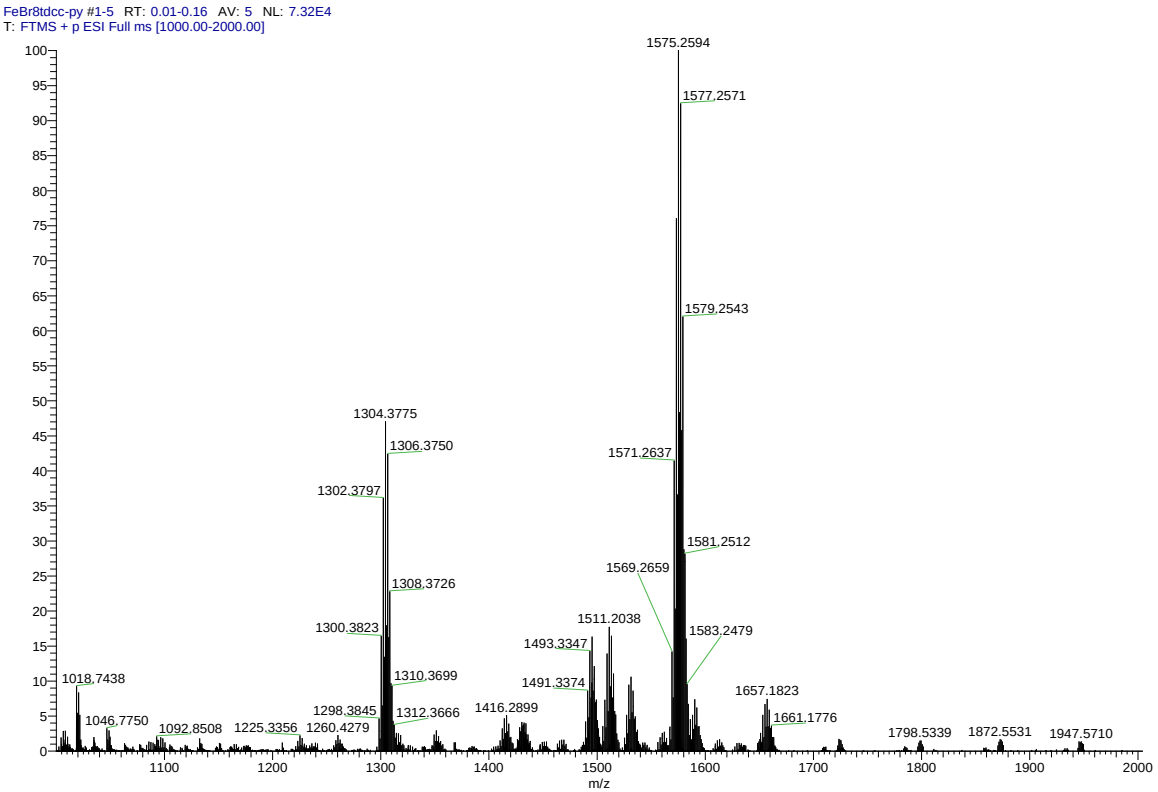

Figure S33. HR-ESI mass spectrum of Fe[Br_8TDCPC](py)$_2$.